Characterization of Laser Modified Surfaces for Wood Adhesion

Jeffrey Alan Dolan

Thesis submitted to the faculty of Virginia Polytechnic Institute and State University in partial fulfillment of the requirements for the degree of

Master of Science In Macromolecular Science and Engineering

Scott H. Renneckar, Chair
Charles E. Frazier
Kevin J. Edgar

February 21st, 2014
Blacksburg, VA

Keywords: Wood adhesion, Surface Chemistry, Mechanical Performance, Thermal decomposition, CO_2 Laser Modification

Characterization of Laser Modified Surfaces for Wood Adhesion

Jeffrey Alan Dolan

Abstract

The controlled degradation of wood surfaces with infrared light from a CO_2 pulsed laser facilitated adhesion without the use of additional resins. Laser modification creates a surface phenomenon that physically and chemically alters the natural biopolymer organization of lignocellulosic materials in a way that promotes adhesion when hot pressed using typical industrial equipment. Laser optimization was determined through mechanical and microscopic observation. It was determined that a mild level of laser surface modification (scale of 30 W/mm^2) resulted in the highest bond-line strength. The large spot size of the laser beam resulted in evenly modified surfaces. Surface analysis revealed that laser modification changed native wood morphology, hydrolyzed and vaporized hemicellulose, and enriched the surface with cellulose II and lignin. Attenuated Total Reflectance Fourier Transform Infrared Spectroscopy (ATR FTIR) was used to analyze the bulk of the laser material. This experiment revealed a change in the hydroxyl region related to hydrogen bonding conformations between wood polymers, mainly cellulose. X-ray photoelectron spectroscopy (XPS) provided an elemental composition of the top 5 nanometers of the surface, which resulted in increased carbon-carbon/carbon-hydrogen linkages and decreased oxygen containing bonds due to laser ablation. Static acid-base contact angle analysis was conducted using three probe liquids to find the Lewis acid, Lewis base, and dispersion components of the top nanometer of surface chemistry. Contact angle analysis revealed laser modified samples had a surface free energy that remained similar to the control wood sample. In addition, the dispersion component of the surface free energy

increased due to laser ablation while acid-base components were reduced. Atomic force microscopy (AFM) visually displays a reduction in surface roughness due to the laser technique. An additional set of experiments like thermal gravimetric analysis, thermal pre and post treatments, and heated ATR FTIR and XPS support findings which require more investigation into this adhesion phenomenon.

Acknowledgements

I would like to take this opportunity to thank my major adviser Dr. Scott Renneckar, who took me into his lab as sophomore and encouraged me to continue into graduate school. His unique approach to science and learning along with his continuous optimistic perspective was inspiring. I would also like to thank my committee members, Dr. Charles Frazier and Dr. Kevin Edgar for their valuable guidance through this work.

A big thank you to USDA NIFA Critical Agricultural Materials Program grant for funding this research. Moreover, thank you to the Joint BioEnergy Institute at Lawrence Berkeley National Laboratory for NMR testing and analysis.

The faculty and staff in the Department of Sustainable Biomaterials are terrific and I would like to thank all of them for their assistance in my research. I am grateful to all my friends and graduate students in Sustainable Biomaterials and the Macro program for all their help and support.

To my parents, thank you for everything without your support none of this would have been possible. Your constant encouragement to pursue education and my dreams was invaluable and greatly appreciated.

Last but not least, my fiancé Jillian Esham, who through it all was by my side and supported me. Her love and devotion was unsurpassed during my time in graduate school and for that I have endless gratitude and love for her.

Table of Contents

List of Tables

List of Figures

CHAPTER 1. Introduction

1.1 Problem Statement and Current State of the Forest Products Industry

The forest products industry has a unique opportunity to influence future building materials based on its low energy requirements for manufacturing and high performance capabilities. Engineered wood products utilize the natural properties of a tree for a broad range of applications, mostly residential construction and furniture. However engineered wood products like plywood, oriented strand board, and fiber board require the use of petroleum derived adhesives for bonding. Formaldehyde based resins and polymeric isocyanates are common because of their availability and cost benefits. Phenol-formaldehyde (PF) and Urea-Formaldehyde (UF) are synthesized from two non-renewable resources of natural gas and petroleum accounting for over two billion pounds of resin produced annually.[1] Recent pushes in environmental standards and customer's recognition of sustainable products may hinder the forest products industry in the United States if they cannot find alternative means for bonding wood products. Growing concerns with formaldehyde from urea formaldehyde emissions, listed as a possible carcinogen, have caused some wood adhesives to be regulated.[2] In response to these regulations along with declining petroleum resources, soybean based adhesives were developed. However these resin systems still require the use of fossil fuel derived reactants. From an environmental standpoint the objective is to create materials with enhanced properties from a single natural resource, in this case sustainably harvested trees. Therefore, an alternative to resin is the utilization and modification of wood polymers to create bonded composites with laser light. Laser treatments are not new to wood products and have been used for engraving surfaces, cutting, edge banding, and discoloring wood.

Innovation in the production of engineered wood products and the use of readily renewable natural resources for bonding are necessary in order to sustain cheap building material costs as the price of petroleum continues to rise.[3] Wood drying is the most energy intensive process for any engineered wood product. Most wood elements require moisture content less than 5% for sufficient adhesion. Producing adhesives that operate at higher moisture contents will save in energy costs. Also, the continuous costs of liquid adhesives and transportation of those adhesives contribute to overall engineered forest products manufacturing costs.

Forming effective bonds between wood elements is a complex science due to the inconsistent nature of the material. However, the performance and surface interactions between liquid adhesives and wood is understood. In contrast, photo and thermally degraded lignocellulosic polymer interactions create a bond between two elements without added adhesives.

The application of laser energy to treat surfaces for the use in bonding is a novel development. Surface modification is traditionally a sanding or machining operation that increases the wood surface energy for liquid adhesive application. But wood modification, in this communication, refers to different degrees of laser ablation which resulted in a chemically and physically altered surface. This research resembles the decade of research in wood welding the only previous technique known to utilize wood to wood interactions for adhesion. Mechanical wood welding research claims that interfacial vibration of solid wood causes lignin and hemicellulose to mobilize or melt creating fusion of intercellular components.[4] By contrast, understanding chemical and structural changes of surface degradation by laser modification is the focus of current research to understand wood to wood bonding. The conditions needed to form bonds between wood elements with laser light, heat, and pressures were determined in this thesis. Chemical changes due to laser ablation and the potential interactions of degraded

lignocellulosic materials to form adhesive bonds were revealed through detailed analysis of the modified surface layers.

1.2 Objectives

The goal of the research is to find the most effective laser treatment for bonding wood elements after hot pressing and investigate the chemical and structural changes due to laser ablation that enable adhesion. The research is divided into two parts: a) microscopy and chemical analysis of the laser modified wood surface, and b) surface analysis of the modified wood as a function of depth

CHAPTER 2: Review of Literature

2.1 Wood Chemistry and Ultrastructure

Wood is composed of three different classes of structural polymers that occur in varying amounts depending on the genus and species. There are number of polysaccharides starting with the most abundant cellulose which in woody cells makes up 40-50% of the composition of the cell wall composite. Cellulose consists of β(1→4) linked D-glucose and has a typical degree of polymerization (DP) around 10,000 making the chains up to 5 microns in length. Cellulose is deposited in semi-crystalline microfibrils containing numerous hydrogen bonds making it insoluble in most solvents. The extensive hydrogen bonding provides cellulose in trees with a monoclinic crystal structure called cellulose Iβ, but also contains non-crystalline regions making it a semi-crystalline polymer where water can bind to the amorphous areas of this homopolymer. Cellulose is synthesized in microfibril bundles that contain 24-36 individual cellulose chains.[5] Cellulose makes the wood cell wall matrix rigid and is the primary reinforcing polymer.

Hemicellulose or more accurately described as heteropolysacchrides are branched low DP chains that surround cellulose either with extensive hydrogen bonding or are entrapped in cellulose crystalline regions.[6] These hemicellulose can range from 25-35% composition in the wood cell wall. Moreover, hemicelluloses consist of alternating and branched chains of only monosaccharaides. They differ greatly from hardwood and softwood species where hardwoods contain primarily glucoroxylan and glucomannan and softwoods contain galactoglucomannan and arabinoglucuronoxylan. To demonstrate the complexity of these hemicelluloses Table 2.1[7] highlights structure associated with these cell wall components. The branching, substitution, and linkage differences in hemicellulose make them amorphous. Hemicelluloses can be covalently bonded to lignin which is the polyaromatic network surrounding hemicelluloses.

Hemicellulose Type	Wood Type	Percent Composition	Units	Molar Ratios	Linkages	Degree of Polymerization
Galactoglucomannan (Galactose-rich)	Softwood	5-8%	β-D-Manp	3	1→4	100
			β-D-Glup	1	1→4	
			α-D-Galp	1	1→6	
			Acetyl			
(Galacto)Glucomannan (Galactose-poor)	Softwood	10-15%	β-D-Manp	4	1→4	100
			β-D-Glup	1	1→4	
			α-D-Galp	0.1	1→6	
			Acetyl	1		
Arabino-glucouronoxylan	Softwood	7-10%	β-D-Xylp	10	1→4	100
			4-O-Me-α-D-GlupA	2	1→2	
			α-L-Ara*f*	1.3	1→3	
Glucuronoxylan	Hardwood	15-30%	β-D-Xylp	10	1→4	200
			4-O-Me-α-D-GlupA	1	1→4	
			Acetyl	7	1→2	
Glucomannan	Hardwood	2-5%	β-D-Manp	1-2	1→4	200
			β-D-Glup		1→4	

Table 2.1 Major hemicellulose monosaccharides, percent composition, linkages, branching, and Degree of Polymerization

Lignin is composed of phenylpropane units linked together creating what has historically been classified as a three dimensional network. There are different precursors that make up lignin in the cell wall including p-coumaryl alcohol, coniferyl alcohol, and sinapyl alcohol. These precursors have methoxy functional groups attached to the 3 and/or 5 position on the phenol ring, Figure 2.1. The polymerized precursors in lignin are termed syringyl units (S-units) related to sinapyl alcohol, guaiacyl units (G-units) related to coniferyl alcohol, and p-hydroxyphenyl (H-units) related to p-coumaryl alcohol. Enzymatic dehydrogenation and radical coupling reactions polymerize and branch the lignin precursors to form a matrix material. [7] The β-O-4 connections dominate lignin structure and makes up 46-60% of the overall linkages. The lignin network makes up 15-25% of the total composition of the cell wall. [8]

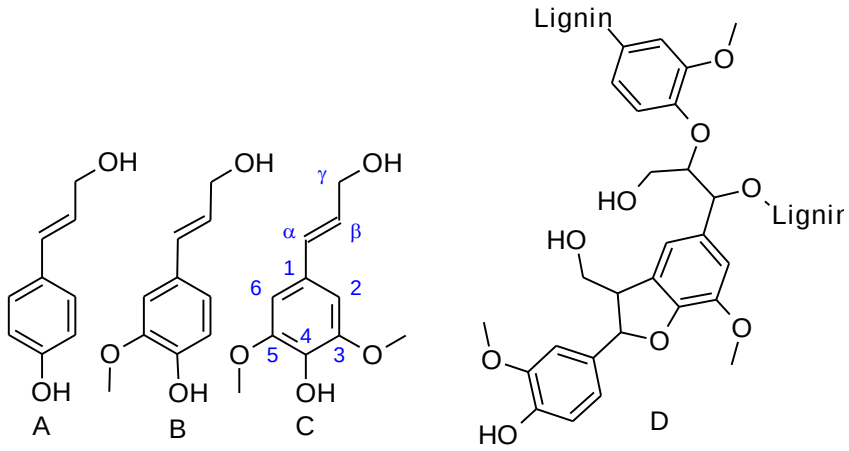

Figure 2.1 **A**. p-coumaryl alcohol/ p-hydroxyphenyl **B**. coniferyl alcohol/guaiacyl units **C**. sinapyl alcohol/syringyl units **D**. lignin structure composed of linked gauiacyl units

Wood ultrastructure is composed of a middle lamella, primary, and secondary layers. The middle lamella and primary layers are composed of up to 50% by weight of lignin and greater amounts at the cell corners.[9] The primary cell wall is composed of randomly oriented cellulose fibrils while the secondary layer has three distinctly oriented sub-layers. [10] The secondary layer is composed of sub layers S_{1-3}. The S_1 and S_3 cellulose microfibril angles are greater than 45° taken from the longitudinal direction. The S_2 is the largest sub-layer and makes up approximately75% of the total wood cell wall with a microfibril angle essentially parallel to the direction of the tree stem. Microfibiril and cell wall orientation creates anisotropic mechanical properties in wood. Moreover, the S_2 sub layer influences the shrinkage and swelling properties of wood.[11]

2.2 Wood Welding

Bonding wood without adhesives was discovered through a process similar to mechanically induced metal welding. It was found that vibrating two contacting solid wood elements fuses the wood surfaces together to form effective joints. This fusion of wood cell wall material is said to occur by polymer entanglement of the amorphous components in wood like lignin and some hemicellulose as well as some crosslinking of lignin, cellulose and

hemicellulose degradation products. Wood welding investigates the chemical and physical conditions used to join wood together mainly using friction to heat the interfacial wood surfaces for adhesion. Wood welding and laser modified wood amalgamation contain key similarities including localized surface degradation, platen pressure and temperature, and no added adhesives for adequate bonding.

There are many contributing factors relating to the effectiveness of wood welding including vibrational time, pressure, holding time after vibration, holding pressure, and vibration amplitude and frequency. The optimized combinations of these factors have created bond-line strengths adequate for structural applications. The vibrational amplitude or linear shift parallel to the bonding plane needs to be around 3 mm to sufficiently bond wood elements. When welding pressure, or the applied force perpendicular to the bonding plane, is increased the bond-line strength increases. As the welding pressure reaches 2.3 MPa the bond-line degrades to a point where the strength decreases. A 3 second welding time and a 5 second holding time with a 2 MPa pressure resulted in the best tensile strength bond-lines.[12] Water in the bond-line seemed to have no effect on the tensile strength of the resulting wood joint. These particular experiments used hardwood species only because softwood cellular structure could not withstand the welding process and collapse. Even though these experiments do not require a severe conditioning step the authors explain the bond-line is hydrolytically unstable and can delaminate in the presence of water after adhesion. The temperature of the bond-line can reach close to 225°C but all samples reach over 170°C. It was found that lignin demethoxylation occurred during vibrational welding, amorphous carbohydrates increase during welding, auto condensation reaction of lignin on its aromatic ring appears to have occurred, furfural appears to have been produced and reacted with lignin and lastly deacetylation of hemicelluloses occurred.[13]. Scanning electron microscopy

shows fiber adhesion is occurring through the movement of the middle lamella composed mostly of lignin where the flow of these components results in an inter-fiber network. [12]

Other studies utilizing ^{13}C solid state NMR have chemically mapped the changes to the wood surface at different vibration frequencies being 100Hz and 150 Hz. The authors propose that heating the wood by vibration created furan molecules from cellulose and hemicellulose as well as cleavage of aromatic ethoxylates species from lignin. Also, bond strength increased with increased frequency due to the interactions and cross-linking of lignin with other wood functional groups or itself.[14] This claim has insufficient data to suggest covalent bonding between surfaces especially referring to the NMR peaks generally associated with etherified syringyl units at C3 and C5 positions (152 ppm) and etherified/non-etherified C3 and C4 guaiacyl lignin structures.[15]

2.3 Wood Pyrolysis and Thermal Degradation

Laser modification of wood is a high heat and energy application sometimes resulting in combustion at the surface. However, the laser does not always combust the wood and other thermal degradation pathways are plausible.

Lignocellulosic materials, like wood do not burn directly. Wood polymers thermally degrade and volatilize. The volatiles can combust if oxygen and an ignition source are present. Products from combustion that utilize open flames are used on a daily basis and include charcoal briquettes for cooking or heating, activated carbon for waste water and air purification, and charred wood barrels for wine, liquor and beer flavoring.[16] [17] [18]In the absence of oxygen pyrolysis occurs. Pyrolysis is often referred to as destructive distillation and products derived from these processes are a direct result of the starting material, such as hardwood and softwood

sources. Wood pyrolysis is categorized as rapid or fast due to quick heat transfer. Fast pyrolysis utilizes fluid bed reactors, specialty tube furnaces, and microwaves to rapidly heat wood. However, slow thermal degradation in a vacuum, a special case, can also yield molecules similar to fast pyrolysis. Manufactured products like heat treated wood for anti-shrinkage/anti-decay applications occur in a vacuum.[19] [20] The final degradation products from pyrolysis include tar or bio-oils for fuel sources, resins, waxes, flavor additives, and derived chemicals like levoglucosan and furfurals.[21] [22]

The anisotropy of the cellular configurations in various wood species creates even more chemical and anatomical complexity that impacts heat and mass transfer. Also the addition of wood extractives and inorganics impacts the complexity of the degradation products as well as the generation of ash.

Gases like carbon monoxide, hydrogen, formaldehyde, and methane are emitted from the chemical decomposition of wood and combust if oxygen is present. A flame occurs at a certain distance from the material where oxygen from air and the emitted combustible gases combine. The material is still oxygen deprived as it is being consumed by fire and thermal degradation continues and the flames are thus retained until only inorganic material remains. Moreover, at higher temperatures copious amounts of carbon dioxide and water are volatilized.[23] Thermal treatment in the presence of air contributes to degradation through oxidation of the material which can lower spontaneous ignition temperatures and increase degradation rates. [24]

A slow thermal degradation characterization approach taken by Su and Luo et al. involved a controlled oxygen concentration environment using thermal gravimetric analysis from 0-800°C coupled with mass spectroscopy. However the goal was to determine the effects of oxygen concentration on pine wood oxidative thermal decomposition. The results showed

increased CO and CO_2 emissions as oxygen composition increases with temperature and were determined as primary volatilization products. An interesting theory posed by the authors was that during thermal treatment for low oxygen concentrations the emission of volatiles like methane, hydrogen, and carbon monoxide prevented the diffusion of oxygen onto the sample surface known as boundary layer resistance. This would mean pyrolysis occurs at low oxygen concentrations. However, at higher oxygen concentrations the efflux of volatiles is overcome and oxygen can penetrate the surface of degrading wood particles.[25]

Another form of pyrolysis is rapid or fast which is a high-temperature process always in the absence of oxygen where heat transfer is very important for the generation of products like liquid bio-oils, non-condensable gases, and solid char. According to Bridgwater et al. common methods of pyrolysis included ablative pyrolysis where a heated inert surface is brought into contact with rapidly moving wood that deposits bio-oil residues on the surface. Another is fluid bed reactors where hot inert gases are transferred to the wood resulting in heating by a mixture of convection and conduction which is very dependent on wood surface volume or particle size. Additional methods include vacuum pyrolysis which is a slow pyrolysis technique however it quickly removes volatiles so it creates products similar to fast pyrolysis.[26] Recent literature describes additional pyrolysis methods such as microwave emission degradation.[21]

For rapid pyrolysis the target product is bio-oil. Bio-oil chemical composition is dependent upon treatment temperature, starting particle size, and wood species or other biomass sources. An interesting study determined the effects of temperature on the molecular weight of the bio-oil produced from a fluid bed reactor. Fluid bed reactors use high temperature liquids or gases to pass through solid particles which then are suspended in the mixture as a “fluidized solid” and degradation products were separated. The experiment utilized a pyrolysis pilot plant to

degrade pine wood particles and separate char, non-condensable gases, and bio-oils. Higher temperatures of the fluid bed reactor caused the char amounts to decrease during pyrolysis. Gel permeation chromatography was used to determine the molecular weight of water insoluble fractions of bio-oil according to reactor temperatures. As a result of increased temperature the molecular weight of the bio-oil compounds increases until 530°C and then starts to decrease (M_n 170 g/mole at 360°C, ~230 g/mole at 450°C, 250 g/mole at 530°C and 210 g/mole at 580°C). The authors claim that the conversion of more lignin into insoluble bio-oil is the reason for molecular weight increases.[27] This explanation justifies an increase in concentration of lignin degradation products but not molecular weight increases. The formation of radical species during lignin fragmentation and recombination of those radicals to form larger units is a possibility leading to increased molecular weight at similar pyrolysis temperatures.[28]

During fast pyrolysis moisture is generated and can account for 15-30% of the bio-oil that cannot be removed by conventional distillation. Water can affect bio-oil stability, viscosity, pH, and corrosiveness and many times is separated for analytical purposes.[26] A powerful analytical tool for bio-oil characterization is gas chromatography coupled with mass spectroscopy in which Sipila et al. analyzed a mixture of oak and maple wood along with Scotts pine with a fluid bed pyrolyzer at 530°C. This author separated water soluble and insoluble fragment material consisting mainly of monomeric materials. The author identified over 45 chemicals in the bio-oil and distinguished what wood component they were derived from.[29]

2.4 Wood Component Degradation

Understanding how each wood component thermally degrades is important for this research. The various macromolecules that make up wood decompose differently depending on

temperature and exposure time. Degradation pathways are important to not only identify reactive molecules but also understand the intensity of the laser treatment.

2.4.1 Heteropolysaccharides

When wood is thermally degraded it forms gaseous and liquid products. The first products are formed from labile functional groups such as the acetate side groups on hemicelluloses. Most of the acetic acid formation comes from the degradation of hemicelluloses that are acetylated including glucuronoxylan and glactoglucomannan in hardwoods and softwoods respectively. Carbon-to-oxygen bonds in pentoses are cleaved resulting in gaseous products such as acetic acid, formaldehyde or carbon monoxide and hydrogen. Degradation of the hemicelluloses after chain cleavage occur via dehydration of xylose residues leading to the formation of furfural and furan derivatives as seen in Figure 2.2.[4]

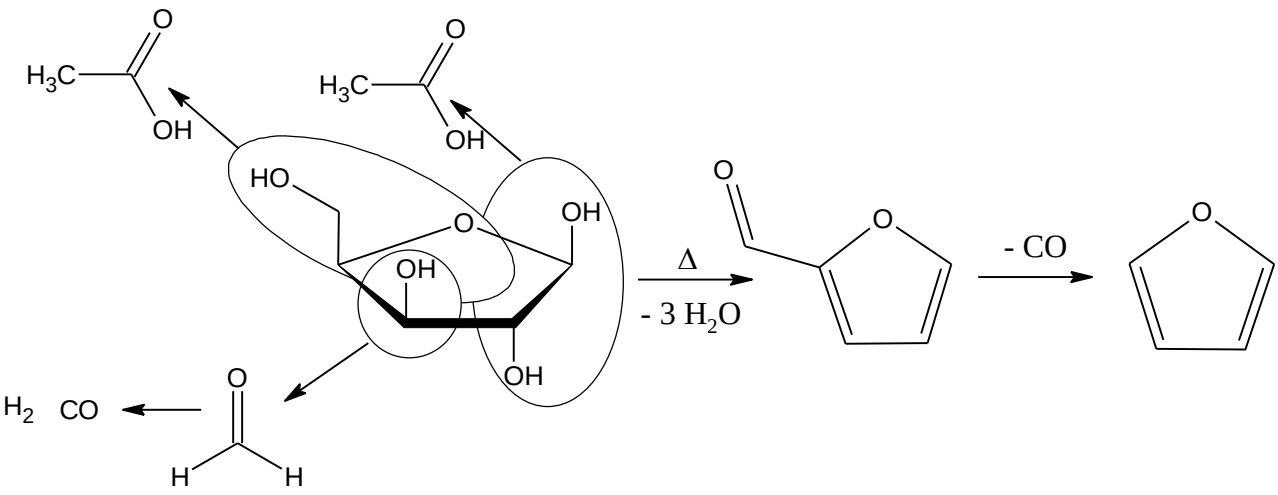

Figure 2.2 Thermal decomposition and dehydration of xylofuranose, a hemicellulose residue

2.4.2 Cellulose

Cellulose is an abundant component in most woody cells and consists of β(1->4) linked glucose residues with native cellulose I lattice structure. Its decomposition starts with the

removal of bound water followed by the cleavage of glycosidic linkages that results from the protonation of the glycosidic oxygen and subsequent bond breakage catalyzed by the acid produced from hemicellulose. This chemical change results in a decreased degree of polymerization and formation of monomeric compounds. Glucose and other cellulose degradation materials can form a multitude of products ranging from levoglucosan, furfural derivatives, phenolic compounds and cross-linked structures. Figure 2.3 A shows the crosslinking of C-6 oxidized cellulose where the carboxyl group on oxidized cellulose may esterify with a hydroxyl group on an adjacent molecule with water removal. The bottom left Figure 2.3 B shows the reaction of a hydrolyzed reducing end glucose residue to form levoglucosan and Figure 2.3 C shows the crosslinking reaction of cellulose by protonation of the primary hydroxyl group.[30] Cellulose crystalline structure is also disrupted and the amount of crystallinity goes up then down with intermediate temperatures (225°C) this is expected because of the removal of amorphous cellulose and then random cleavage of glycosidic bonds in ordered regions which disrupts regular packing. [31]

2.4.3 Lignin

Early mechanisms of lignin degradation were conducted by studying the effects of thermal treatment on phenethyl phenyl ether as a model of β-O-4-alkyl-aryl ether linkages, common in lignin structure. Mechanistic studies determined that styrene and phenol are products from lignin fragmentation after pyrolysis. However this mechanism did not include oxygen functionality at the α-position for free radical products and so Figure 2.4 was the theoretical mechanism established to understand the free radical reactions in lignin during pyrolysis. Free radical mechanisms are a major debate because with the addition of free radical scavengers the degradation products still form. Another theory is called cage effect where solids trap reactive

intermediates and are likely to recombine leading to no new products. These reactions happen at intermediate temperatures before the major production of char. [32]

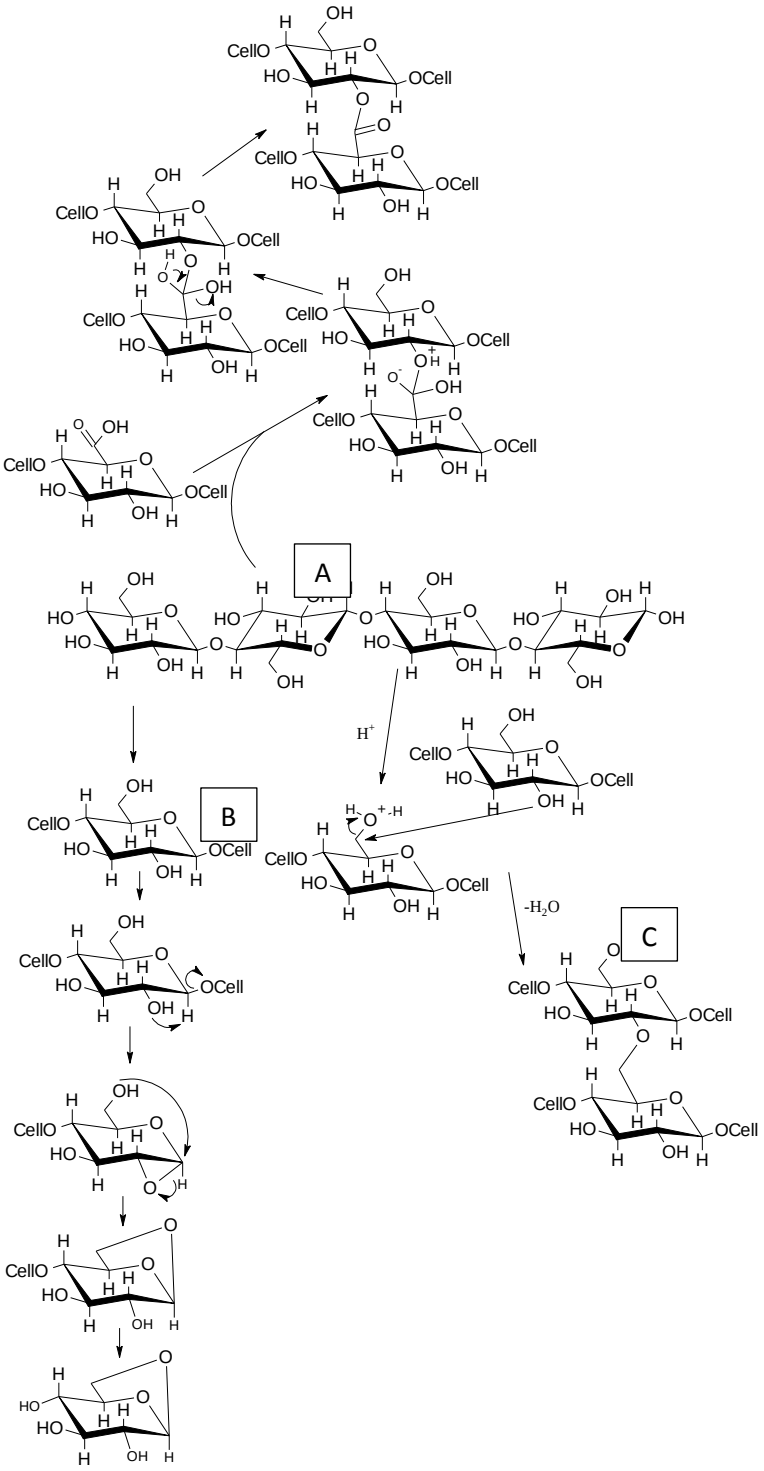

Figure 2.3 **A.** Thermal degradation reaction mechanism of acetylated cellulose **B.** mechanism of cellulose into levoglucosan **C.**Reaction mechanism of crosslinking cellulose in the presence of acid

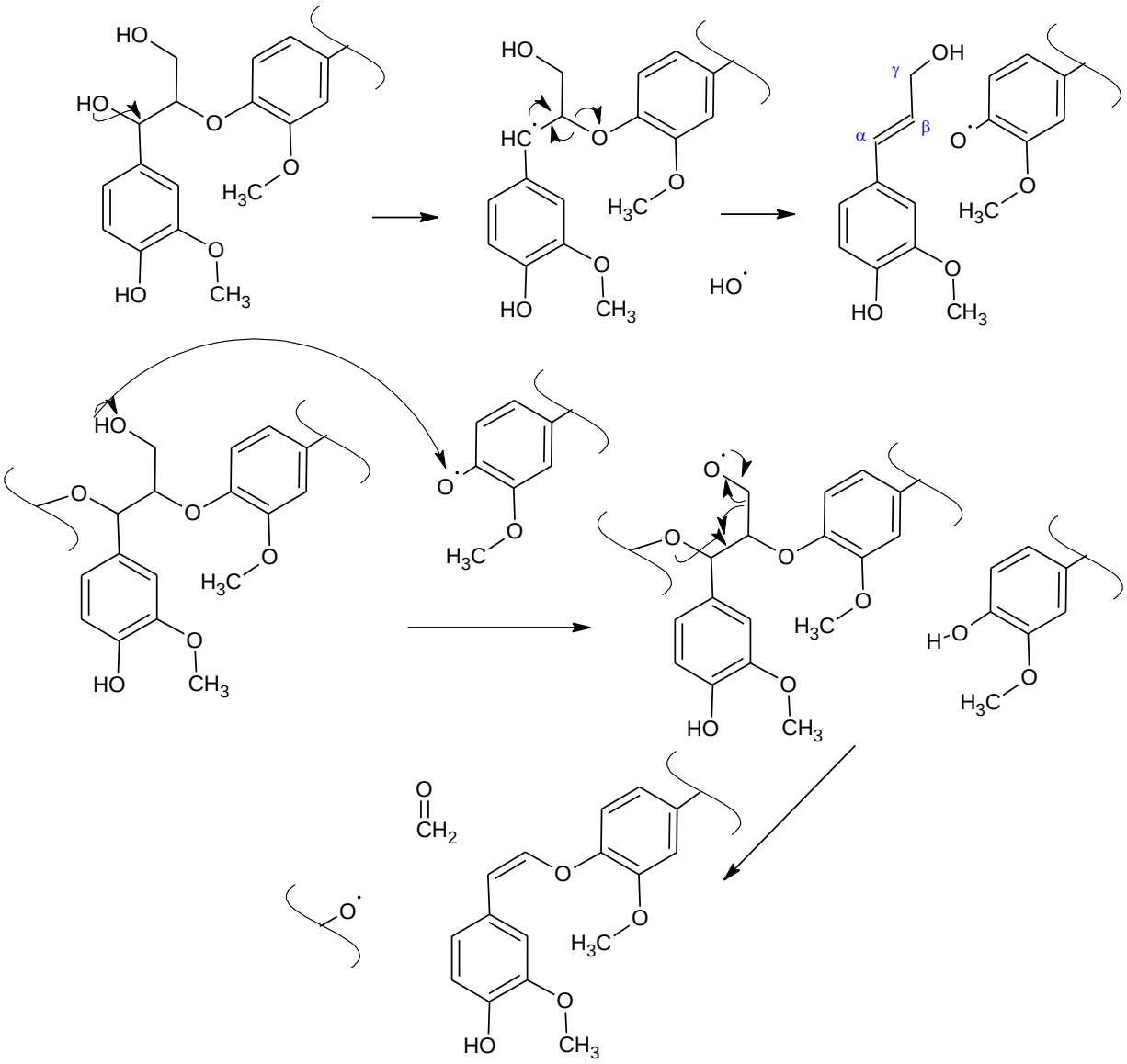

Figure 2.4 Theoretical free radical recombination mechanism of lignin during decomposition

2.5 Light Degradation of Wood

Laser light in this research refers to photons emitted at 10.6 micron wavelengths or in the infrared spectra. This infrared light has high energy which generates heat but also promotes photodegradation. Photodegradation in the infrared spectra is not often researched because wood is not commonly exposed to high levels of this light source. Ultraviolet light degradation of wood is commonly studied due to woods propensity for exterior applications.

2.5.1 UV Light

Ultra violet (UV) radiation has great influence on the physical and chemical structure of wood. Lignin in wood is most susceptible to chemical modification due to light degradation. The aromatic and phenolic groups associated with lignin substructure absorb light in UV wavelengths leading to the degradation of these polymeric units. Three subsequent effects of light degradation on lignin structure are increased phenolic hydroxyl groups, decrease in β-O-4 linkages, and increased number of aromatic carbonyl groups. Photodegradation often decreases molecular weight of lignin as well.[33] These changes contribute to further absorption of light and break down of the lignin polymer matrix.[34] The range of wavelengths usually studied on wood is from 100 to 400 nanometers where many phenolic type compounds associated with lignin absorb from 200 to 350nm. The other components of wood like cellulose are more stable in UV and visible light because they do not absorb photons of this wavelength like lignin molecules. Cellulose can go through UV light degradation where chain scission at C1 and C4 occur, also reducing the degree of polymerization. This happens through the abstraction of hydrogen and the production of free radicals produced along the cellulose chain.[35] Another interesting study suggests that UV irradiation may change the morphology of cellulose chains from cellulose I to cellulose II. [36]

2.5.2 Infrared Light

Authors Kacik and Kubovsky have utilized a CO_2 infrared laser to irradiate Beech wood to chemically change the surface for coloring purposes. This method of coloring wood is untraditional compared to steam or thermal treatments however there are other coloring techniques that utilize visible light, sunlight, and ultra violet light. [37] It was found that with increasing irradiation intensity the Beech wood surface darkened. Chemical changes detected included cleavage of aliphatic side chains in lignin and possible condensation reactions with increasing laser irradiation. Acetyl groups associated with hemicelluloses are cleaved and released as acetic acid. The authors claim this causes an acidic hydrolysis of lignin's ether linkages to form carbonium ions. These ions lead to further condensation reactions. The laser modification also causes depolymerization of the hemicelluloses which indicates degradation of structural components in woody tissue. Laser light affects and degrades thermally unstable portions of woody polymers including amorphous cellulose. As the irradiation dosages increase the yield of carbohydrates like xylose (hemicellulose) and glucose (cellulose) decreases. Overall effects of increased irradiation include condensation of lignin, degradation of hemicelluloses, and degradation to amorphous cellulose which are responsible for darkening the Beech wood. [38]

2.6 CO_2 Laser Fundamentals

Two precursory theories were developed in the early 20th century leading to the development of the first laser in the 1960's. In 1900 Planck's law described electromagnetic radiation and provided the basis of quantum theory.[39] Albert Einstein later in 1917 established the foundations for the laser and maser in his paper "On the Quantum Theory of Radiation."[40] The first maser (Microwave Amplification by Stimulated Emissions of Radiation) was built in 1954 and was energized with ammonia molecules. Later in 1960 the first light emitting maser

was created, renamed laser, and in 1964 the Novel Prize in physics was awarded to Charles Townes for this discovery.[41] Since this time numerous lasing materials have been discovered and utilized for industrial purposes. One of the first known laser applications for CO_2 laser source was plywood cutting for packaging.

Carbon dioxide is a linear and symmetric molecule with three fundamental vibration modes consisting of a symmetric stretch mode (V_1), bending mode (V_2), and asymmetric stretch mode (V_3). These different modes correspond to the vibrational quanta and are identified though the numeric code [V_1 V_2 V_3] (i.e. [0 1 0] means no quanta in the symmetric stretch mode, one quanta in the bending mode, and no quanta in the asymmetric stretch mode). In order to generate light as photons, the CO_2 molecules must relax from a high energy state to a lower energy condition which typically occurs from [0 0 1] to [1 0 0] this type of energy decay releases a quanta of energy at 10.6 micron wavelengths. Lasing action continues with an incident photon that collides with an excited state molecule and produces a "twin" photon and this cascade continues. Carbon dioxide also has various rotational states in which energy is stored and released as a result of torsional conformations. The energy related to molecular torsion is smaller than vibrational energy but gives rise to a spectrum of possible output energies which controls the emitted photon and the wavelength ($E=h\nu$, E-change in energy states, h-Planck's constant, ν-frequency of the light emitted). There is variation between photon energy in this process however a dominate transition occurs because of selective competition between the numerous energy states resulting in a single wavelength of 10.6 microns. Pure carbon dioxide lasers are not efficient due to slow re-excitation rates and loss in energy states therefore to increase efficiency a mixture of molecules is needed.

Nitrogen a diatomic molecule is added to the mixture to enhance the excitation of carbon dioxide molecules. Nitrogen has only one possible vibrational mode that is very close to carbon dioxide's [0 0 1] energy level. Consequently when nitrogen collides with carbon dioxide it transfers the energy to the carbon dioxide molecule which can subsequently take place in the lasing action. Also in pure CO_2 lasers the relaxation step from [0 1 0] an intermediate energy level to [0 0 0] ground state is very slow. The addition of helium to the mixture increases the rate of de-excitation due to its high collision rate which is about 40 times higher than CO_2 at 1 torr. The mixture consists of a 1:5:20 by volume ratio of CO_2, nitrogen, and helium respectively. It is important to note that cooling these gas mixtures is important for lasing action because changes in the energy spectra will occur with increasing temperature which lowers efficiency and could change the wavelength of the laser. The laser tube containing the gas mixture is cylindrical composed of a fully reflective mirror on one end and a semi-transparent mirror on the other end. The incident photons contribute to the direction of the cascade and release of stimulated molecules however the incident photons that initiate perpendicular to the mirror are sustained because of the dominate direction of those reflected photons. The semi-transparent mirror reflects some of the photons to sustain this direction but the remaining photons escape as polarized light. [42] [43]

As mentioned before the cascade or multiplication of photons is necessary so that there is a majority of excited molecules in the laser cavity. The term population inversion was given to the event where there are more molecules in an upper energy level than a lower energy level. The term "pumping" is often used in CO_2 laser systems to describe the electrical input resulting in population inversion. High energy electrons are produced from these electrical inputs like a glow

discharge which creates a continuous laser source or a radio frequency excitation used for pulsed CO_2 lasers.[44] [43]

Another important aspect of CO_2 lasers are the resulting beam modes. Due to oscillation in the laser cavity from the sustained energy reflected off of the mirrors there are energy distributions modes. These modes are identified by a three-dimensional index termed TEM_{mnq} for transverse electromagnetic mode where m, n, and q are the X, Y, and Z direction respectively and map the energy of a laser beam. It is common to only report the m and n values because the Z direction (q) nodes are taken as the number of half wavelengths of light between the two mirrors along a line joining these mirrors. Generally the q node value is very large whereas the spaces between the nodes in the X and Y direction are small (0-3). For a Gaussian energy distribution the beam has the most intense energy towards the center and has the best focusing ability and is termed TEM_{00}. Another common energy distribution is called a "doughnut" mode and consists of a laser beam with a hollow center. This type of mode is produced by placing a mirror in the center of the semi-transparent cap of the laser cavity which allows photons to reflect off the center circular mirror, sustaining lasing action, while photons escape around the mirror creating a hollow tube beam. This beam is not as focusable as a TEM_{00} but is useful for heat treatments or processes that do not require a very small spot size. Multimode beams are purposely made but could also be the result of poor laser cavities or optics. [43]

Acrylic imprints are made to test the mode of a laser beam where polymethylmethacrylate is used because it vaporizes into methyl methacrylate and leaves a three dimensional representation of the laser beam including focal point, distribution, and shape.[45] The laser system utilized in this thesis has a Gaussian type beam distribution. The laser tube is located in the back of the system and a series of mirrors delivers the laser beam to the laser head

that houses the final focal optic and a calibration tool aligns the focal point of the optic with surface of the material. This is called a gantry laser system and utilizes an X-Y coordinate system to drive the laser head on specified pathways. For this work the focal point was moved for defocused lasing to increase spot size and broaden the beam distribution.

2.7 Analytical Techniques for Wood Characterization

Wood is a complex material and often analytical techniques can only generalize changes in wood chemical structure. Using an abundance of techniques can minimize the error in describing a wood structural or chemical change. The next section describes techniques used throughout the thesis to determine and characterize the differences between wood and laser modified wood.

2.7.1 ^{13}C Solid State Nuclear Magnetic Resonance

The principles of NMR spectroscopy are based around atomic nuclei specifically protons that exhibit both angular momentum and a magnetic moment. These protons have spin states that have equivalent energy without magnetic field intervention. However nuclei are exposed to a magnetic field through the use of a superconducting magnet their energy states separate with increasing field strength known as nuclear Zeeman splitting. The nuclear spins can have parallel or antiparallel orientations in relation to the induced magnetic field that will have different energy states. Commonly β spin state is related to the excited or high energy state while α refers to nuclear spins in a low or ground energy state. When an interfering wave, commonly at a radio frequency, is introduced the aligned nuclear spin acts like a gyroscope around its magnetically induced principle axis. In a molecule the nucleus is surrounded by electrons of that atom and adjacent chemical bonds and the magnetic field is influenced by the chemical environment. This results in a variant resonance frequency known as a chemical shift. The energy fluctuation or

gyroscopic movement due to the introduction of the radio wave are detected and mathematically manipulated using a Fourier transform which then can be interpreted as an NMR spectrum. [46]

A powerful tool for studying wood and lignocellulosic materials is solid state ^{13}C nuclear magnetic resonance (NMR). This technique works on the principle of probing the spin of carbon atoms. NMR spectroscopy is useful at detecting atoms with odd nuclear spin quantum (*I*) numbers such as ^{13}C where *I* is equal to ½. Another important factor involving the sensitivity of NMR spectroscopy is natural abundance where 1.1% of carbons are ^{13} C. [47] Solid state NMR has weak spectral resolution because of the interference of detectable atom spins due to localized and overlapping abundance of atoms which broadens spectra. A common way to improve spectral resolution is using magic angle spinning where rapidly spinning a sample at a specific angle, 54°, to the magnetic field reduces signal to noise ratio. Cross polarization also helps to reduce noise by transferring abundant spins from protons to the dilute ^{13}C spins.[48] Solid state ^{13}C NMR was used to measure specific chemical products of wood like char residues and chemical changes at different temperature treatments. [49] This technique is also useful for determining changes in overall wood structure during heat treatments.[50]

2.7.2 Heteronuclear Single Quantum Coherence Spectroscopy

Heteronuclear Single Quantum Coherence spectroscopy (HSQC) is a two dimensional approach using the principles of nuclear magnetic resonance that probes proton and usually ^{13}C or ^{15}N nuclei.[51] HSQC utilizes the phenomena similar to cross polarization where the transfer of magnetism from the proton to another nucleus occurs and the signal produced from the proton is mapped on a primary axis and the signal of the second nuclei is plotted on a second axis. This technique unlike solid state NMR is conducted in solution state. For woody cell wall material this is a difficult, but some solvent systems can dissolve cell wall components like LiCl

/dimethylsulfoxide and imidazolium-based ionic liquids. These woody cell walls must be balled milled in order to fully dissolve in solution. Deuterated solvents of sufficient purity are used to abate proton signals of the wood.[52] The advantage of solution state is the quantitation of spectra that can determine molecular size, aromatic content, lignin subunit type, component ratios, polysaccharide types, linkage types and much more. This technique is much more accurate at describing components that have already been separated, especially lignin which is hard to analyze using one dimensional NMR.[53]

2.7.3 Fourier Transform Infrared Spectroscopy and Attenuated Total Reflectance

Infrared spectroscopy utilizes infrared light to induce vibrational modes of molecules by changing their dipole moments. Bonds that change dipole moments due to light radiation at a certain frequency are called infrared active. The infrared spectrophotometers can then detect the minute energy changes from the absorbance of the light energy by the sample and convert it into spectra.[54] Infrared signals that are produced as a wave signal are mathematically transformed (Fourier Transform) into a one quadrant spectra. Infrared spectroscopy works on the principle that asymmetric, bending, and symmetric vibrations occur in molecules with a conceptual spring like moment that when excited by infrared light radiation are detected by the absorbance of that light. In the case of attenuated total reflectance FTIR, solid or liquid samples are placed on a crystal, i.e. a diamond, which directs the incident laser light into the sample and measures the light reflection from the sample. In the case of transmittance FTIR, a transparent or translucent film is made of the material or mixed with a film making material that is not infrared active and the difference in incident light is detected. [55]

Infrared spectroscopy is useful for probing functional groups on wood polymeric material, observing changes in structural linkages and bonds, indicating crystallinity changes,

and can also detect changes in hydrogen bonding .[56 57] This technique can also be coupled with thermal degradation systems like thermal gravimetric analysis for degradation pathways for lignocellulosic materials.[58]

2.7.4 X-ray Photoelectron Spectroscopy

The photoelectric effect, defined by Albert Einstein, is the concept behind X-ray photoelectron spectroscopy (XPS or ESCA). The technique uses an X-ray source to bombard a sample surface with photons of a certain wavelength and energy. Photons collide with the atoms at the surface where there is a statistical probability that an electron from the atoms core orbital will be displaced and that escaping electron, or photoelectron, can then be quantified through the detection of that electrons particular escape energy. The equation $h\nu = E_{bind} + E_{kin} + \Phi$ where h is Planck constant, ν is the frequency of light, E_{bind} is the binding energy, E_{kin} is the kinetic energy of photoelectron, and Φ is the additional energy transfer from Fermi level to vacuum level. For this spectroscopy to work the radiation source is known ($h\nu$), the additional energy (Φ) is also known and the photoelectron kinetic energy has to be detected (E_{kin}) which leaves the binding energy to be solved for and is unique to all elements. The technique also requires a particular angle of incident photon bombardment that corresponds to the depth of penetration into the sample. At a right angle to the sample surface the depth of penetration is the greatest while lowering the angle will result in shallower surface penetration. High vacuum is also necessary for this spectroscopy and has to be above 10^{-8} mbar.[59] Wide scanning can determine the total elemental composition of a surface while high resolution scanning can determine bond associations with an element through the deconvolution of the spectra at specific binding energies associated with that atom.[60]

For wood since it is an organic material the two most studied elements are carbon and oxygen. Carbon and oxygen ratios are important for understanding the oxidation and polar characteristics of that surface. The deconvoultion of the carbon spectra can provide information on four carbon linkages being C-C/C-H, C-O, C=O/O-C-O or O-C=O which represent different wood functional groups and structural features. Oxygen spectra deconvolution can give information on O-C bonds and O=C bonds.[61] [62] This technique is often used in combination with a number of other solid state spectral analyses because of the broad interpretation of the bonds.[63] XPS is also good for sample contamination detection and functional groups quantities that could contribute to the wetting of solids by liquids, mainly for adhesive research.[64]

2.8 Liquid Chromatography

Chromatography started in the mid 1800's with scientists like Runge and Schonbein who used paper to separate organic and inorganic materials through the capillary and adsorption action of filter paper. [65] It wasn't until scientists like L. Reed and Tswetts around the turn of the century started experimenting with packed columns of inorganic material, like $CaCO_3$, to separate materials. [66] From there in the 1930's partition chromatography was invented followed by ion-exchange (1950), gel-filtration chromatography (late 1950's), gel-permeation chromatography (1960's), and then in the mid 1960's high-performance liquid chromatography was developed. Column's use a plethora of different packing materials, particle packing sizes, pore sizes, solvent setups, column lengths, column widths, pH sensitivities, and temperature requirements.[67]

With the use of a computer and detection capabilities liquid chromatography has become a powerful tool for quantitatively determining molecular compositions of mixtures. The high performance (also was known as high pressure) liquid chromatography systems include pumps,

sample injection setups, columns, and detection devices. Pumps are used to move the solvents, known as a mobile phase, to the columns for separation. These pumps are programmed to run in several modes including isocratic, constant pressure or flow rate, or gradient pressure or flow rate in which two or more mobile phases are varied for molecule isolation based on their elution time though the column. An auto-sampler is commonly used for delivery of the sample into the mobile phase which is then carried to the column. The sample then enters the column, is separated and detected using a variety of methods.

2.8.1 Ultra Violet and Visible light Detection High Performance Liquid Chromatography

The CO_2 laser is a high power and high heat application where molecules from wood polymers are degraded and separated from the main polymeric structures. Therefore understanding the typical degradation pathways of the different wood components is needed to find the correct column and detection devices to use for HPLC analysis. Common wood degradation products are from two major sources. Holocellulose which is cellulose and hemicellulose composed of linked monosaccharide residues, and lignin that are composed mostly of phenolic molecules. Lignin degrades over a broad temperature range from 200 to 500°C because of the different functionalities off of the lignin matrix making the stability of these linkages different. The lignin polymer structure is affected at temperatures from 200°C and up where the β-O-4 linkages are cleaved and products form including small molecules.

The small molecules that separate from the lignin structure are of importance to this work because certain degradation products develop at certain temperatures and these monomeric structures could have sufficient reactivity for cross-linking. The literature had a few common degradation products from hardwood species including 4-hydroxybenzoic acid, syringic acid, vanillin, syringaldehyde, ferulic acid and coniferyaldehyde.

The model compounds, also called standards, are used for the elution or retention time measurements and calibrations. The standards retention times are then compared to unknown mixtures to determine the composition of the mixture. Each of the compounds after eluting from the column is detected using an ultraviolet and visible light detector. The UV detector emits light at a particular wavelength which is absorbed into the sample and the difference in incident to absorbed light is measured and plotted by software. The intensity of light measured depends on the concentration of these compounds so a calibration is established where different concentrations of mixtures of the standards are produced and tested at particular injection volume amounts. The resulting plots that correspond to the different concentrations of standards were graphed and an equation was derived for every molecule relating the intensity and retention time to the concentration of that molecule in the sample mixture. Determining the amount and type of thermally reactive degradation products from the laser treatment could infer a covalently bonded adhesion mechanism.

2.8.2 Ionic Chromatography

The delivery of sample and solvent to a column is much the same for ionic chromatography (IC) compared to the above UV/HPLC system however the solvents, columns, and detection methods vary. Ionic chromatography was utilized to find the concentrations of monosccharides in acid hydrolyzed wood and solid residue from laser ablation. It was also used to identify sugars from the water soluble compounds evolved from laser modification of wood. The column used to separate monosaccharides for this type of chromatography is composed of a polystyrene and divinylbenzene copolymer stationary phase. With just the use of water as a mobile phase all sugars were separated. The particle size was 7 microns and a high pH is most efficient for this type of column because sugars are weak acids and are partially ionized at high

pH. Traditional silica based columns cannot withstand neutral to high pH, hence the use of polystyrene and divinylbnezene. Once the sugars have been isolated they go through a post reaction with sodium hydroxide with a low concentration of 350 mM. This is called a post column reaction reagent and it effectively charges the molecule through oxidation or reduction of that molecule that can then be detected through the use of a pulse amperometric detector. This detector measures small electrical currents between a gold anode and cathode that when an analyte is passed through the current a change is observed and plotted. Monosaccharides are reduced by the sodium hydroxide post column reaction reagent and thus are detectable by this technique.

Chapter 3. Laser Optimization and Chemical Characterization of Extracted Laser Modified Wood

3.1 Methods and Materials

3.1.1 Wood and Laser Modification

Yellow-poplar (*Liriodendron tulipifera)* a hardwood and southern yellow pine (SYP, *Pinus spp.)* a softwood were utilized as solid wood, 3.175 mm rotary cut veneers, and 0.5 mm maximum knife milled wood elements. A Universal V460 60 Watt CO_2 pulsed laser, at 10.6 µm wavelength, was used to modify wood surfaces. The laser's calibrated focal length (5.08 cm), average power (wattage) and carriage speed were varied to increase spot size and influence surface degradation. AutoCAD vector programs were used to control laser carriage movement to accurately separate line ablation based on spot size for complete surface modification. Carriage vectors or laser line direction was parallel to the longitudinal direction of all solid and veneer wood samples. Surface temperatures were recorded by an infrared thermometer (Fisherbrand™ Traceable™ Infrared Dual Lasers Thermometer with Type-K Probe) 15 cm from the veneers during modification.

3.1.2 Compression Shear Block Analysis

A modified ASTM D-905 compression shear block analysis was conducted to determine shear strength of laser modified and hot pressed laminate composites. The laminate and block dimensions were set to 31.25 mm in length, 25.00 mm in width and 9.375 mm in thickness with an offset of 6.25 mm creating 625 mm^2 shear area. Laminates were planed to thickness and conditioned in an environmental chamber at 20°C at 65.8% humidity (12% moisture content (MC)) for two weeks. Three different laser treatments were used to modify laminate surfaces and reconditioned to 12% MC prior to bonding. The samples were matched according to grain

orientation (i.e. tangential surface to tangential surface) . Hot pressing conditions consisted of a Micromets Instrument MP2000 Minipress under a constant pressure of 2.0 MPa at 180°C for 10 min achieving a bond-line temperature above 170°C. Bonded samples were conditioned at 12% MC and machined to final dimensions and reconditioned to 12% MC until tested.

3.1.3 Light, Reflection and Scanning Electron Microscopy

Two specimens of SYP and yellow-poplar solid wood were cut into approximately 1 cm cubes with a razor blade and soaked in water for 24 h under vacuum. The samples were microtomed to produce two parallel surfaces one with tangential grain orientation and the other sample with radial grain orientation. Samples were conditioned to 12% MC and laser modified on the microtomed surfaces. The cubes were soaked in 95% ethanol for 24 h, which limited modified wood and solvent interactions yet provided enough softening for microtoming. The cubes were microtomed through the cross-sectional surface until uniform 30-40 µm thick specimens were obtained. These specimens were placed on a glass microscope slide with a drop of glycerol for bubble minimization. A Nikon Eclipse LV100 light microscope with digital camera and optics at 400X and accompanying Nikon measurement software was used to quantify laser penetration into wood cells. A Nikon SMZ1500 reflective microscope was used to capture images of laser induced geometries of yellow-poplar shear block specimens.

Two 12% MC 51x51x3.175 mm (length x width x thickness) yellow-poplar veneers were laser modified and pressed with matching longitudinal surface orientation under 2.0 MPa at 180°C for 5 min. The sample was cut into a 6.5 mm cube and microtomed through the cross-sectional area containing the bond-line. The sample was dried at 103°C for 24 h and adhered with double sided copper tape to a stage. The sample was sputter coated with approximately 10

nm of Gold/Palladium (60/40) and analyzed in a NeoScope JCM-5000 JEOL scanning electron microscope operating at 15 kV under high vacuum.

3.1.4 Ionic Chromatography

Pulse amperometric detection ionic chromatography (IC) was used for sugar analysis of the laser modified yellow-poplar compared to the remaining bulk wood. Brush extraction with water loosened the thin layer of modified wood from veneers and was collected before and after hot pressing. Figure 3.1 contains the flow chart of the surface extraction procedure. The solid material was isolated with a centrifuge for 30 min at 5000 RPM then decanted. The residue was freeze dried at -40°C and 40 mTorr for one week. The supernatant was analyzed with IC for laser hydrolyzed and dehydrated monosaccharaides.

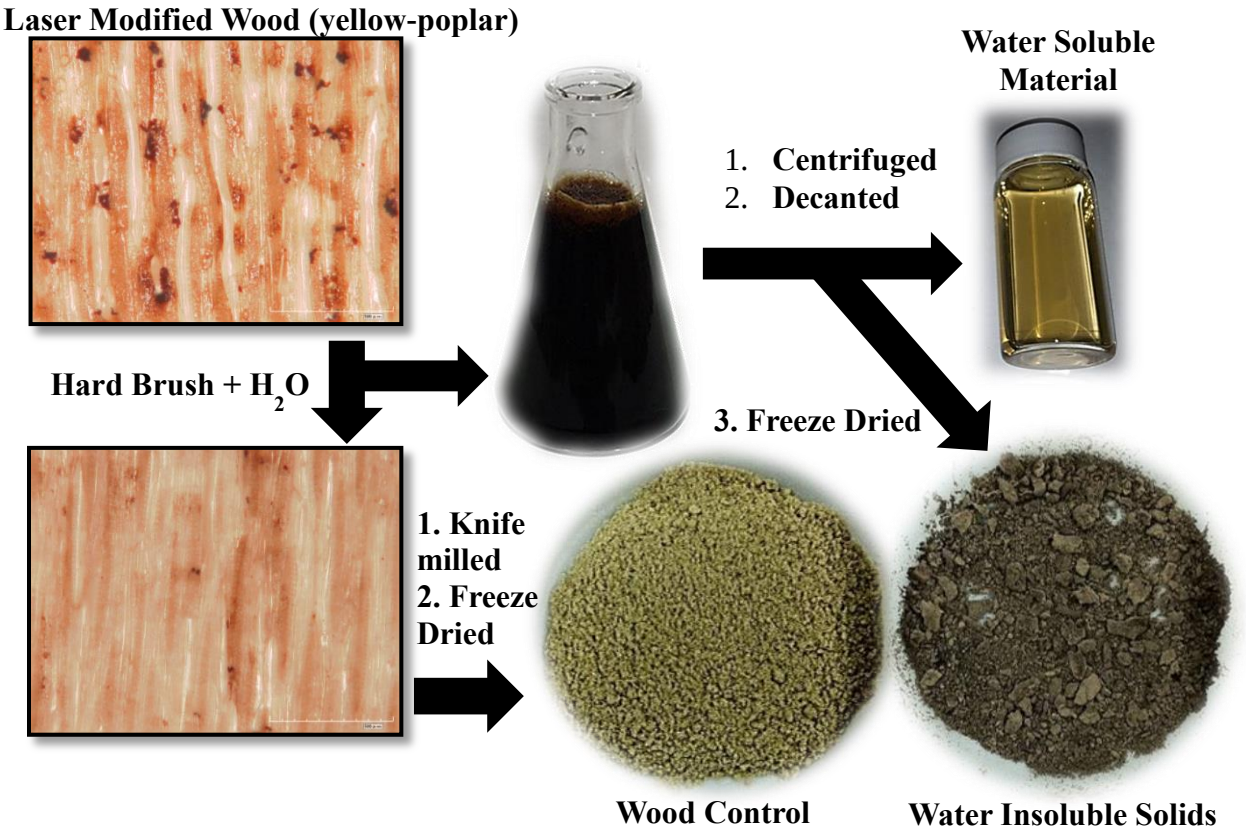

Figure 3.1 Flow chart of extracting laser modified material for chemical characterization from yellow-poplar wood

The dried precipitant and oven dried bulk yellow-poplar veneer were knifed milled to obtain a 0.5 mm maximum particle size and then subsequently acid hydrolyzed as adapted from "Determination of Structural Carbohydrates and Lignin in Biomass."[68i] Modification to this procedure consisted of analyzing non-neutralized filtered carbohydrate supernatant due to the broad pH tolerance of the IC column. IC parameters consisted of a Metrohm auto-sampler and pump system with ultrafiltration, Hamilton RCX-30 250-mm column, deionized water eluent, 1mL/min flow rate, post column reaction (PCR) reagent was 350 mM NaOH, 32°C column temperature, 1h determination time, 200 µL injection volume, and Dosino partial loop dilution of samples and standards for calibration. Aqueous sugar standards for calibration included D-

arabinose (Sigma-Aldrich), D-galactose (Sigma-Aldrich), and D-mannose (Sigma-Aldrich) at 100 ppm and D-glucose (Sigma-Aldrich) and D-xylose (Sigma-Aldrich) at 1000 ppm with six separate dilutions of 40x, 20x, 10x, and 4x. Hydrolyzed samples were diluted 40x and laser modified supernatant was not diluted. Water soluble compounds in supernatant were determined through an additional series of sugar standards including D-sorbitol (Sigma-Aldrich), D-xylitol (Sigma-Aldrich), and levoglucosan (Sigma-Aldrich). The standards and supernatant were compared with retention times for molecule determination.

3.1.5 High Performance Liquid Chromatography

A C-18 column for reverse phase chromatography was used to separate molecules due to the correct pore size and packing material. The C-18 column had a stationary phase of octadecyl functionalized silica with a particle size of 5 microns and pore size of 10 nanometers. This hydrophobic stationary phase column works best in low pH range because the residual silanols are neutral and cation exchange is reduced. For this particular case a buffered system was utilized; the buffer keeps the pH stable during sample injection and within the column. The buffer utilized was phosphoric acid and potassium phosphate aqueous solution where phosphoric acid was used to adjust the pH just above 2. Molarity also effects elution time and was adjust experimentally from 0.01 to 0.025 M where the highest molarity provided the best spectral resolution. Trial and error led to a gradient mobile phase setup with the buffer and methanol. Where the buffered water phase was used to prolong elution time or increase the interaction of the stationary phase and the molecules. Methanol was slowly increased in overall flow rate from 0 to 70% of the mobile phase composition and was used to increase the hydrophobic environment of the eluent so that the molecules would have fewer interactions and elute.

The water soluble phenolic compounds were tested with high performance liquid chromatography for identification using retention times. The high performance liquid chromatography (HPLC) system included Shimadtzu LC-10ADVP pumps, SIL-10ADVP auto injector, SPD-10AVVP UV/Vis detector, SCL-10A VP system controller, CTO-10AS VP column oven and LC solutions software. A Nucleosil 100-5C18 (25 cm by 4.6 mm) was used at 70°C with a total flow rate of 0.7 mL/min. The gradient eluent consisted of 0.025M KH_2PO_4 buffer with a pH of 2.24 (A) and Methanol (B) where the concentration of B increased from 0-50% over 20 min and then increased from 50-70% over the next 10 min. Acquisition time was 30 min, 15µL injection volume, and UV/vis detector calibrated to 280 nm. Standards composed of 4 mg/mL in methanol were used including gallic acid (Sigma), trans-ferulic acid (Aldrich), syringaldehyde (Aldrich), syringic acid (Sigma), 4-hydroxybenzoic acid (Aldrich), 4-hydroxy-3-methoxycinnamaldehyde (coniferaldehyde) (Aldrich), caffeic acid (Sigma), vanillin (Sigma-Aldrich), 5-(hydroxymethyl) furfural (HMF) (SAFC), and furfural (Sigma-Aldrich). Decanted laser modified material was filtered to 0.2µm and tested.

3.1.6 CPMAS ^{13}C solid state Nuclear Magnetic Resonance

Water extracted laser modified material and knife milled yellow-poplar particles were used for spectroscopic evaluation. Solid state cross polarization magic angle spinning (CPMAS) ^{13}C NMR analyses were performed on a Bruker Avance 300 MHz spectrometer operating at 75.47 MHz, with an acquisition time of 15 ms, a relaxation delay of 1.7 s, and 1,024 scans. Post-acquisition corrections were made with MestReNova software including a segmental baseline correction, Savizky-Golay normal smoothing, and spectra normalization using the highest peak.

3.1.7 Wide Angle X-Ray Diffraction

Samples were prepared from water extracted laser modified material and knifed milled yellow-poplar. X-Ray (XRD) was performed using a Bruker D8 Discover XRD system, Cu Kα (λ = 0.154 nm) radiation operating at 40 kV/40 mA. Diffraction profile was detected using a locked couple 2θ scan from 10 to 50°. Using Origin Pro 8, XRD data was baseline subtracted and noise reduction was conducted using spectral data averaging. Peak fit was used to deconvolute peaks for crystallinity index and fit to $r^2 > .99$.

3.1.7 2D ^{13}C-^{1}H HSQC NMR spectroscopy

Laser modified yellow-poplar and control samples were extracted to remove extractives and ball milled as previously described [69]. The samples were sealed and sonicated until homogenous in a Branson 2510 table-top cleaner (Branson Ultrasonic Corporation, Danbury, CT). The temperature of the bath was closely monitored and maintained below 55 °C. The homogeneous solutions were transferred to NMR tubes. HSQC spectra were acquired at 25 °C using a Bruker Avance-600 MHz instrument equipped with a 5 mm inverse-gradient $^{1}H/^{13}C$ cryoprobe using a q_hsqcetgp pulse program (ns = 200, ds = 16, number of increments = 256, d_1 = 1.0 s) [70]. Chemical shifts were referenced to the central DMSO peak (δ_C/δ_H 39.5/2.5 ppm). Assignment of the HSQC spectra was described elsewhere [69a, 71]. A semi-quantitative analysis of the volume integrals of the HSQC correlation peaks was performed using Bruker's Topspin 3.1 (Windows) processing software. A cosine squared function was applied to both F_2 (LB = -0.05, GB = 0.001) and F_1 (LB = -0.01, GB = 0.001) prior to 2D Fourier Transformation. Semi-quantitative evaluation of interunit linkages in lignins has been typically expressed as number of specific interunit linkages per 100 aromatic (lignin) monomers or C_9 units. Yellow poplar contains both guaiacyl (G) and syringyl (S) type lignin units. To perform quantitative evaluation of interunit linkages of lignin from yellow poplar sample, it is necessary to use an internal standard that

represents aromatic C_9 units in the lignin. The C_2-H_2 position of the guaiacyl unit and the $C_{2,6}$-$H_{2,6}$ positions in the syringyl unit are considered to be stable [72]. The integral of the correlation peak due to these resonances in syringyl units corresponds to twice the amount of syringyl C_9 units present. The overall amount of C_9 units present in yellow poplar can then be quantified by the sum of half the syringyl signal plus the guaiacyl signal. In the aliphatic oxygenated region, the relative abundances of sidechains involved in the various interunit linkages were estimated from the C_α–H_α correlations to avoid possible interference from homonuclear ^1H–^1H couplings. This is except for cinnamyl alcohol end-groups, for which Cγ–Hγ correlation was used. In the aromatic/unsaturated region, $C_{2,6}$–$H_{2,6}$ correlations from G and S lignin units were used to estimate their relative abundances. Lignin aromatic units were expressed in molar percentages (H + S + G = 100) [73].

3.2 Results and Discussion

Wood surfaces were exposed to laser treatments of varying severities. The severities of laser treatments were based on laser power, spot size, and line separation. These parameters were quantified as laser line intensity, which is the numerical value relating diameter of the spot size (d_{spot}), average power (P_a), laser head speed (v_{scan}), pulse duration (τ_D), and repetition rate (ν) to provide the infrared energy density at the surface, equation 3.1&3.2

$$I_{spot} = \frac{4P_a}{\nu^2 \tau_D {d_{spot}}^2 \pi} \quad (eq.3.1) \qquad Line\ Intensity = \frac{I_{spot}}{V_{scan}\, d_{spot}} \quad (eq.3.2)$$

Where the laser pulse duration was 120 microseconds and the repetition rate was 5 KHz. The laser system parameters shown in Table 3.1 correspond to the imposed micoscale surface

roughness of the samples. The degree of laser modification of the wood was controlled impacting the resulting surface geometry.

All laser line vectors moved parallel to the longitudinal direction of the wood and corresponding geometries are shown in the cross sectional view (Figure 3.2). Treatment 1 resulted in ablated channels that are approximately 330 microns in width and 50 microns in depth. The depth of the channel is about the same size as the diameter of a yellow-poplar vessel. Treatment 2 created deep ablated channels that are on the order of 500 microns in width and depth that mimic wood bonding techniques like finger jointing, aptly named 'micro-finger joints' in this work. Treatment 3 ablates 300 microns of surface material away leaving shallow channels of 60 microns spanning a width of 870 microns and an additional 430 microns of minimally ablated material on the periphery of the Gaussian shaped laser beam imprint. This treatment, overall, created the most even surface in which degradation products remained on the surface until further hot pressing.

Table 3.1 Laser treatment parameters that influence surface properties for bonding

Treatment	Spot size (mm)	Laser Power (Watts)	Laser Head Speed (m/s)	Line Intensity (W/mm^2)
1	0.35	30	0.25	1164.2
2	0.69	60	0.10	763.0
3	1.75	60	0.17	28.3

Compression shear block testing of southern yellow pine (SYP) and yellow-poplar species showed an adhesive layer performance dependence on laser treatment (Figure 3.3). Based on lowest to highest performance, laser Treatment-2 showed the worst performance, while laser Treatment-3 had the highest values. For the lowest performing samples, bond-lines with micro-finger joint geometries resulted in the lowest ultimate shear strength amongst the laser

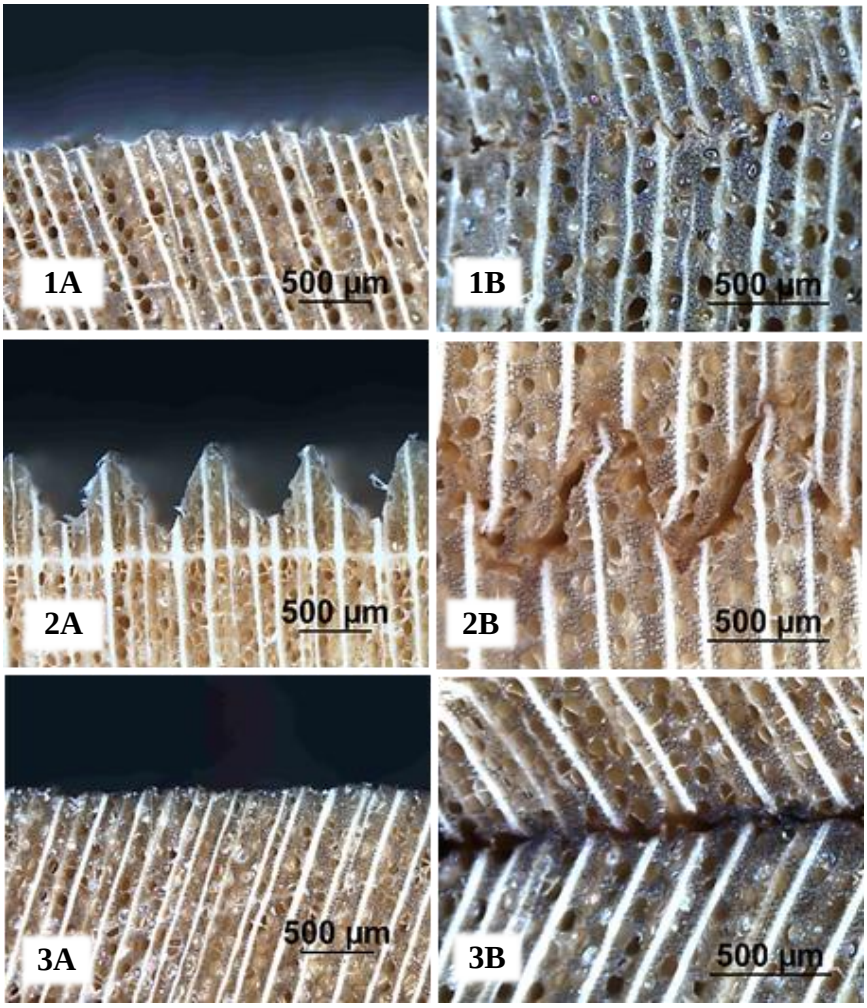

Figure 3.2 Cross sectional images of Yellow-poplar wood by reflective microscope of laser induced surface geometries (A1-3) and subsequent bond-lines (B1-3) corresponding to Table 3.1

treatments. These specimens delaminated without additional wood failure and this was consistent for both wood species. Wood failure indicates that the adhesive layer is stronger than the surrounding wood. Delamination of 75% of the yellow-poplar samples and 29% of SYP samples with Treatment-2 occurred during reconditioning after hot pressing. Swelling stress induced by moisture and hydrolytic instability of the bond-line are possible causes for laminate separation. For these samples microscopy revealed discontinuous and void-filled interfaces suggesting a decrease in frictional interactions between the surfaces. Samples with disjointed surfaces would explain the low test values as frictional coefficients are often used to estimate the mean shear

stress in the adhesive layer.[74]Treatment 1 resulted in bond-lines that had intermediate ultimate strengths without additional wood failure. Compared to the other two laser treatments, Treatment-3 resulted in the highest test values for both species. SYP samples had wood failure surrounding the bond-line averaging 33% of the total bonding area with some specimens reaching 85%. With failure near the proportional limit, the stress and displacement curves indicated brittle bond-lines for all laser treatments. However, SYP with treatment 3 showed the greatest strength and strain at break values. For a comparison to solid wood in compression shear parallel to grain, SYP species have a range in values

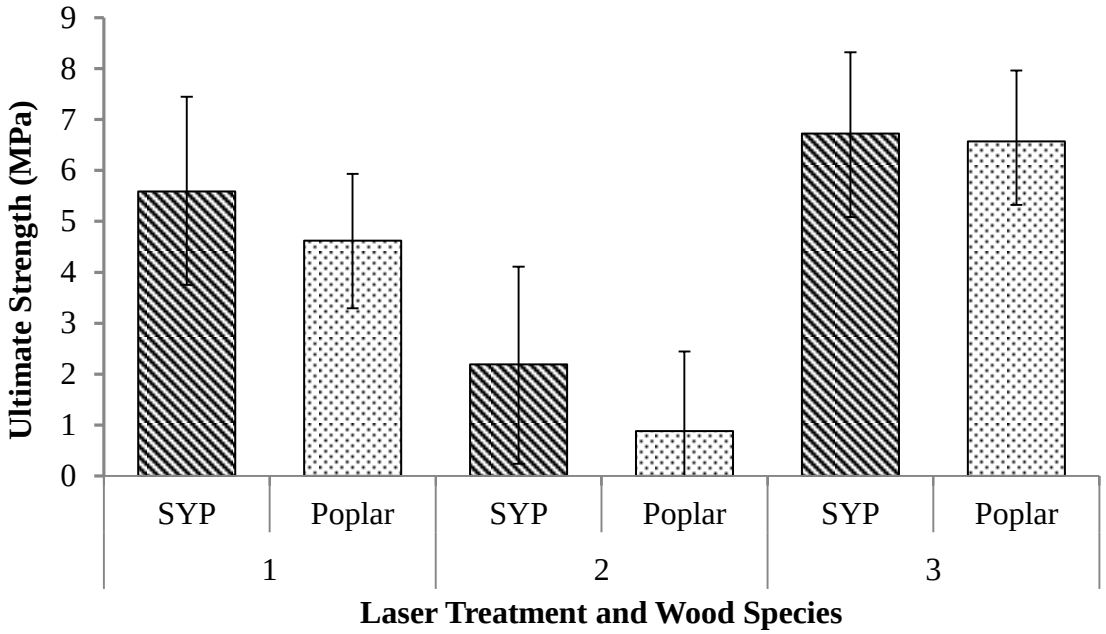

Figure 3.3 Compression shear block results of bond-line strength of yellow-poplar (Poplar) and Southern Yellow Pine (SYP) specimens using various laser ablation techniques that correspond to Table 3.1

of 4.7-11 MPa, while yellow-poplar ultimate shear strength is around 8.2 MPa. [75] Depending on the SYP species (unknown when in veneer form) the laser bonded wood can be equivalent in shear strength while yellow-poplar in some instances is higher for individual samples, but the average is slightly lower. The laser conditions for treatment 3 were used adopted for further analysis and all subsequent discussions on laser modification refer to this treatment. Quantitative

microscopy was employed to determine the effects of laser light on different anatomical features unique to these wood species. Cross-sectional segments (30-45 µm in thickness) were taken from tangentially modified surfaces and examined through transmission light microscopy, Figure 3.4. Transition from translucent wood to dark discolorations concentrated at the top 25 microns of the surface provided evidence of laser penetration and wood modification. Ablation and wood penetration is dependent upon wood cellular structure. Earlywood (referring to rapidly growing cells in a seasonal growth ring) longitudinal tracheids, the major structural cells in SYP, contained an average of 19.7 µm of light penetration. However, the denser latewood longitudinal tracheids showed an average 8.07 µm of laser penetration. The abrupt transition from earlywood to latewood in SYP resulted in uneven laser ablation because of extreme density differences. It should be noted with the compression shear block tests, increased wood failure in shear testing correlated to SYP earlywood to earlywood interactions that could be a result of laser penetration with a larger residue of laser treated wood at the surface. Yellow-poplar species structural cells (libriform fiber and fiber tracheids) resulted in an average laser penetration of 11.0 microns. Yellow-poplar is a diffuse hardwood in which cells are uniform across a growth ring, thus modification of this wood is consistent compared to SYP. Lower standard deviations for yellow-poplar over SYP in the adhesive layer shear strength tests could be a consequence of bond-line regularity. The adhesive layer for yellow-poplar (Figure 3.5) resulted in a bond-line that was approximately 20 µm in width, or the combined laser penetration depth for two yellow-poplar surfaces. Sapwood yellow-poplar, a low extractive content hardwood, was utilized for chemical characterization to eliminate the effects of resinous liquids on wood to wood adhesion between softwood SYP species. Yellow-poplar also has the benefit of uniform laser modification, making it preferential for chemically characterization of the adhesive mechanisms.

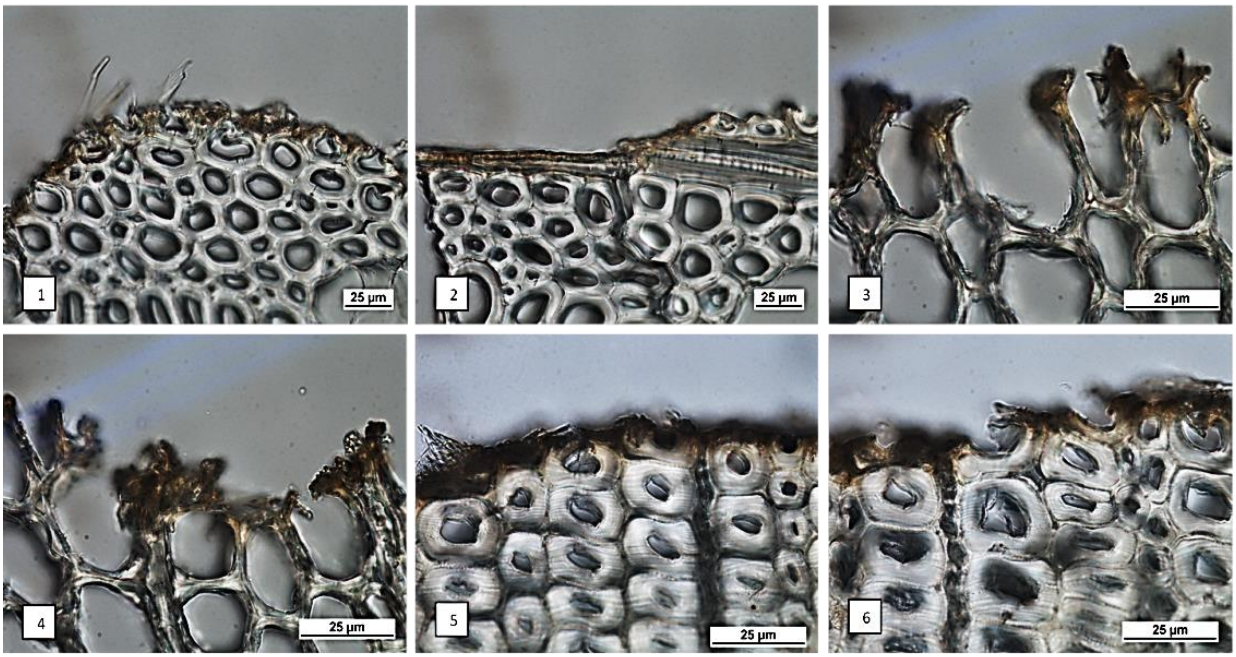

Figure 3.4 images 1-6 transverse sections of woody cell wall penetration due to surface ablation. Chemical modification of woody tissue from lasing results in dark discoloration at the surface. -- 1: Yellow-poplar libriform fiber and fiber tracheid -- 2: Yellow-poplar radial parenchyma -- 3 & 4: Southern Yellow Pine earlywood longitudinal tracheid -- 5 & 6: Southern Yellow Pine latewood longitudinal tracheid

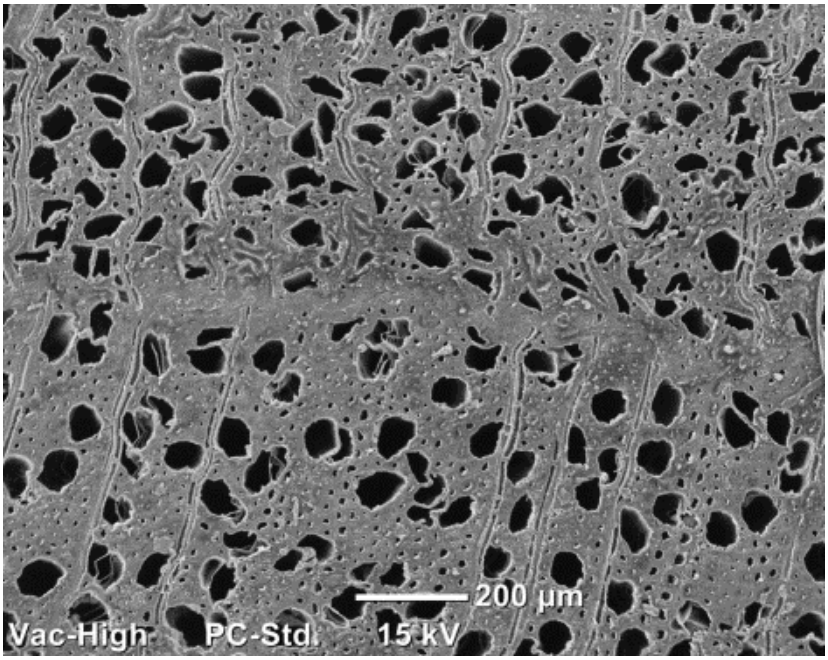

Figure 3.5 Cross-sectional SEM image of laser modified Yellow-poplar interfacial bond-line

For compositional analysis, the isolated solids portion of the laser modified material was hydrolyzed with sulfuric acid to determine the relative amounts of structural polymers in the laser degraded adhesive layer compared to unmodified yellow-poplar. Chromatography of the hydrolysate revealed that the lased surface layer had increased D-glucan from cellulose and a very small percentage of xylan, mannan, aribinan, and galactan remained from hemicellulose relative to the control (Table 3.2). Glucuronoxylan is a major hardwood hemicellulose comprised of a β-D-xylose backbone. This polysaccharide was significantly affected by laser modification as seen by the decrease in D-xylose concentration. Acid insoluble lignin increased due to laser modification while the acid soluble portions are not detected but commonly represent less than 3% of total hydrolyzed hardwood in comparable conditions.[76] Hemicelluloses are less thermally stable compared to other wood components [77] and are susceptible to degradation and potentially volatilization during laser modification dependent upon the degree of degradation.

Ionic chromatography of the water soluble portion of the extracted laser modified wood revealed degraded, dehydrated, and hydrogenated products not found in native or the control wood specimens. The detected compounds include D-glucose, D-xylose, arabinose, sorbitol, xylitol, and levoglucosan. These compounds are the result of laser modification leading to the breakdown of major structural wood polymers, for this technique most detectable compounds

Table 3.2 Extracted Laser Modified and Control Yellow Poplar Carbohydrate and Acid Insoluble Lignin breakdown in wt%

Sample	Glucose (%)	Xylose (%)	Arabinose (%)	Galactose (%)	Mannose (%)	Acid Insoluble Lignin (%)	Ash (%)
Control	49.18	13.47	0.36	0.81	0.85	21.09	0.30
Laser Modified	63.23	3.83	0.23	0.20	0.36	27.93	0.70
Change	14.05	-9.64	-0.14	-0.61	-0.49	6.84	0.40

*oligomeric material, cellobiose, acid soluble lignin, and extractives not included

were a result of holocellulose degradation. The most abundant monosaccharide was D-xylose indicating that the laser modification does not vaporize all hemicellulose material. In lesser extent, levoglucosan and arabinose were also present indicating a thermal degradation product and another hemicellulose monosaccharide. Residual monosaccharaides are known to create sticky surfaces, an issue encountered by cotton processing, and may provide initial tack for adhesion.[78]

Furfural and hydroxymethylfurfural are dehydration products of xylose and glucose that were analyzed with UV/Vis detection and reverse phase chromatography. Through HPLC analysis both lignin and polysaccharide degradation products were determined. Degradation of propanoid side chains in lignin occurs around 230 to 260°C which coincides with the measured surface temperature during laser modification found with an infrared (IR) thermometer (average of 233°C, Table 5.1). These temperatures typically evolve compounds such as vanillin. The C-C and β-β linkages in lignin cleave around 275 to350°C producing syringyl molecules from radical recombination.[79] This could be likely as the IR thermometer may not accurately reflect instantaneous surface temperatures. Aldehyde containing compounds were more prevalent than acids suggesting limited oxidation to the lignin monomers. Most likely dehydration is occurring due to amount of unsaturated monomeric lignin units, mainly syringaldehyde. This result suggests a degradation pathway similar to an intermediate pyrolysis technique.

Heteronuclear single quantum coherence spectroscopy, probing ^{1}H and ^{13}C nuclei was used to compare wood structure from a control to laser modified wood solubilized in ionic liquid (appendix D). The method is an important tool in comparing lignin structure as well as identifying significant changes to the polysaccharide components of modified wood. Syringyl units (S-units) are part this substructure composed of phenylpropanoids with methoxyl groups at

the C-3 and C-5 positions. A guaiacyl unit (G-units), another major lignin substructure, only has a methoxyl group on the C-3 position. According to spectral analysis using the per 100 aromatic molecules S-units decreased, aldehyde containing S-units increases and G units increase. The calculated S/G ratio for the control was 5.86 and there was a decrease in the laser modified material to 4.48. This is consistent with reverse phase chromatography where an abundance of syringaldehyde in the water soluble portions of the extracted laser modified material was detected. Syringyl units are said to have less linkages to the lignin network and could be separated due to modification. [79] Furthermore if G-units remain this could explain the decrease in S/G ratio which is agreement with other literature but is not due to demethoxylation which occurs at temperatures over 400C. [79-80] Cleavage of the β-O-4 linkages suggests a depolymerization of lignin where71.5% of aromatic compounds had this linkage compared to 47.9% in the modified material. Because of the lower bond dissociation energy of C-O bonds the β-O-4 linkages in lignin are thermally labile, especially at these laser induced surface temperatures. Vinyl groups also increased from control to laser modified wood, which is often associated with the breakage of the β-O-4 linkages. As for carbohydrates detected with this technique the acetyl groups associated with xylan have decreased in the modified wood consistent with structural analysis.

All of these changes are consistent with ^{13}C CPMAS solids state NMR results (Figure 3.6) which are non-quantitative compared to the semi-quantitative HSQC. The solid state NMR spectroscopy showed side peak depletion around 65 ppm related to C-6 ordered carbohydrates, mainly cellulose. This change is seen in the conversion of cellulose I as the C-6 it is related to the orientation of the conformational isomers. Also the reduced peak at 72 ppm relating to C2/C3/C5 in cellulose indicates a change in morphology and hydrogen bonding. [81] Neither heat

treatment of wood or UV light degradation causes a similar truncation of peaks at 72 ppm and 65 ppm and seems to be specific to laser modification.[50] The C-4 peak for carbohydrates is significantly affected by laser energy.

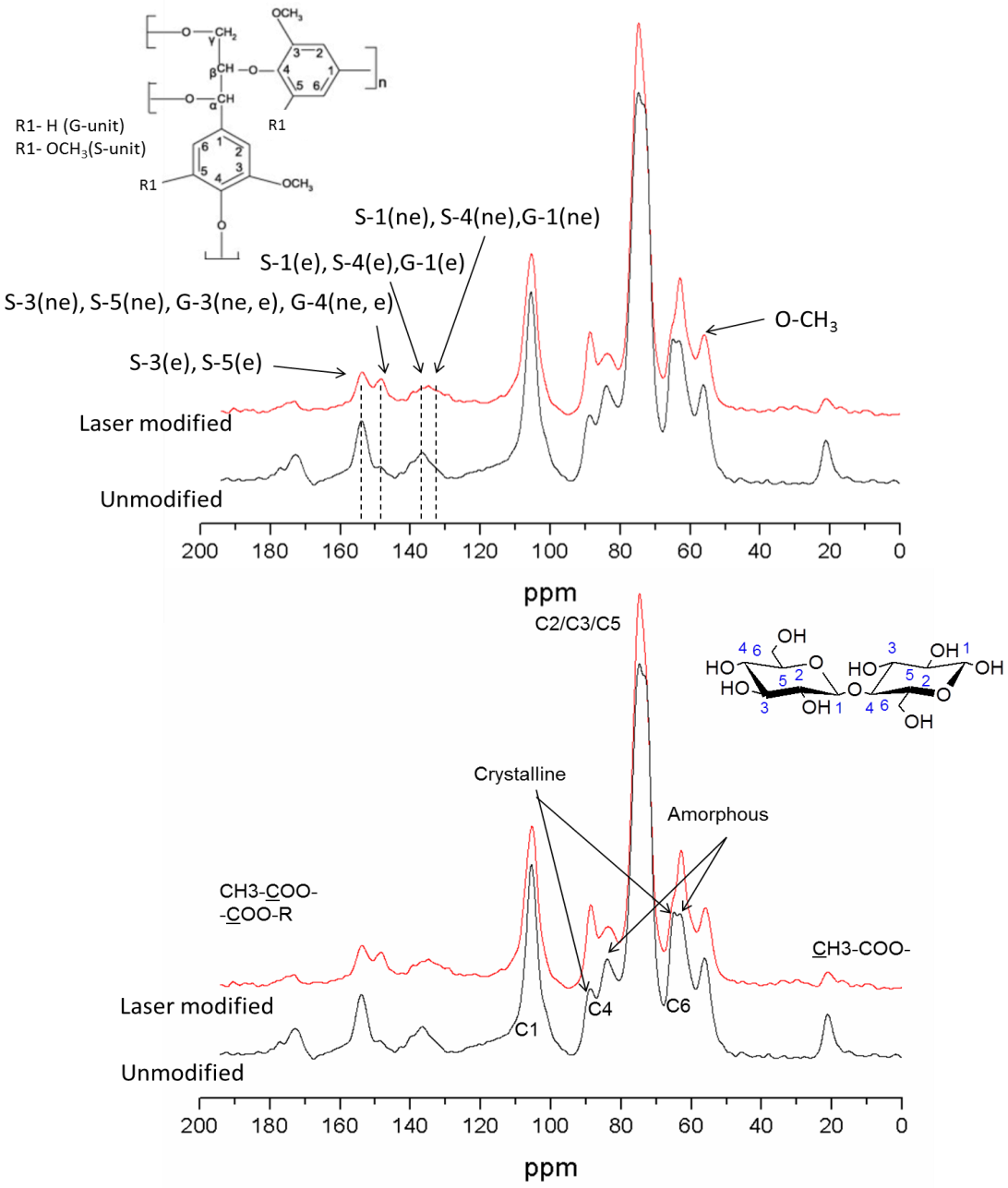

Figure 3.6 ^{13}C CPMAS solid state NMR extracted laser modified Yellow Poplar (Laser modified) vs. reference (Unmodified)

This response is due to amorphous hemicellulose and cellulose cleavage resulting in the increased peak at 89 ppm related to ordered carbohydrates. Moreover, the C1 peak at 105 ppm for carbohydrates is decreased due to laser modification. Hemicellulose carboxylic acid from glucuronic acid and acetyl groups in acetylated xylose are depleted at 172 ppm and 21 ppm respectively, this reinforces hemicellulose loss but also indicates no additional oxidation to the laser material. Along similar lines, the 2-D HSQC data revealed only marginal increase in oxidized lignin compared to the control sample.

The lustrous and glassy appearance of laser modified wood can be a result of morphological changes in native cellulose. The wood cellulose has a crystallinity index of 84% for both laser modified and control wood. Native cellulose Iβ peaks in wood were detected that had four crystalline reflections corresponding to the alignment of cellulose molecules in a lattice including 2θ peaks of 14.5°, 16°, 20.5°, 22° and 34.5°. Cellulose II was found in laser modified wood as indicated by 2θ peaks at 12°,15.25°, 20°, 22°,and 34.5°, Figure 3.7. Baseline subtraction and normalization of the spectra along with Voigt area function deconvolution and amorphous halo addition allowed for the integration of all the peaks. Total crystallinity was found though equation 3. 3. [82]

$$crystallinty\ \% = \frac{area\ under\ peaks}{area\ under\ peaks + amorphous\ halo} \times 100 \qquad (eq. 3.3)$$

There is a combination of cellulose I and cellulose II crystal arrangements in laser modified wood depending on the exposure of wood to laser energy. Moreover, the spectral changes from the control to laser modified wood resembles that of a mercerization treatment of cellulose where NaOH swells the lattice geometry and upon removal crystal structure is irreversibly changed.[83] Mercerization is used to create lustrous and strength enhanced cellulose fibers. The proposed structure of cellulose II infers a change in cellulose hydrogen bonding.

Cellulose II exterior cellulose chains have inter-plane hydrogen bonds involving hydroxyl groups from O2H to O2 and intra-plane from O6H to O2. However, cellulose Iβ hydrogen bonds occur intra-molecular from O2H to O6 and intraplane from O6H to O3.[36, 84] This conformational change can increase inter-molecular electrostatic and van der Waals interactions[36, 84] making it more favorable for adhesion.

3.3 Discussion of Adhesion Mechanism

For adherends to bond together the surfaces must come into intimate contact with an adhesive. For hot melt adhesives this process occurs as the liquid like adhesive flows into contact and subsequently cools solidifying in place. Hemicelluloses and lignin are amorphous polymers that show thermal softening in the presence of moisture around the hot-press temperatures.[85] Softening of the surface with a reduced compliance would lead to increased interactions between modified surfaces and promote adhesion especially due to the enriched lignin content at the surface. Yet, the adhesion mechanism is not entirely a thermoplastic phenomenon because pre-thermal treatment of the laser modified surfaces deactivates the adhesive layer and is incapable of bonding where a thermoplastic material should have the ability to reflow and adhere. Additionally, bonded substrates reheated to temperatures above hot pressing temperatures do not cause delamination.

Besides secondary interactions, thermal polymerization of molecules like levoglucosan is possible [86] and could lead to reactions with structural wood components for a thermosetting adhesion mechanism. Difunctional molecules like HMF and its derivatives can also crosslink with the addition of heat. However, since there was little change in lignin and sugar degradation products before and after hot pressing, significant thermal polymerization is unlikely (Figure 5.1). The key to this data is the slight modification of the lignin, such as the enhanced number

cinnamyl alcohol end-groups and the reduction of the βO4 bonds in lignin. The vinyl end-groups offer the route towards free radical polymerization, directly linking these groups together (beta-beta bonds). A reduction in βO4 provides enhanced mobility of the lignin with multiple degradation products that can repolymerize through free radical mechanisms. Native lignin is sensitive to temperatures in the range of 140C to 200C, with the lower temperatures associated with aryl-ether bond breakage and the upper temperatures associated with oxidative radical coupling. Radical coupling would provide a route for adhesion and explain the limited adhesion after heat treatment, as this method is known to stabilize extruded lignin fibers prior to carbonization.

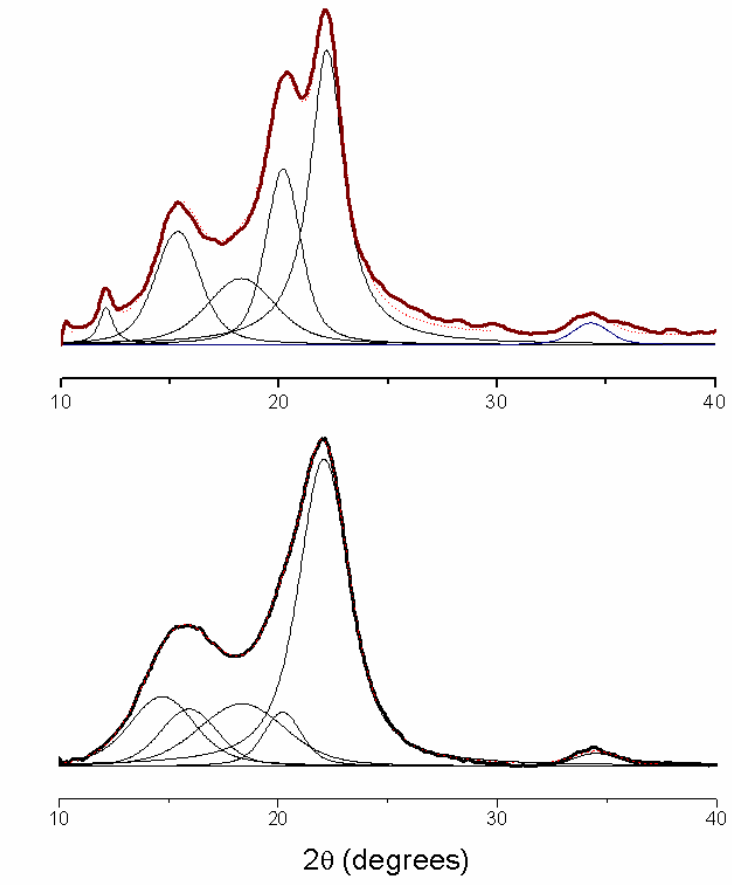

Figure 3.7 X-ray diffraction from 10-40° of Yellow-poplar knife milled (top) and surface extracted laser modified Yellow-poplar (bottom)

Isolated lignin has not been commercially developed to serve as an adhesive and this would suggest a limited mechanism of the lignin itself. However, the laser modified surface is only partially lignin with nearly 2/3rds of the sample cellulose. This structural polysaccharide must still provide mechanical performance and can participate in adhesion. Cellulose hydrogen bonding and non-specific intermolecular interactions such as van der Waals forces may govern adhesion through atomic proximity enabled by reduced surface roughness and thermal conformability of laser modified surfaces. The combination of the mixture of cellulose and lignin with oxidative radical coupling during hot pressing is not too unlike the adhesion framework found within the native cell wall, albeit without the same degree of structural order.

3.4 Chapter Summary and Conclusions

Laser modification causes the following changes to wood surfaces:

- Cellulose morphology changes from cellulose Iβ to cellulose II
- Glucan and liginin structures dominate the modified wood surface
- Glucan and xylan polysaccharides are cleaved and degraded creating furfural derivatives, levoglucosan, sugar alcohols, and various monosaccharides
- Substantial Deacetylation and decarboxylation of all lignocellulosic polymers occurs
- Cleavage of S-unit and β-O-4 linkages
- Enhanced cinnamyl alcohol end-groups.

It is also important to note that no significant changes were detected in degradation products relating to a cross-linking adhesive mechanism (levoglucosan and furfural derivatives) before and after hot pressing.

The chemical rearrangement and degradation of wood components by laser modification creates an adhesive layer activated by hot-pressing. Surface geometry (lock and key) does not play an important role in adhesion and a specific laser energy density is necessary for effective bonding. Laser modified and bonded wood has significant shear strength upwards of 8.5 MPa and wood failure up to 85% meaning the adhesive layer can be stronger than the surrounding wood. Laser modification cleaves and dehydrates cellulose, hemicelluloses and lignin however the monomeric and monosaccharides still remains on the surface during hot pressing. These low molecular weight compounds are highly functionalized and may cross-link the surfaces especially levoglucosan and HMF but are more likely to help plasticize the modified material along with moisture. Surface temperatures during laser modification are predicted between 230-350°C based on IR thermometer readings and the formation of degradation products. Hydrogen bonding is the likely cause for adhesion due to the change in morphology and abundance of cellulose at the surface combined with some degree of oxidative radical coupling.

CHAPTER 4. Surface Chemistry and Microscopy of Laser Modified Wood

4.1 Materials and Methods

4.1.1 Sample Preparation and Method Development for Contact Angle

Yellow-poplar, *Liriodendron tulipifera,* wood was utilized from a freshly cut tree. Flat cut boards containing sapwood and heartwood were collected and machined green into 5 cm x 1.25 cm x 1.25 cm samples. Specimens containing only tangential surfaces were kept and microtomed green with a Leica SM 2500 until flat surfaces were obtained. All samples were vacuum dried at 40°C and -100 kPa for 72 hours then immediately laser modified following laser treatment number 3 in previous work (Table 3.1). The samples were stored in a desiccator using a three cycle vacuum and nitrogen exchange with P_2O_5 to keep samples dry and in an inert environment. For contact angle analysis, the Sessile drop method was used with diiodomethane (Sigma Aldrich), formamide (Sigma Aldrich), and deionized water. Over thirty replications on sapwood and heartwood, control and laser modified, surfaces were performed using a mechanically driven syringe. The initial contact angle formed within .11 seconds (standard deviation of .023 seconds) between the solid and liquid interface was measured with a Sanyo camera from First Ten Angstroms Inc. with FTA 32 video and Drop Shape Analysis version 2 software.

Acid-base and dispersion properties of the surface were found using the probe liquids mentioned above and the thermodynamic work of adhesion was determined through the wetting of solids by liquids. A mathematical formula derived by Fowkes[87] in combination with Dupre's equation was used to determine the work of adhesion done specifically by London dispersion interactions yielding the following relation:

$$W = W^d = 2\sqrt{(\gamma_1^d \gamma_2^d)}$$

Where γ_1^d and γ_2^d are the dispersion components of the surface energy of two interacting molecules. Acidic and basic components related to the work of adhesion, W^{AB}, were determined from the following equation:

$$W^{AB} = 2\sqrt{(\gamma_1^+\gamma_2^-)} + 2\sqrt{(\gamma_1^-\gamma_2^+)}$$

where γ_1^+ and γ_2^+ represent acidic surface energy components, while γ_1^- and γ_2^- are the basic components and the pairs represent the interactions between acidic and basic molecules.[88] Young's equation, $\gamma_S - \gamma_{SL} = \gamma_L \cos(\theta)$, combined with Dupres equation, $W = \gamma_1 + \gamma_2 - \gamma_{12}$, yields $W = \gamma_L(1 + \cos(\theta))$. Finally the combination of the Fowkes, van Oss, Chaudhury, and Good, and Young-Dupre equations resulted in the following relationship:

$$\gamma L(1 + \cos\theta) = 2\left(\sqrt{\gamma_S^{LW}\gamma_L^{LW}} + \sqrt{\gamma_S^+\gamma_L^-} + \sqrt{\gamma_S^-\gamma_L^+}\right)$$

where γL is the liquid surface tension, θ is the contact angle, γ_S^{LW} and γ_L^{LW} are the dispersion component of the solid and liquid surface energy respectively and γ_S^+ and γ_S^- are the acidic and basic components of the solids surface energy. The liquid surface energy of the acidic and basic components are γ_L^+ and γ_L^-.[89] The probe liquids with known surface energies for dispersion and acid-base components are provided in Table 4.1 which were used in combination with the experimentally observed contact angles for each liquid resulting in three equations with three unknowns for the solid surface energy components ($\gamma_S^{LW}, \gamma_S^+, \gamma_S^-$).[90]

	Probe Liquids (mJ/m^2)		
	Diiodomethane	Formamide	Water
γ_L	50.8	58	72.8
γ_L^{LW}	50.8	39	21.9
γ_L^{AB}	0	19	51
γ_L^{+}	0	2.28	25.5
γ_L^{-}	0	39.6	25.5

Table 4.1 Probe liquids for acid-base contact angle analysis with corresponding surface tension components

4.1.2 Sample and System Setup for X-Ray Photoelectron Spectroscopy

Samples for XPS were taken from the cut blocks used for contact angle. Both sapwood and heartwood samples were sectioned in sizes of 500 and 800 microns in thickness with the Leica SM 2500. The 800 micron samples were then laser modified resulting in sample thicknesses of approximately 500 microns. The samples underwent the same drying conditions as for contact angle analysis. Samples were cut to 5 mm by 5 mm with a single edge razor blade and analyzed. The samples were tested with a PHI Quantera SXM-03 Scanning XPS Microprobe with an Al K-α X-ray source operating with beam energy of 1486 eV, pass energy of 280 eV over 15 sweeps, and collected by a hemispherical analyzer under a pressure less than $5x10^{-8}$ Torr. The instrument detected the elemental average over a spot size of 200 microns.

Low resolution scans were obtained from four different samples of heartwood and sapwood four both microtomed control and laser modified surfaces for total elemental composition. High resolution scans of carbon and oxygen species were analyzed and peak

deconvolution with PeakFit v4.12 software at specific binding energies and automatic Gaussian fits were applied with resulting Chi Squared values of .999.

4.1.3 Atomic Force Microscopy Techniques

The sectioned pieces from XPS that were not analyzed were used for AFM imaging. A MFP-3D-BIO Asylum Research system was utilized in tapping mode under ambient conditions. An Olympus TR800PSA silicon nitride triangular probe was used that had a spring constant of 0.57 N/m and operated at a frequency of 73 kHz. High resolution images were taken over 512 scans in tapping mode along the longitudinal direction of fibers cells on the tangential surface.

4.1.4 Fourier Transform Infrared Spectroscopy Settings

Dried samples from contact angle analysis were used for attenuated total reflectance infrared spectroscopy (ATR FTIR). A Nicolet 8700 FT-IR was utilized with a Pike Technologies GladiATR attenuated total reflectance accessory with heating stage and diamond window. Omnic software was used to operate the FT-IR over 128 scans at a resolution of 2 cm^{-1} and gain of 8.

4.1.4 Scanning Electron Microscopy

Dried samples from contact angle analysis were cut into 3 mm by 3 mm dimensions, microtomed, and laser modified. Subsequently, the samples were fixed to double sided copper tape on an SEM pin mount. The sample was sputter coated with approximately 10 nm of Gold/Palladium (60/40) and analyzed in a NeoScope JCM-5000 JEOL scanning electron microscope operating at 15 kV under high vacuum.

4.2 Results and Discussion

4.2.1 Laser Effects on Wood Chemical Linkages

The depth of penetration for the ATR with the diamond accessory at 1000 cm^{-1} is 2 microns. This analysis depth probes the bond vibrations of the subsurface for the control and laser modified materials. Previous work showed laser depth of penetration or chemically modified material within the top 8 microns of the yellow-poplar surface. The laser has a wavelength of 10.6 microns that is associated with the wavenumber 940 cm^{-1}. This wavenumber is between the bond vibration energies associated with asymmetric, out of phase ring stretching in cellulose at 897 cm^{-1} and 1100 cm^{-1} associated with asymmetric bridge C-O-C stretching in glycosidic linkages in polysaccharides .[91,38, 92] The control sample compared to the laser modified wood spectra in Figure 4.1a showed a peak shift from 1100 to 1106 cm^{-1} along with relative peak decrease. Moreover the peak at 892 in the control shifts to 897 cm^{-1} for laser modified samples along with relative peak increase. This change suggests an overall decrease in the glycosidic linkages or a depolymerization of polysaccharides while the increased band could suggest that the bulk material is comprised of increased pyranose rings from either increased cellulose content or more anomeric carbons from depolymerized chains and unordered chains.

There was also a band decrease and shift related to unconjugated carbonyl compounds from 1737 to 1728 cm^{-1}. This change arose from a decrease in acetyl group content on hemicellulose xylan chains. The conjugated ketone or carbonyl group attached to aromatic structures, primarily lignin, shifted and decreased from 1646 cm^{-1} in the control to 1637 cm^{-1} in the modified wood. The bulk of this material does not show extractive contamination as shown by the sapwood and laser modified sapwood spectra were identical to the heartwood.

The bands at 1327 cm^{-1} and 1319 cm^{-1} are commonly assigned to C-2 or C-3 C-O-H bending and CH_2 wagging in cellulose respectively.[91, 93] Although these bands rarely change with heat treatment in pure cellulose, this portion of the spectrum is influenced by hemicellulose content. A peak shift from 1319 cm^{-1}, a peak maximum, in the control sample to 1327 cm^{-1},a maximum, in the laser modified material, was likely due to the deacetylation or removal of xylan resulting in increased intensity at 1327 cm^{-1} indicative of cellulose character. A change in C-2, C-3 and hydroxyl groups can also suggest different hydrogen bonding conformations. [94] This data confirms previously reported 2-D NMR data that indicated deacetylation of xylan.

Another major spectral difference occurred at 3330 cm^{-1}, Figure 4.1b, related to the hydroxyl groups from polysaccharides especially cellulose. The control sample has a peak at 3322 cm^{-1} while the laser modified wood has shifted to 3347 cm^{-1}. This shift has been found to indicate two different aspects about cellulose morphology. The shift from cellulose I to cellulose II was detected in previous work and the band shifts in hydroxyl group vibrations show a similar trend as in the literature. [93] Other work also suggests that this shift could mean the cellulose is becoming amorphous. The trend happens in two similar ways compared to the laser modified material where the band shift is in the direction of amorphous cellulose and the hydroxyl group band becomes more narrow.[95] The control band at 2894 cm^{-1}, associated with aliphatic C-H stretching, decreases to 2884 cm^{-1} for the laser modified samples. The shift direction is associated with the change in cellulose I to cellulose II, however, the opposite shift occurs during the formation of amorphous cellulose, suggesting these shifts are more indicative of cellulose lattice conformational changes. It is possible with the high energy of the laser, especially at a frequency corresponding to cellulose ring stretching, to displace and cleave cellulose resulting in lattice conformational change and possibly some conversion to amorphous cellulose that is not

detectable in bulk, found in previous work through wide angle x-ray diffraction.

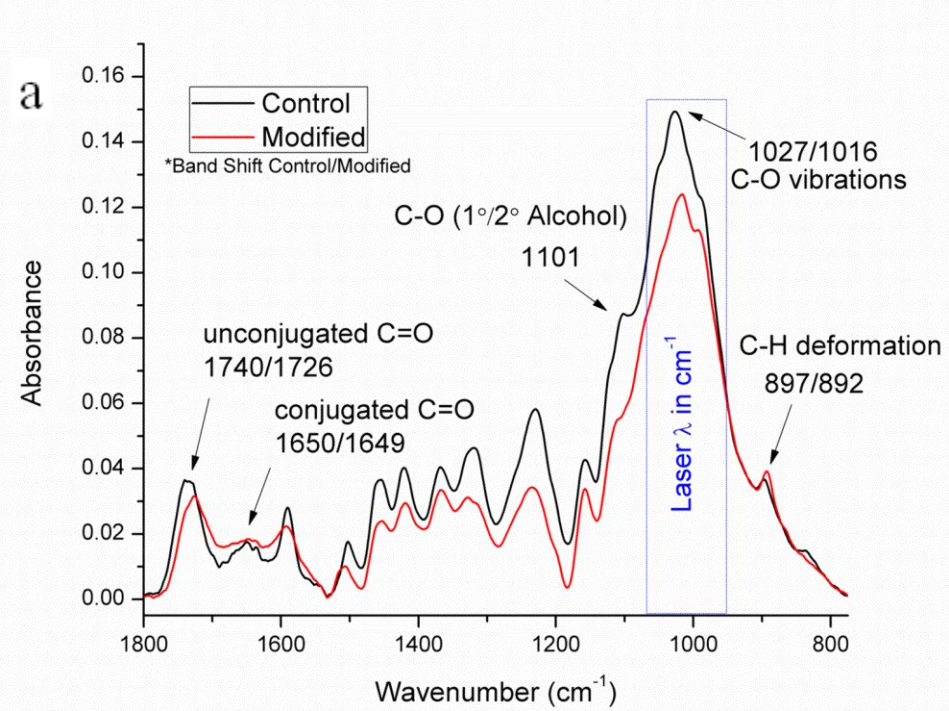

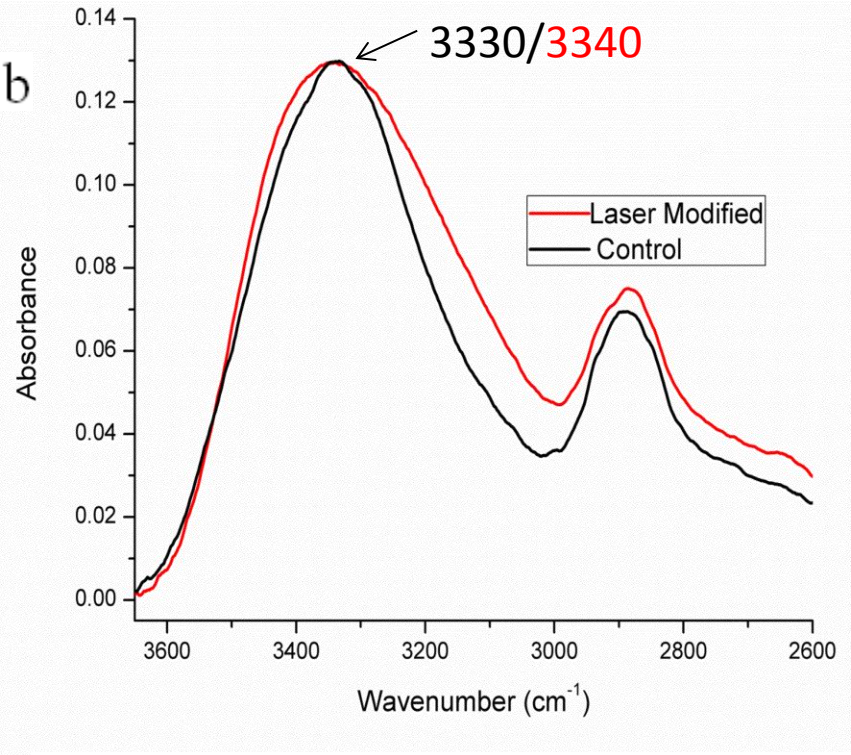

Figure 4.1 FTIR ATR absorbance spectra of Yellow-poplar control and laser modified Yellow-poplar -- a -- Finger print region of spectra with chemical shifts --b --Hydroxyl and aliphatic region

4.2.2 Subsurface Elemental Analysis of Laser Modified Wood

X-ray Photoelectron Spectroscopy high-resolution spectra of carbons were deconvoluted into four specific binding energies. Figure 4.2 contains the deconvoluted spectra for sapwood samples for the control compared to the laser modified sapwood. Heartwood samples were also analyzed and show less change relative to the sapwood possibly due to extractives. The first deconvoluted carbon is C1, which refers to the C-C and C-H bonds that have a binding energy of 284.6 eV. The C1's represent lignin, acetylated hemicellulose and extractives in the wood structure. Moving up in binding energies at 285.9 eV is C2 that corresponds to C-O bonds, mostly related to hydroxyl groups and C-O-C linkages on cellulose, hemicellulose, lignin, and extractives; this peak can also be interpreted as the methoxyl groups of lignin. Carbon linkages related to C3 are C=O and O-C-O that occur at 287.7 eV. The C3 relates to carbonyl linkages in lignin, extractives, and hemicelluloses while O-C-O linkages are related to cellulose and hemicellulose. The C4 corresponds to O-C=O linkages at 288.9 eV mostly relating to ester linkages and carboxylic acid groups on lignin, hemicellulose, and extractives. The high resolution spectrum of oxygen was deconvoluted into O_1 correlating to O=C linkages at 531.0 eV and O_2 related to O-C bonds at 532.9 eV (Figure 4.2).[61-62, 64]

The quantification of the deconvoluted carbon linkages is shown in Figure 4.3, highlighting a difference in C_1 percentages in both sapwood and heartwood before and after laser modification. The increased existence of C-C and C-H bonds in laser modified wood samples indicates an increased hydrophobic surface.

From previous work, it was found that laser modified wood surfaces have increased lignin content in conjunction with literature that provides evidence that lignin dominates surface

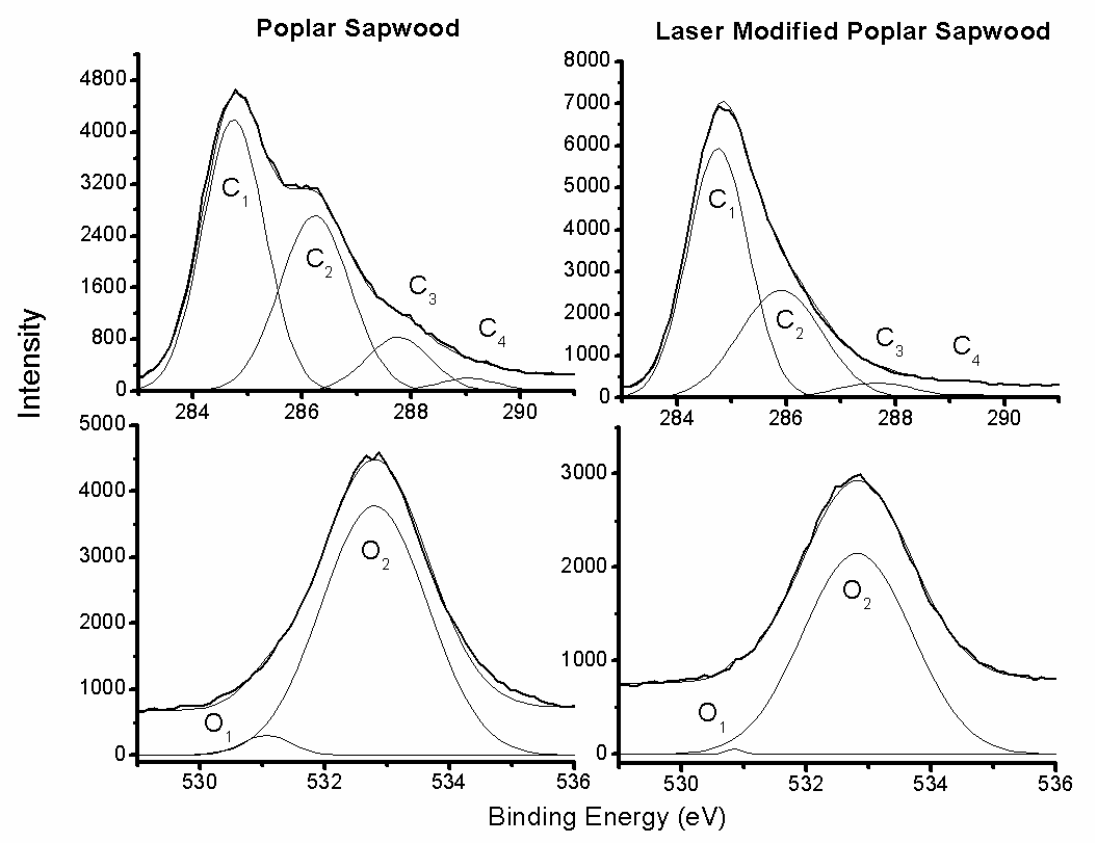

Figure 4.2 XPS High resolution carbon (top) and oxygen (bottom) spectra of Yellow-poplar sapwood (left column) and laser modified sapwood (right column)

composition at this probing depth.[96] Moreover, the bonds related to C_2 remain similar comparing the control to laser modified surfaces, which is not common for even mild heat treatments; this results suggests the laser modification is different than for samples exposed to high heat. [62] The C_2 linkages specifically C-O related to hydroxyl groups may not be greatly affected by laser energy due to a major portion of this material being cellulose chains. Hemicelluloses especially acetylated xylan chains are decomposed leaving degradation products that contain appreciable amounts of hydroxyl groups. Additional chromatography analysis had found residual syringe aldehyde and furfural derivatives contained in the modified surface layer, but XPS data suggests

a very small presence of aldehyde containing compounds (C3) at the surface. Fowkes theorized that by utilizing XPS analysis, atoms like carbon and oxygen could be characterized as acidic or basic by binding energy, where at lower binding energies substances are more likely to be electron-donors, or basic, and at higher binding energies substances are suspected to be electron acceptors or acidic.[97] For wood this assignment is complicated and other studies have adopted a modified theory to find that C_2 and C_4 in XPS analysis can relate to acidic surfaces while C_1 and C_3 would contribute toward basic surfaces.[64] By percentage, C_1 and C_2 are the two highest values that should reflect a dominantly basic and acidic surface. Whereas for Fowkes theory, C_1 and C_2 combined would be very basic with little acidic contributions. Other noteworthy changes occur in acidic functional groups like carboxylic where there is a decrease in intensity due to laser ablation in sapwood samples, yet there is a slight increase in heartwood samples. The difference could be caused by the contamination of extractive compounds at the surface layer. Low resolution scans provided total elemental analysis where the control samples of both sapwood and heartwood contained around 2% nitrogen from amino acids in proteins or also from other wood extraneous molecules. Extractives in yellow-poplar contain mostly alkaloid type molecules with different functionality of nitrogen and carbon including hydroxyl, methoxyl and ketones.[98] Moreover, the outermost boundary of the heartwood and sapwood transition is known to have highest extractive content which was used in these experiments.[99] The extractives migrate to the surface when a board is cut, especially during the drying process. The presence of these small molecule extractives can contaminate the surface and make it more polar or non-polar depending on orientation and extractive type. However, minimal amounts of nitrogen were found in the laser modified wood at the XPS probing distance approximately 5-9 nanometers

.

Polarity can be found by analyzing carbon linkages probed by XPS where C_1's are non-polar and C_2's are polar. The laser modification technique increases the C_1 content, increasing non-polar carbons. The C_2 remains relatively stable and does not decrease dramatically because of laser ablation compared to the control. Chemical composition of this laser modified surface in

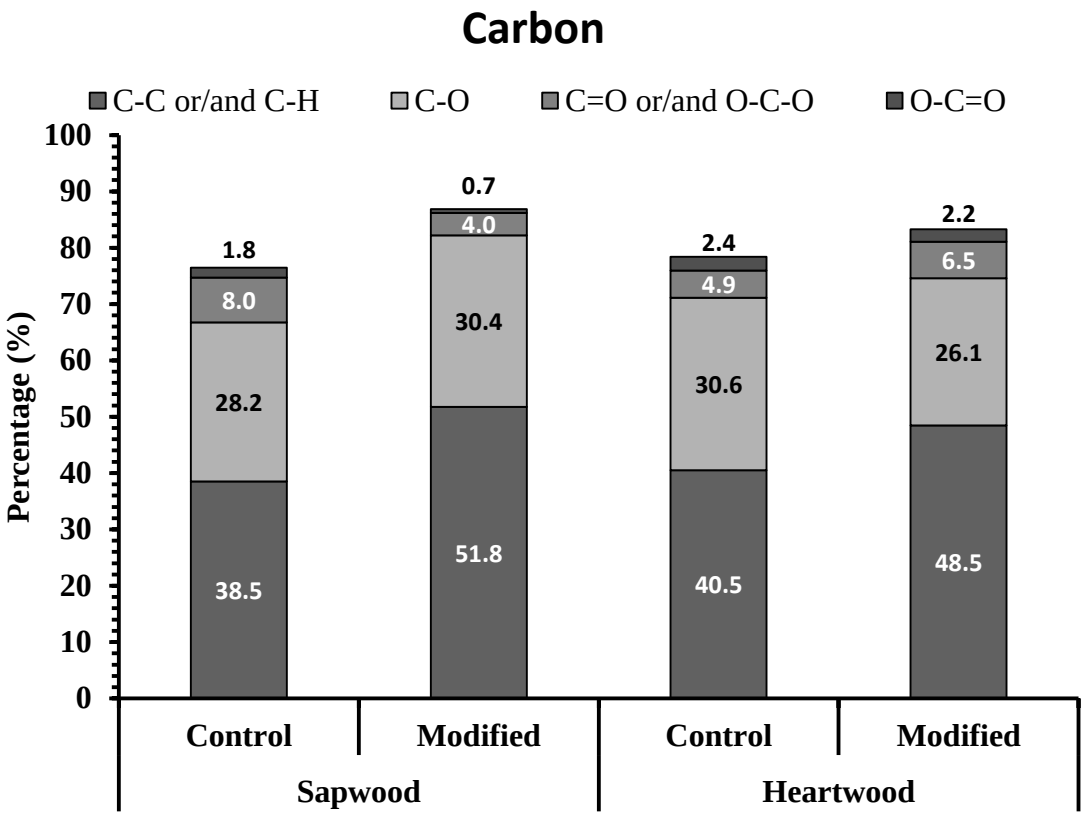

Figure 4.3 Breakdown of carbon linkages from high resolution XPS spectra of yellow-poplar control and modified wood and heartwood and sapwood

previous work suggests lignin and cellulose both increase due to modification, which is consistent with this XPS data if we consider C_1 to mostly probe lignin and C_2 to mostly probe cellulose and hemicelluloses. Another means of interpreting wood structure polarity is by oxygen

to carbon (O/C) ratios where oxygenated species related to polar bonds decreases due to laser modification. XPS analysis revealed that sapwood compared to laser modified sapwood had an O/C ratio decrease from 0.28 to 0.15, while heartwood samples compared to laser modified heartwood had less of a decrease from 0.24 to 0.20.

4.2.3 Acid-Base Contact Angle Analysis

To understand the surface chemistry of the top nanometer of the yellow-poplar surfaces from control to modified wood, contact angle analysis, specifically, acid-base and dispersion components of the solid surface free energy were determined. Contact angle analysis using static or sessile drop approach can approximate the surface energy components utilizing the combined Fowkes, van Oss, Chaudhury and Good, and Young-Dupre equations. Since wood surfaces are non-ideal due to chemical heterogeneity these calculations are only approximate, providing a good indication of the differences purely between the treatment of sapwood and heartwood and between control and laser modified samples. The contact angles associated with diiodomethane, formamide, and water are presented in Figure 4.4, where standard deviations over all samples are less than 5 degrees. Contact angles decrease from control to laser modified wood for every probe liquid. Sapwood shows a greater decrease in contact angle with all liquids when compared to heartwood from control to modified wood.

Dispersion forces were probed, consisting of instantaneous and permanent dipole-induced dipole interactions, which are associated with long distance van der Waals interactions. Diiodomethane is a liquid that only interacts with these forces and is also non-polar making it a very useful probe. Water is a polar liquid that acts, in theory, as both a Lewis acid and Lewis base and thus the acid-base components are split in half which is used to probe either acidic or basic components. Formamide is also a polar liquid that has little acidic contributions and is

mostly basic. Acid-base character is important in the work of adhesion because strong associations, intermolecular interactions, or hydrogen bonding can exists between the electron donor and electron withdrawing groups at the surface. Ideal adhesion conditions would be reflected by high acid-base character because it is related to hydrogen bonding potential.

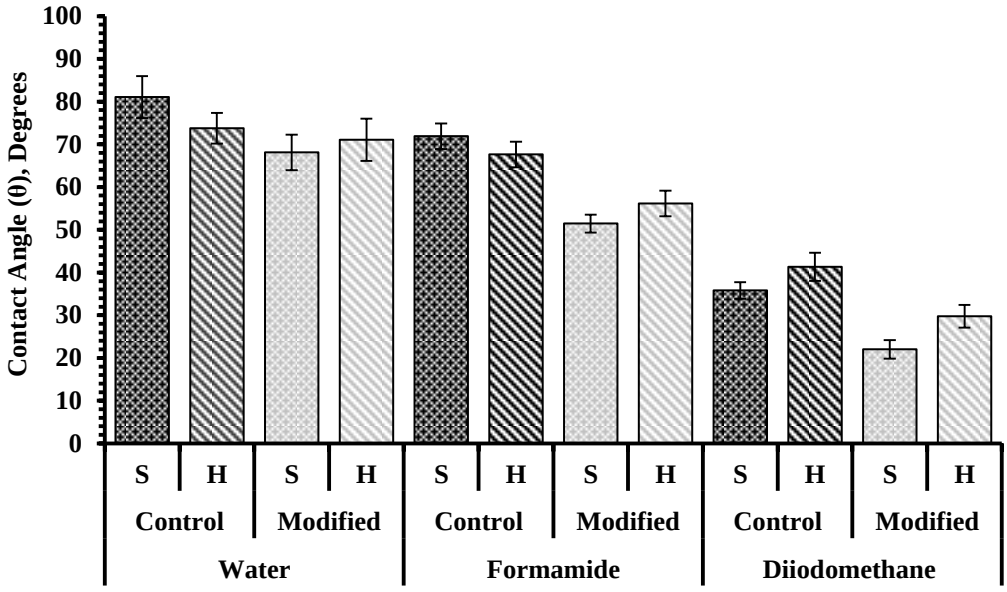

Figure 4.4 Contact angle average and standard deviation from 30 drops of different probe liquids on Yellow-poplar control and laser modified sapwood (S) and Heartwood (H) specimens.

Acid-base theory predicts the thermodynamic work of hydrogen bonding between molecules through acid, or electron acceptor, and base, or electron donator, while the strength and is not related to chemical polarity.[100] Wood surfaces consist mostly of London dispersion forces and are also amphoteric with a small portion of acidic character but more contribution toward basicity.[90] Base-base and acid-acid interactions do not contribute toward the work of adhesion between surfaces.

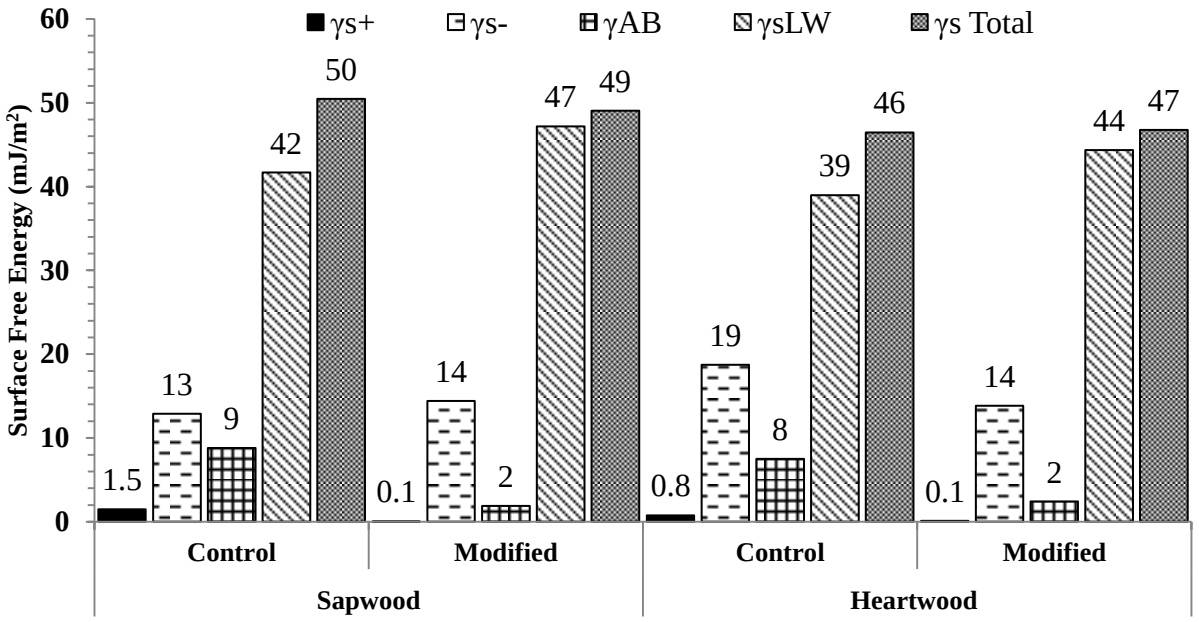

Figure 4.5 Acid, base, acid-base, dispersion, and total solid surface free energy components of Yellow-poplar laser modified and control samples with both sapwood and heartwood

According to the derived free energy surface components (Figure 4.5) there were little acidic contributions toward the acid-base work of adhesion associated with the control wood surfaces, however after laser modification the acidic portion drops even lower. This effect was also seen in the XPS analysis of the acidic type linkages (C4) in sapwood specifically uronic acid groups. This change can indicate the absence of surface oxidation, which is atypical for wood after light and thermal decomposition in the presence of oxygen.[101] This change could be explained by the laser technique in which the efflux of volatiles can overcome the penetration of oxygen into the surface layer, essentially acting as pyrolysis type degradation process.[25] The total surface energy including the dispersion component and acid-base components is low for laser modified wood because the acidic component is close to zero resulting in little contributions toward the acid-base adhesive force, thus the dispersion component accounts for a majority of the total surface energy (Figure 4.5). It is common that the wood surfaces are dominated by basicity, which suggests an abundance of electron donor groups at the surface. Bulk wood is

acidic in nature because of primary and secondary hydroxyl groups on woody polymers plus contributions from carboxylic acid groups. However this was not found to be true for these surfaces in which the basic portion dominated the acid-base contribution. This is particularly evident for laser modified wood in which the surface resembles a monopolar substance. If these surfaces have high basic and low acidic content then it would suggest that hydrogen bonding potential is decreased due to the surface ablation technique, where the increase in dispersion component and decrease in acid-base components makes the total surface energy very similar for control and laser modified wood. This result may also indicate that the van der Waals interactions have increased and over large surfaces could contribute to the adhesion between laser modified wood samples. The surfaces have to be flat enough to come into atomic contact over large areas for this adhesive mechanism to be plausible.

4.2.4 Atomic Force Microscopy

The surfaces of yellow-poplar for both control and laser modified wood, Figure 4.6, were obtained by AFM imaging in tapping mode in the longitudinal direction on a tangential surface. The phase images are produced from a change in viscoelastic material behavior when the probe deflection has a delay from material contact compared to the tapping frequency. For example a perfectly elastic material will exhibit instantaneous contact deflection resulting in a zero degree phase shifts while a purely viscous material will have a phase shift of 90 degrees. In the case of these images the white areas could be established as softer regions compared to the dark stiff regions. Young's modulus in ambient conditions from 3 to 12% moisture content of lignin is reported to be in the range of 3 GPa to 7 GPa this would correspond to the softer material in the AFM images.[102] Pure xylan corresponding to model hemicellulose material has an effective Young's modulus of 8 GPa in similar moisture conditions which would also show a more

viscous phase delay.[103] Cellulose is the stiffest of wood polymer matrix material having a Young's modulus around 25GPa in comparable moisture conditions.[104] The wood control samples have a much larger range of soft to stiff materials as seen by the larger degree change. The laser modified samples have a much lower degree change corresponding to surfaces with more homogenous physical properties.

The images reveal relative surface roughness; the laser-modified wood has about half the surface roughness of the control. The control wood specimen had fiber protrusions on a micro-scale and nano-scale interfering with over 95% of the surface. The images shown for the control sample are the smoothest fiber surfaces viewed in the work. The laser-modified material is well represented by the image shown because the entire surface was able to be imaged except for deep vessel elements. Control samples had distinct cellulose microfibril regions in the horizontal direction as seen by the height image and obvious orientation of the surface. No such orientation exists for laser modified samples but areas of homogenously spaced nano-sized residues appear. The modification from cellulose chain direction to no direction indicates the structure at the surface is significantly disrupted. It should also be noted in light of the contact angle work note above, the control samples have major surface roughness compared to the laser modified wood in which the contact angle may be affected. If a surface is hydrophilic ($\theta<90°$) and it is roughened then the contact angle will decrease.[105] The laser-modified surface was smoother and yet still had a smaller contact angles for water meaning that the surface roughness played a less significant role than chemical interactions.

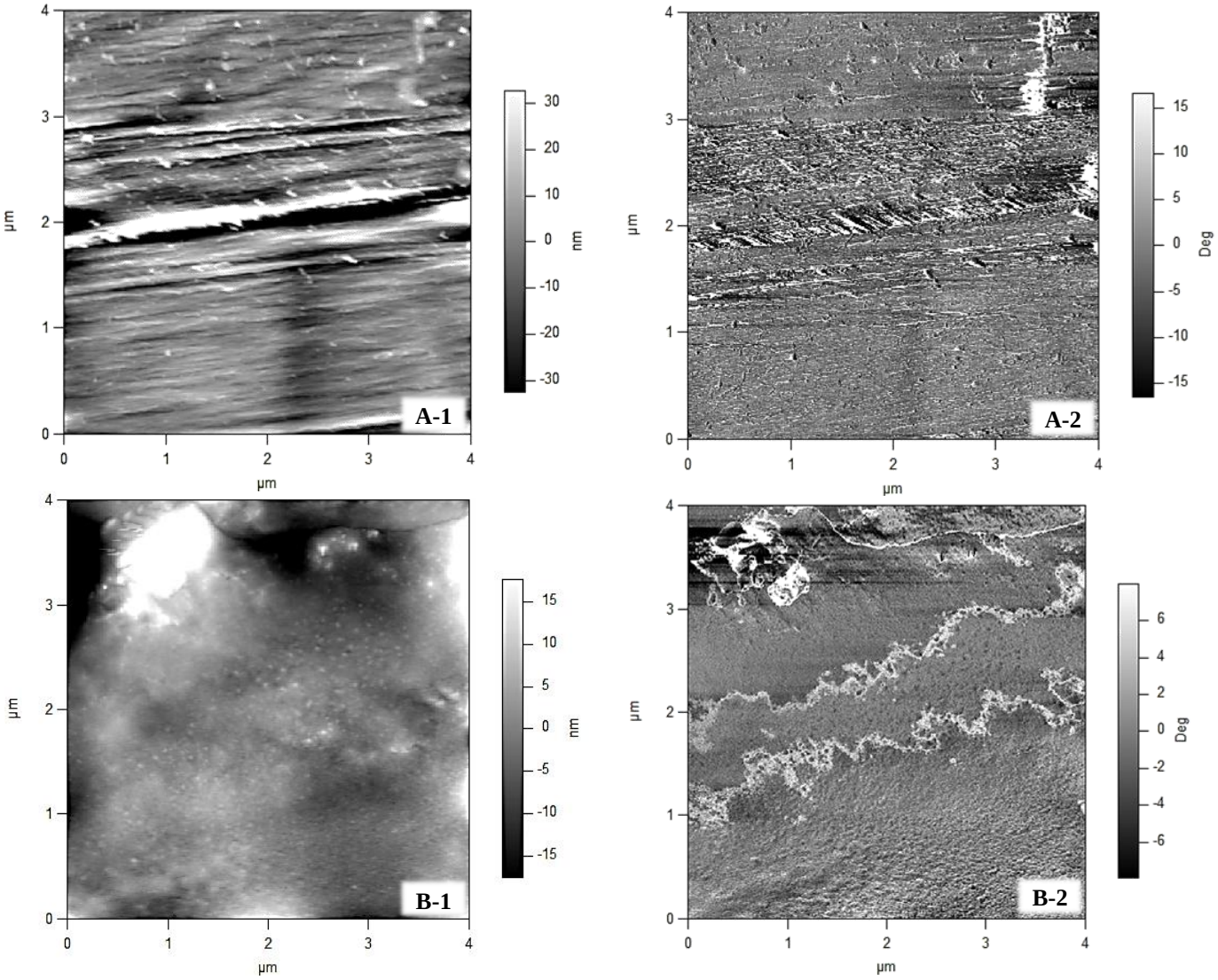

Figure 4.6 A—Microtomed Yellow-poplar surfaces, B—Laser modified Yellow-poplar surfaces, 1—Flattened Height image, 2—Phase image

4.3 Scanning Electron Microscopy

The microscale features of wood anatomical changes after laser modification were observed by scanning electron microscopy, Figure 4.7. At 50X magnification the surfaces appear similar with the largest of wood anatomical features still intact, like vessel elements and perforation plates. Accumulated laser modified material, 2-15 micron sized deposits, for the laser modified surface appears to create greater surface roughness. However, at 500X magnification,

specifically fiber tracheid bundles surrounding vessels and ray cells, there is a clear difference and reduction in surface roughness. The microtomed fiber surfaces are fibrillated from the tearing involved with surface preparation while the modified surfaces have a cauterized appearance reducing the protrusions of these wood features. At this magnification some wood anatomical features are identifiable in the laser modified samples, whereas ray cell walls are fused unlike the control sample. The dense fiber bundle sections are obvious and clearly defined in the unmodified wood, however after modification these sections merge together creating larger sections of flat and homogeneous material. Holes also appear in these regions which maybe a result of material cooling or the translocation and accumulation of radial cell wall deposits.

At high magnification, 5000X, fiber tracheid cells are identifiable in the control as the images shows a grouping of these cell types. The S_2 layer of the cell wall with vertical microfibril orientation is visible within the control image (Fig. 4.7 A3). The laser modified wood image shows no such orientation and fiber tracheid cell wall ultrastructure is absent. Similar to surfaces imaged by AFM there are nanometer sized aggregates on the cell surface (Figure 4.7 B3). The fused cell wall regions provide evidence that the laser energy has the capability to coalesce degraded wood polymeric material by either laser induced thermal flow or from the condensation of volatiles produced from rapid cooling, similar to wood tar formation. Another possibility is the degradation and accumulation of degraded material.

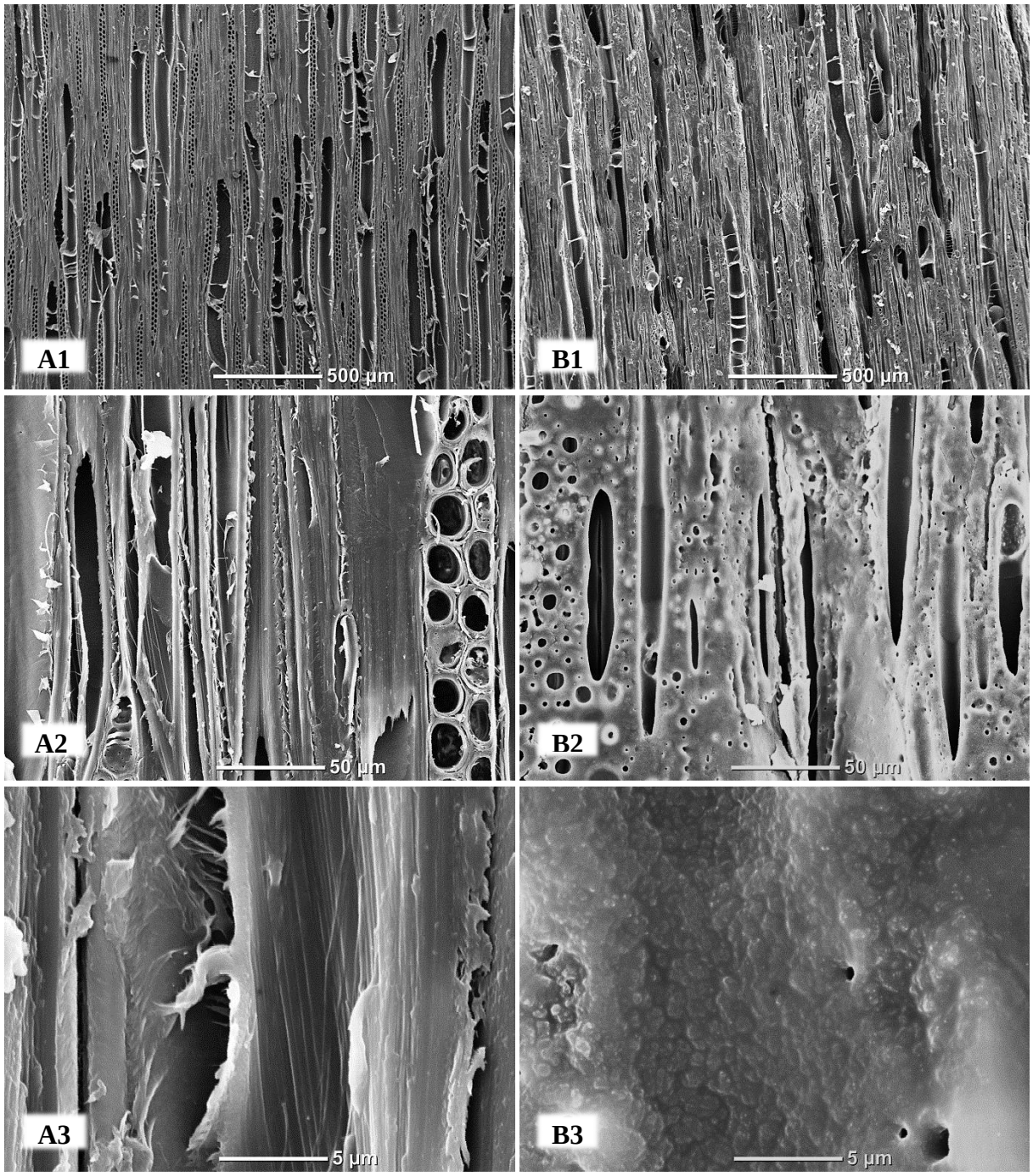

Figure 4.7 A1-B3 Scanning Electron Microscopy images of microtomed Yellow-poplar wood (A) and laser modified wood (B) at magnifications of 50X(1), 500X(2), and 5000X(3)

4.4 Chapter Conclusions

The bulk laser modified wood is chemically similar between heartwood and sapwood probed by FTIR ATR averaging the top 2 microns of the surface. The spectra's between control and modified wood suggest a partial conformational change from cellulose I to cellulose II as well as deacetylation of hemicellulose like glucuronoxylan and loss of aromatic carbonyl groups. The laser has a wavelength associated with the absorption energy of the skeletal vibrations of cellulose pyranose rings, possibly responsible for the chemical changes in polysaccharides. XPS analysis shows an increase in non-polar C-C and C-H bonds while C-O bonds remain similar between modified and control samples. There is also a decrease in acidic functional groups like carboxylic acid associated with hemicellulose in sapwood, however the heartwood maybe contaminated with extractives showing a smaller change. The O/C ratio for sapwood is dramatically decreased compared to laser modified and heartwood shows a less severe decreases suggesting the laser reduces oxygen containing bonds at the surface. Contact angle suggests that the dispersion component of the solid free surface energy increases. Electron donating groups are minimized due to laser modification while electron acceptor groups remain high for all samples. Since the acidic portion of the surface is minimized by laser modification, the potential for hydrogen bonding between surfaces is reduced related to the work of acid-base adhesion. This result may mean that van der Waals forces may be the driving factor in adhesion if sufficient contact area between surfaces is met. Atomic force microscopy revealed that the laser-modified surface is overall much smoother than the wood control, which has micro scale fiber protrusions. Moreover, the hydrophilic ($\theta<90°$) wood control that had increased surface roughness showed less favorable wetting when compared to the smoother laser modified surface with water as a probe liquid. Microscopy also revealed a more homogeneous physical surface with the laser

modified wood where the phase shifts are less prominent. The decreased surface roughness in addition to heat and pressure may allow for atomic interactions. Moreover, SEM provides evidence that laser modification merges degraded cell wall components for a continuous surface. This surface may have the ability to undergo further flow when in contact with similar surfaces under high heat and pressure.

CHAPTER 5. Supporting Experimentation

5.1 Before and After Hot Pressing HPLC Analysis

A veneer sheet of yellow-poplar was cut into four 20cm x 20 cm x 3.175 mm sheets. Two of the sheets were laser modified at 12% moisture content and immediately bonded at 2.4 MPa at 200°C for 5 minutes. After bonding the sheets were mechanically separated to expose bond-line material. The bond-line material and control laser modified material was brush extracted with similar quantities of water and tested for differences.

The hypothesis being if the laser byproducts decrease in quantity then it is possible they are recombining with lignin or carbohydrate structure from either the decomposed surface or the adjacent bonding surface, creating a covalent bonding. Since the amount of water was not exactly the same and brushing technique was not always consistent the data was normalized using the largest peak in the chromatogram to determine relative differences. The chromatograms are seen in Figure 5.1A where the data was vertically subtracted due to baseline drifting during sample detection. The peaks were integrated and data for percentage change before and after hot pressing are presented in Figure 5.1B. Approximately 55% of the total composition of the mixture is identified with the standards used. The results show an increase in most of the degradation products as a result of the hot pressing step suggesting further degradation of lignin and carbohydrates. Polymerization or recombination of two different components is possible due to the decrease in content of syringaldehyde and ferulic acid. The aldehyde and carboxylic acid groups on these molecules could react without the presence of moisture. Other possibilities leading to the decrease of these components is radical coupling or further decomposition leading to volatilization. An indication that covalent bonding is limited in

the system is seen by the laser bonded sample low hydrolytic instability where liquid water causes delamination.

5.2 Heated X-Ray Photoelectron Spectroscopy

The samples used for XPS is previous work were heated to 200°C in a vacuum to observe the chemical changes as a sample is heated. A slight variation in response during testing was noticed during the vacuum stage. The control heartwood sample required at least 30 minutes during the load lock stage, while the laser modified heartwood sample required 10 minutes. The vacuum thermal treatment revealed a number of important aspects that should be further investigated. The first aspect being the volatilization of compounds from the control sample vs. the laser modified sample as the vacuum length was dependent on the amount off-gassing; thus

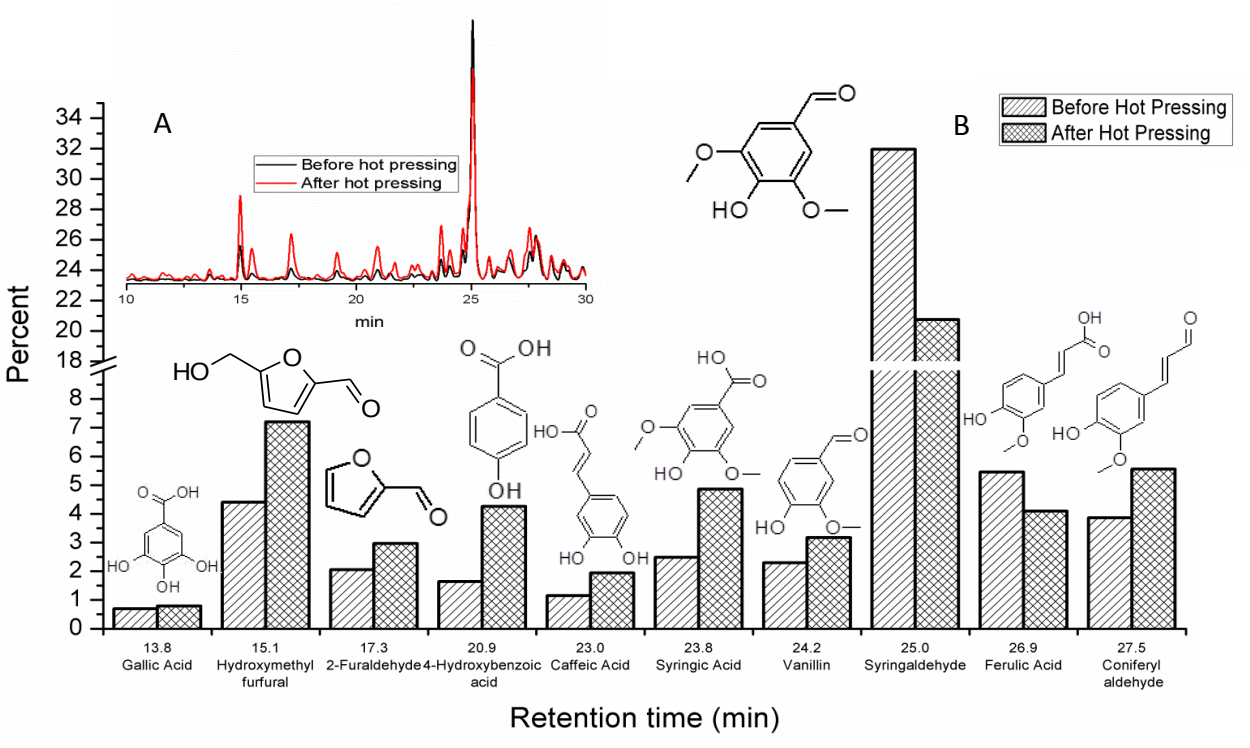

Figure 5.1 A. Chromatogram of phenolic compounds removed from surface extraction before and after hot pressing B. Percent changes in chromatogram and composition from before and after hot pressing with retention times and compound structure

the load lock time was three times longer for the control sample. This result may indicate that laser modified surfaces resist or minimize the efflux of volatiles which could be a result of the surface layer absorbing these volatiles or the lased residues creating a continuous surface where the escape of volatiles are trapped by the modified surface layer (consistent with AFM). Further investigation on the diffusion of molecules through laser modified wood could is pertinent. Another possibility is that the wood is sufficiently modified where volatile output occurred during the laser treatment and would require increased thermal input to increase volatile yield.

The deconvolution of the XPS spectra, as done for previous XPS data, from heat treatment was summarized in Figure 5.2. Comparing the effects of heat treatment on both laser modified and control heartwood samples, the overall carbon content decreased and oxygen content increased. The oxygen to carbon ratio of the heartwood control sample and laser modified wood is 0.24 and 0.20, respectively. After heat treatment both increase to 0.29 and 0.27. Carbon to oxygen linkages, related mostly to cellulose and hemicellulose are decreased according to deconvolution. Extractives and lignin may increase after heating the surfaces due to the increase in C-C/C-H bonds and a minimal decrease in nitrogen content is found related to extractive materials in yellow-poplar wood. However, this increase does point out a distinct difference between typical thermal degradation and laser modification; laser modification reduces oxygen content and simple heat treatment causes an increase in oxygenated species at this probing distance. If the laser modified surface does inhibit the volatilization of wood then entrapment of reactive volatiles like formaldehyde may lead to oxygenated species at the surface where laser modified heated samples observe a greater increase in O/C ratios. This explanation is only a hypothesis and requires further investigation, as no other data is consistent with this

phenomenon in the literature.

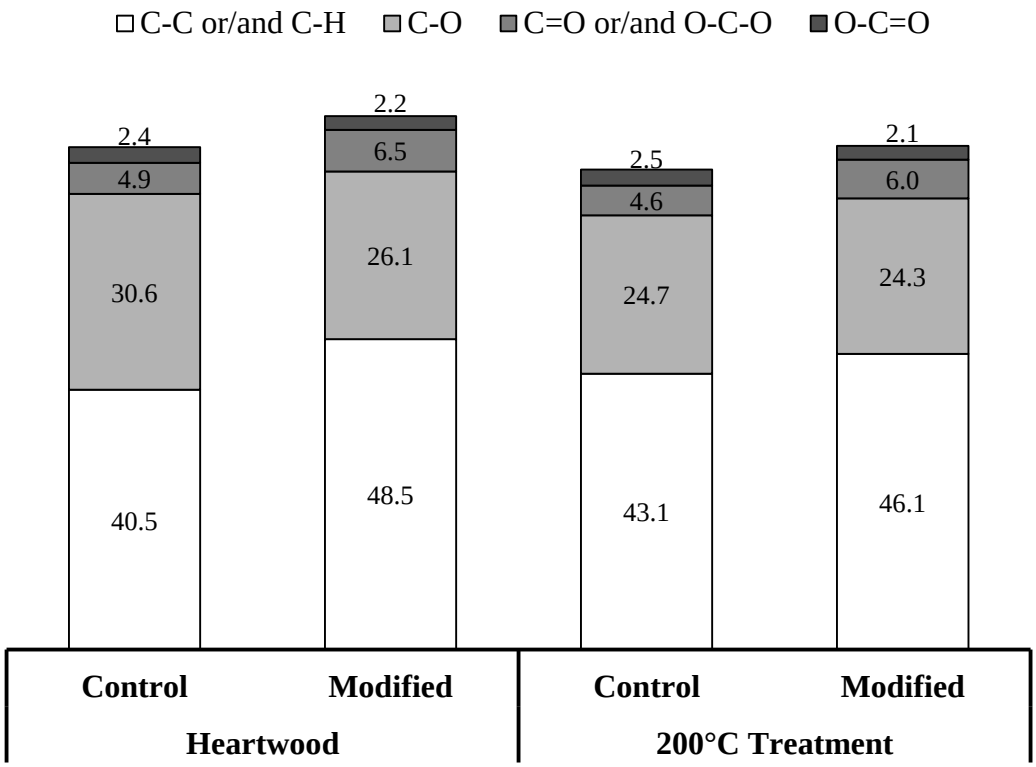

Figure 5.2 XPS Carbon data summary for yellow-poplar "control" sample and laser "modified" yellow-poplar samples before (heartwood) and after heat treatment (200°C treatment)

5.3 Heated ATR FTIR

Laser modified yellow-poplar and unmodified yellow-poplar wood were compared using a heated ATR accessory of the FTIR spectrometer. The ATR accessory has a heated stage that was controlled for a temperature ramp where the laser modified material was pressed onto the diamond probe and heated from room temperature to 200°C at 10°C/minute with spectra taken every minute consisting of 32 scans with a resolution of 4 cm^{-1}. The spectra were baseline corrected and meshed into a 3D graph with an axis for wavenumber (x), temperature (y), and

intensity (z). The graphical representation of the data was split into hydroxyl and aliphatic signals from 3800 to 2800 cm^{-1} and the finger print region from 1800-400 cm^{-1}, Figure 5.3 A and B. For hydroxyl region the change from cellulose I to cellulose II, as discussed previously, is enhanced with the addition of heat found through the shift in wavenumber 3339 cm^{-1}. Other cellulose characteristic peaks that shift toward the formation of cellulose II are compared to the mercerization of cellulose with NaOH with corresponding absorbance change in Figure 5.3 C. Other wood components like conjugated carbonyl groups in lignin structure are gradually depleted with the addition of heat at wave number 1637 cm^{-1}. Depletion of these groups may relate to the chemical oxidative coupling of lignin species, and these species will be further explored in additional study.

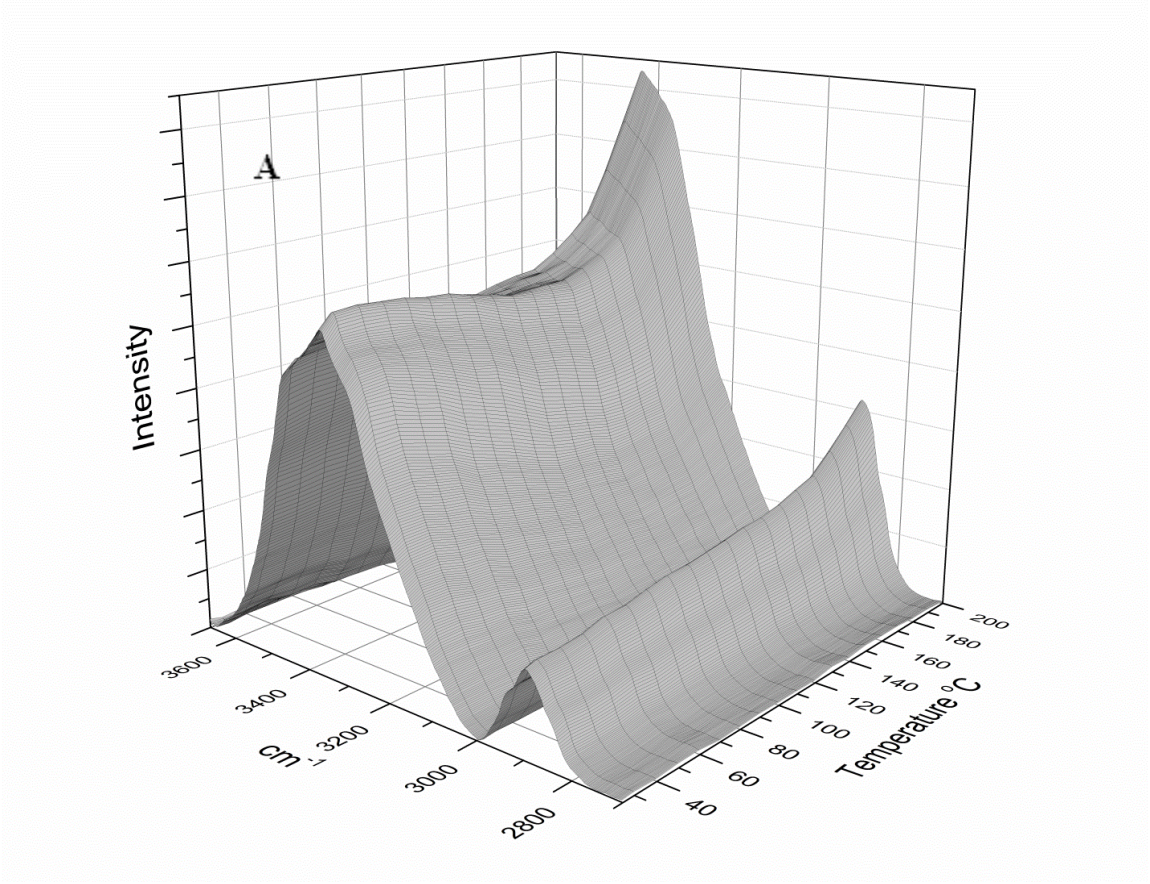
A
Intensity
3600
3400
3200
3000
2800
cm -1
200
180
160
140
120
100
80
60
40
Temperature °C

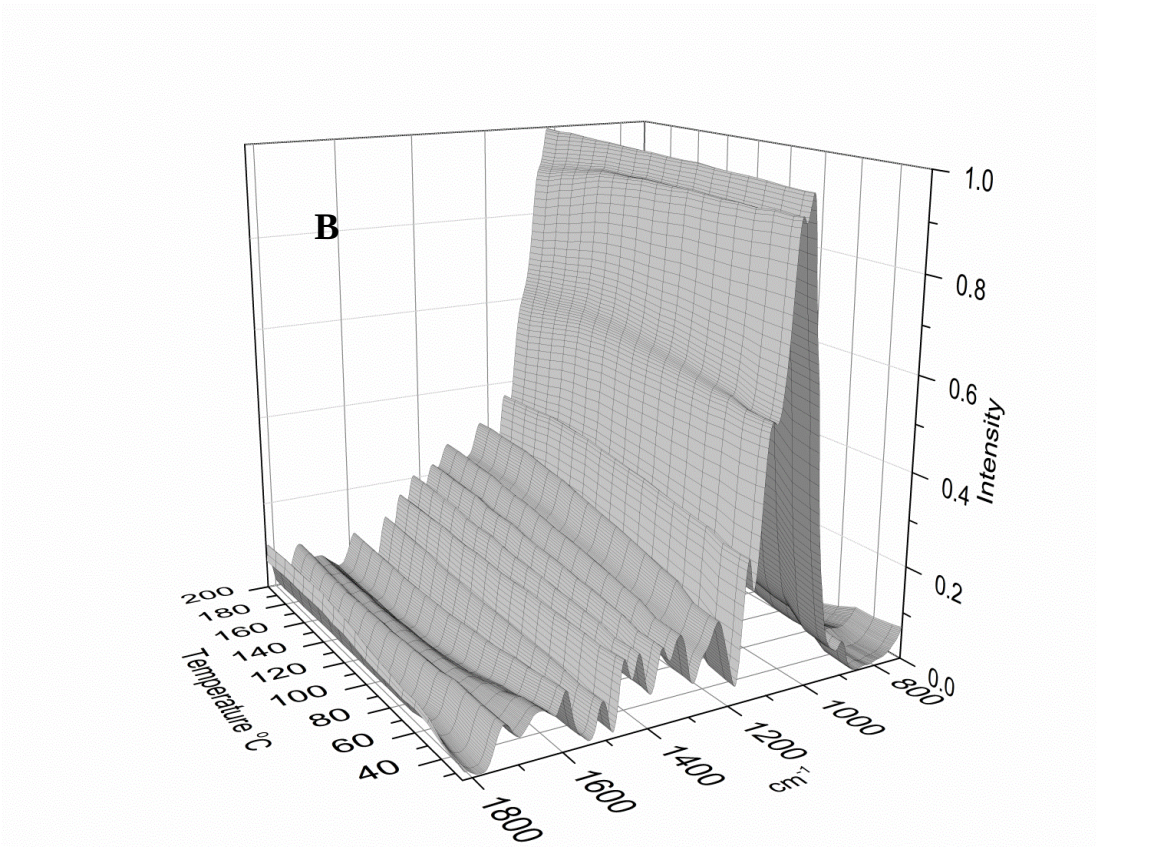
B
1.0
0.8
0.6
0.4
0.2
0.0
Intensity
800
1000
1200
1400
1600
1800
cm-1
200
180
160
140
120
100
80
60
40
Temperature °C

C	Cellulose I (cm^{-1})	Cellulose II (cm^{-1})	Assignment	Absorbance Change (cm^{-1})	Literature Values (cm^{-1}) (NaOH)
Peaks	3339	3442	H-Bonded OH	+102	+95
	1236	1228	C-OH in plane at C-6	-8	-8
	1030	1021	C-O at C-6	-9	-13
	896	894	C-O-C β-glycosidic linkage	-2	-3

Figure 5.3 Heated heartwood Yellow-poplar FTIR ATR data with temperature range of 25°C to 200°C over wavenumbers 2800-3800 cm^{-1} (A) and 1800-800 cm^{-1} (B) with peaks associated with absorbance changes from cellulose I to II from spectras (C)

5.4 Thermal Gravimetric Analysis

Thermal gravimetric analysis (TGA) is a technique that measures mass loss as a result of constant or increased thermal stimulus by isothermal or ramped temperature programs respectively, that are used to determine degradation pathways in materials. TGA was used to show the degradation of the wood control sample compared to laser modified wood in a nitrogen atmosphere (sample flow rate 60 mL/minute and balance flow rate 40 mL/minute) at a 15°C/minute ramp to 600°C. The degradation of the wood sample has three distinct stages as seen in Figure 5.4 the first is the degradation of hemicellulose and amorphous cellulose around 300°C.[106] The degradation profile of hemicellulose and crystalline cellulose overlap however at 350°C there is a distinct slope change in the control most likely a result of just cellulose degradation. Lignin degradation is also occurring at these first stages but as the lignin structure condenses it become more thermally stable and degrades slowly over a broad range specifically evident from 375 to 600°C.[107] Laser modified wood shows two distinct degradation events the first near the hemicellulose and cellulose degradation temperature at 300°C. This curve is more indicative of cellulose degradation, which is consistent with previous finding that hemicelluloses are degraded from laser energy and cellulose is in higher quantities. The degradation profile then changes at 350°C with a slight slope change followed by an immediate and distinct slope change

related to lignin thermal decomposition. The degradation of both cellulose and lignin occur sooner compared to the control due to partially degraded material from laser modification. Even though most polymeric materials have a molecular weight dependence on onset degradation temperature where larger chains have higher thermal stability, this is not true for cellulose. However, thermal degradation does dramatically decrease chain length in cellulose as temperature is increased. [108]

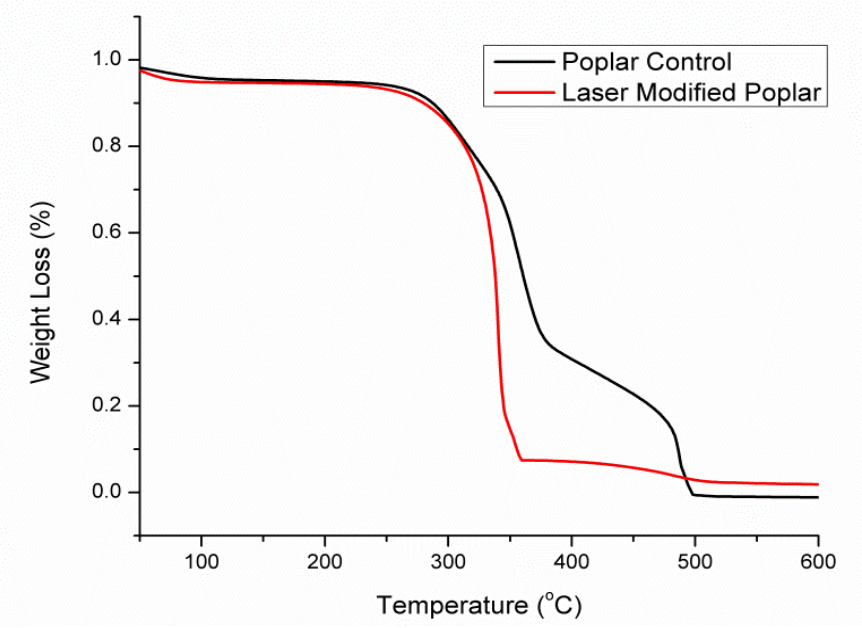

Figure 5.4 TGA thermogram of extracted laser modified yellow-poplar compared to the control sample

5.5 Liquid Nitrogen Pre-treated Veneer before Laser Modification

Localized heating of wood samples by laser modification was measured utilizing an infrared thermometer. The infrared thermometer may not instantaneously measure the maximum temperature at the contact between the laser and modified wood but gives an approximation of the local temperature change. The infrared laser also works more accurately closer to the heat source. All measurements were taken from 15 cm away from the wood surfaces being ablated.

Yellow-poplar wood that had a moisture content of 12% with 5 cm x 5 cm x 3.175 mm dimensions were submerged in liquid nitrogen for 10 minutes, immediately removed and modified over the entire surface. Measured surface temperatures from a control sample at room temperature and pretreated liquid nitrogen are compared in Table 5.1. The values show that even with the liquid nitrogen pretreatment the samples still achieved high localized temperatures. The hypothesis involved with this experiment was to reduce the impact of heat on laser modification. Reduction in heat may separate thermal and light degradation events to have more insight on how infrared light at high energy density affects the wood structure. However the test results indicated that no matter the starting temperature of the surface the laser energy was too high to reduce any the effects of heat or thermal degradation. Additionally, the measured thermal temperatures are below the temperatures at which cellulose typically degrades.

Table 5.1. Liquid nitrogen wood pretreatment before laser modification (minimum) and during laser modification (maximum) compared to control at room temperature

	Room Temperature (°C)		**Liquid Nitrogen (°C)**	
Sample	Minimum	Maximum	Minimum	Maximum
1	21	235	-43	233
2	23	238	-43	230
3	22	242	-45	230
4	22	246	-52	231
5	23	227	-46	226
6	22	217	-45	233
7	21	229	-58	235
Average	**22**	**233**	**-47**	**231**
Standard Deviation	0.8	9.9	5.6	2.9

5.6 Pre and Post Hot Pressing Heat Treatments

To identify the possibility of a thermoplastic type adhesive material created from laser ablation, veneer samples were laser modified and then thermally treated at 200°C for 5 minutes

and brought back to room temperature and 12% moisture content and then hot pressed together. The result of the test demonstrated that there was no adhesion between pre-thermally treated veneers. A second approach was to rebond, once bonded material. Bonded veneer samples were separated by mechanical force, with no wood failure, and subsequently the samples were reconditioned to 12% moisture content and hot pressed again. The samples resulted in no adhesion.

After bonding the laser modified wood it was found that a post heat treatment of the bonded wood over long periods of time at 200°C could enhance water stability. Solid wood samples that were bonded were subjected to a 24 hr heat treatment in a furnace and were able to withstand boiling water tests and solvent submersion without delamination. The optimization of heat treatment for two veneer bonded wood was accomplished by varying composite exposure time within a 200°C furnace environment and submersing the samples in boiling water until they delaminate. The bonding times correspond to 3 and 6 minutes to see if there was any effect on longer bonding times and subsequent heat treatment. The results in Table 5.2 indicate that with increased exposure to 200°C thermal treatment the bond-line becomes more hydrolytically stable and will not delaminate if treated up to 4 hours. Thermal treatment of solid wood is known to decrease the modulus of rupture and increase the modulus of elasticity[109] resulting in the solid wood sample to become more brittle.To determine if there was a tradeoff between water stability and mechanical bond strength, wood veneer samples were bonded for 3 and 6 minutes and heat treated at 200°C for 2 and 4 hours. The samples were bonded and immediately thermally treated then cut according to ASTM D2339 placed in an environmental chamber at 20°C in 65.8% humidity (12% MC) for two weeks and subsequently tested in shear tension. This test is effective at measuring bond-line strength between veneer samples. The results from half a sample

population for the standard are shown in Figure 5.5 where tests show no thermal exposure time dependence on ultimate shear strength. From control to 2 and 4 hour thermal treatments there is no clear trend in mechanical response, however ultimate shear strength does not seem to be significantly affected by the thermal treatment. With a larger sample size a trend might emerge but these initial tests are promising for improving water stability without losing mechanical properties of the heat treated composites.

Table 5.2. Boiling water tests on laser bonded wood for 3 and 6 minute hot press times and varying thermal treatment time at 200°C

Post heat treatment (min)	3 min hot press time in boiling water (min)	6 min hot press time in boiling water (min)
0	1.2	1
5	2.3	1.7
10	3.3	1.7
20	4.5	1.9
30	5.7	2
60	8.3	3.3
120	56	11
240	over 180	over 180

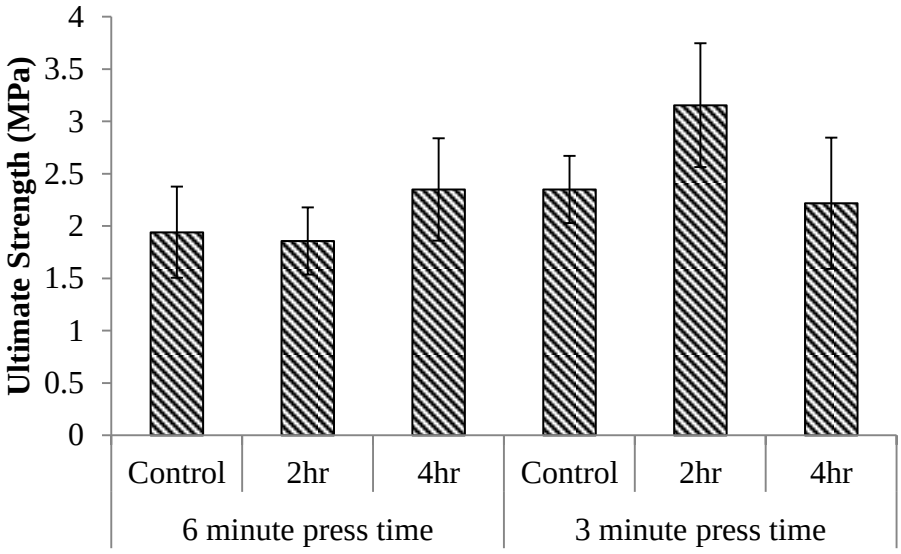

Figure 5.5. Shear tension results for two ply laser bonded wood between different press times and thermal treatment times

CHAPTER 6. Conclusions

6.1 Summary

The CO_2 laser treatment of wood samples was investigated to create veneer composites without added adhesives. A number of laser parameters were screened to determine the amount of laser energy needed and the resulting surface geometries. Induced surface roughness with interlocking (lock and key) type adhesion does not enhance bond-line strength. An unfocused divergent beam with a large spot size and an energy density of 30W/mm^2 was the most efficient and effective for the modification of southern yellow pine and yellow-poplar wood for hot pressing and subsequent bonding. The approximate measurable surface temperature due to laser modification reaches 230°C for the 30W/mm^2. Furthermore, platen temperature and pressure for adequate adhesion is 200°C and 2.3 MPa, respectively.

For the residual wood sample after laser modification, it is observed that laser ablation penetrates up to 10 microns into the surface of wood cell walls. The resulting surface has fused degraded lignocellulosic material between large vessel elements suggesting flow of the surface material. The surface of this modified material compared to the wood control has decreased surface roughness. Moreover, the modified surface has a more homogenous viscoelastic surface compared to wood as determined by AFM images..

The following was determined about the chemistry of laser modified yellow-poplar compared to the wood reference:

- Hemicellulose content decreases
    - Xylose, arabinose, and xylitol are present in the modified material
    - Furfural a dehydration product of xylose also occurs at the surface
- Cellulose content increases

        - Morphological change from native cellulose I to cellulose II
        - Degradation products occur at the surface including levoglucosan, glucose, sorbitol, and hydroxymethyl furfural
    - Lignin content increases
        - Degradation products remain on the surface most notably syringaldehyde
        - β-O-4 linkages are broken and vinyl groups increase during modification
    - Surface analysis revealed
        - Total surface free energy is similar to control
        - London dispersion component of surface free energy increases
        - Acid-base component of the surface free energy decreases
        - Oxygen containing linkages decrease
        - Nitrogen containing extractives (alkaloids) decrease

Supplemental experiments concluded the following:

- Cellulose I to cellulose II content increases due to ramping heat treatment to 200°C
- The degradation profile of modified wood indicate decomposition of two components mainly cellulose and also lignin
- After hot pressing a majority of aromatic degradation products increase
- Pre laser veneer treatment with liquid nitrogen does not decrease overall surface temperature due to infrared light energy
- Post heat treatment of bonded wood improves hydrolytic stability and does not substantially effect mechanical properties

- Thermally treated laser modified surfaces and subsequent hot pressing resists adhesion

The adhesion mechanism is not fully resolved for the laser modification process. It is known that adhesion requires intimate contact between surfaces; laser modification impacts the local surface roughness allowing for intimate association of substrates under pressure. This process is not reversible, so the adhesion is not a simple diffusion/entanglement mechanism. Both secondary interactions and chemical bonding may play a role in the adhesion between the laser modified surfaces. Limited hydrogen bonding potential because of a low acidic surface energy component, combined with increased cinnamyl alcohol groups, and additional degradation products forming after hot pressing, suggests that chemical bonding is important in achieving adhesion. Finally, thermal treatment has shown enhanced performance of the bondline for durability, and the temperatures used for this treatment are equivalent temperatures used to stabilize lignin carbon fibers during heat treatment that cause oxidative radical coupling. Further studies will investigate this potential mechanism in detail.

6.2 Future Work

A deeper understanding of the surface features after hot pressing may suggest a more defined adhesion mechanism. Regarding post heat treatment, the fact that stability increases while mechanical strength remains the same could mean covalent bonding of those surfaces, possibly through oxidative radical coupling, or increased dimensional stability through degradation of hemicelluloses. Further characterization of the water soluble portion of the extracted wood with techniques like gas chromatography paired with mass spectroscopy could identify all degradation compounds within the system. This may lead to a more detailed degradation pathway to further understand the unique effects of the laser technique compared to

heat treatments. Scale up of this process was also underway and may require another look at energy density laser beam optimization. To have an industrially significant process the conditioning of the wood before and after laser treatment and hot pressing to improve bond-line strength needs to be fully developed. Fracture analysis of bonded laminates will further investigate the adhesive performance of the laser modified surfaces.

References

1. Wilson, J. B., Life-Cycle Inventory of Formaldehyde-based Resins Used in Wood Composites in Terms of Resources, Emissions, Energy and Carbon. *Wood and Fiber Science* **2009,** *42* (Corrim Special Issue), 18.
2. USEPA, Formaldehyde Standards for Composite Wood Products Act. Agency, U. E. P., Ed. City of Washington, 2010; pp 1-9.
3. Petroleum product prices. December 5, 2012 ed.; U.S. Energy Information Administration: 2012; p 2.
4. Gfeller, B.; Properzi, M.; Zanetti, M.; Pizzi, A.; Pichelin, F.; Lehmann, M.; Delmotte, L., Wood bonding by mechanically-induced in situ welding of polymeric structural wood constituents. *Journal of Applied Polymer Science* **2004,** *92* (1), 243-251.
5. Fernandes, A. N.; Thomas, L. H.; Altaner, C. M.; Callow, P.; Forsyth, V. T.; Apperley, D. C.; Kennedy, C. J.; Jarvis, M. C., Nanostructure of cellulose microfibrils in spruce wood. *Proceedings of the National Academy of Sciences* **2011,** *108* (47), E1195-E1203.
6. Cosgrove, D. J., Growth of the plant cell wall. *Nature Reviews Molecular Cell Biology* **2005,** *6* (11), 850-861.
7. Sjöström, E., *Wood Chemistry: Fundamentals and Applications*. Academic Press: 1993.
8. Chu, S.; Subrahmanyam, A. V.; Huber, G. W., The pyrolysis chemistry of a [small beta]-O-4 type oligomeric lignin model compound. *Green Chemistry* **2013,** *15* (1), 125-136.
9. Meshitsuka, G.; Nakano, J., Structural Characteristics of Compound Middle Lamella Lignin. *Journal of Wood Chemistry and Technology* **1985,** *5* (3), 391-404.
10. Cote, W. A., Jr. AN ELECTRON MICROSCOPE INVESTIGATION OF THE ORGANIZATION AND FINE STRUCTURE OF THE SECONDARY CELL WALLS OF WOOD. Ph.D., State University of New York College of Environmental Science and Forestry, Ann Arbor, 1958.
11. Walker, J. F., Basic wood chemistry and cell wall ultrastructure. In *Primary Wood Processing*, Springer Netherlands: 2006; pp 23-67.
12. Gfeller, B.; Zanetti, M.; Properzi, M.; Pizzi, A.; Pichelin, F.; Lehmann, M.; Delmotte, L., Wood bonding by vibrational welding. *Journal of Adhesion Science & Technology* **2003,** *17* (11), 1573.
13. Leban, J. M.; Pizzi, A.; Properzi, M.; Pichelin, F.; Gelhaye, P.; Rose, C., Wood welding: A challenging alternative to conventional wood gluing. *Scandinavian Journal of Forest Research* **2005,** *20* (6), 534-538.
14. Delmotte, L.; Mansouri, H. R.; Omrani, P.; Pizzi, A., Influence of Wood Welding Frequency on Wood Constituents Chemical Modifications. *Journal of Adhesion Science & Technology* **2009,** *23* (9), 1271-1279.
15. Gil, A. M.; Neto, C. P., Solid-State Nmr Studies Of Wood And Other Lignocellulosic Materials. In *Annual Reports on NMR Spectroscopy*, Webb, G. A., Ed. Academic Press: 1999; Vol. Volume 37, pp 75-117.
16. Li, D.-n.; Ma, X.-j., Preparation and characterization of activated carbon fibers from liquefied wood. *Cellulose* **2013,** *20* (4), 1649-1656.
17. Antal, M. J.; Gronli, M., The art, science, and technology of charcoal production. *Industrial & Engineering Chemistry Research* **2003,** *42* (8), 1619-1640.
18. Fernández de Simón, B.; Cadahía, E.; del Álamo, M.; Nevares, I., Effect of size, seasoning and toasting in the volatile compounds in toasted oak wood and in a red wine treated with them. *Analytica Chimica Acta* **2010,** *660* (1–2), 211-220.
19. Windeisen, E.; Strobel, C.; Wegener, G., Chemical changes during the production of thermo-treated beech wood. *Wood Sci.Technol.* **2007,** *41* (6), 523-536.

20. Pakdel, H.; AmenChen, C.; Roy, C., Phenolic compounds from vacuum pyrolysis of wood wastes. *CANADIAN JOURNAL OF CHEMICAL ENGINEERING* **1997,** *75* (1), 121-126.
21. Miura, M.; Kaga, H.; Tanaka, S.; Takahashi, K., Rapid Microwave Pyrolysis of Wood. *Journal of chemical engineering of Japan* **2000,** *33* (2), 299-302.
22. Di Blasi, C.; Branca, C.; Galgano, A., Biomass Screening for the Production of Furfural via Thermal Decomposition. *Industrial & Engineering Chemistry Research* **2010,** *49* (6), 2658-2671.
23. Martinka, J.; Kačíková, D.; Hroncová, E.; Ladomerský, J., Experimental determination of the effect of temperature and oxygen concentration on the production of birch wood main fire emissions. *Journal of Thermal Analysis and Calorimetry* **2012,** *110* (1), 193-198.
24. Browne, F. L., Theories of the Combustion of Wood and its Control. Laboratory, F. P., Ed. pp 1-59.
25. Su, Y.; Luo, Y.; Wu, W.; Zhang, Y.; Zhao, S., Characteristics of pine wood oxidative pyrolysis: Degradation behavior, carbon oxide production and heat properties. *Journal of Analytical and Applied Pyrolysis* **2012,** *98* (0), 137-143.
26. Bridgwater, A. V.; Meier, D.; Radlein, D., An overview of fast pyrolysis of biomass. *Organic Geochemistry* **1999,** *30* (12), 1479-1493.
27. Westerhof, R. J. M.; Brilman, D. W. F.; van Swaaij, W. P. M.; Kersten, S. R. A., Effect of Temperature in Fluidized Bed Fast Pyrolysis of Biomass: Oil Quality Assessment in Test Units. *Industrial & Engineering Chemistry Research* **2009,** *49* (3), 1160-1168.
28. Kitani, O.; Hall, C. W., *Biomass handbook*. Gordon and Breach Science Publishers: New York, 1989.
29. Sipilä, K.; Kuoppala, E.; Fagernäs, L.; Oasmaa, A., Characterization of biomass-based flash pyrolysis oils. *Biomass and Bioenergy* **1998,** *14* (2), 103-113.
30. Molton, P. M.; Demmitt, T. F. *Reaction mechanisms in cellulose pyrolysis: a literature review*; 1977.
31. Weinstetn, M.; Broido, A., Pyrolysis-Crystallinity Relationships in Cellulose. *Combustion Science and Technology* **1970,** *1* (4), 287-292.
32. Evans, R. J.; Milne, T. A.; Soltys, M. N., Direct mass-spectrometric studies of the pyrolysis of carbonaceous fuels: III. Primary pyrolysis of lignin. *Journal of Analytical and Applied Pyrolysis* **1986,** *9* (3), 207-236.
33. SURFACE DEGRADATION OF WOOD BY ULTRAVIOLET LIGHT. *Polym. Chem U6 - ctx_ver=Z39.88-2004&ctx_enc=info%3Aofi%2Fenc%3AUTF-8&rfr_id=info:sid/summon.serialssolutions.com&rft_val_fmt=info:ofi/fmt:kev:mtx:journal&rft.genre=article&rft.atitle=SURFACE+DEGRADATION+OF+WOOD+BY+ULTRAVIOLET+LIGHT&rft.jtitle=Polym.+Chem&rft.date=1984-01-01&rft.volume=22&rft.issue=9&rft.spage=2227&rft.epage=2241&paramdict=en-US U7 - Journal Article U8 - FETCH-proquest_abstracts_9031277541* **1984,** *22* (9), 2227-2241.
34. Davidson, R. S., The photodegradation of some naturally occurring polymers. *Journal of Photochemistry & Photobiology, B: Biology* **1996,** *33* (1), 3-25.
35. Hon, N.-S., Formation of free radicals in photoirradiated cellulose. VIII. Mechanisms. *Journal of Polymer Science: Polymer Chemistry Edition* **1976,** *14* (10), 2497-2512.
36. Zuber, M.; Zia, K. M.; Bhatti, I. A.; Ali, Z.; Arshad, M. U.; Saif, M. J., Modification of cellulosic fibers by UV-irradiation. Part II: After treatments effects. *International Journal of Biological Macromolecules* **2012,** *51* (5), 743-748.
37. Tolvaj, L.; Nemeth, R.; Varga, D.; Molnar, S., COLOUR HOMOGENISATION OF BEECH WOOD BY STEAM TREATMENT. *DREWNO-WOOD* **2009,** *52* (181), 5-17.
38. Kačík, F.; Kubovský, I., Chemical changes of beech wood due to CO2 laser irradiation. *Journal of Photochemistry and Photobiology A: Chemistry* **2011,** *222* (1), 105-110.
39. Kangro, H., *Early History of Planck's Radiation Law*. Taylor & Francis: 1976.

40. Einstein, A., On the quantum theory of radiation. *Phys. Z* **1917,** *18*, 121-128.
41. Bertolotti, M., *Masers and lasers : an historical approach*. A. Hilger: Bristol, 1983.
42. Maini, A., Lasers and Optoelectronics : Fundamentals, Devices and Applications. 1 ed.; Wiley: Hoboken, 2013. http://viva.eblib.com/patron/FullRecord.aspx?p=1343443.
43. Powell, J., *CO_2 laser cutting*. Springer-Verlag: New York, 1993.
44. Williams, D., Laser basics. *Anaesthesia & Intensive Care Medicine* **2008,** *9* (12), 550-552.
45. Kannatey-Asibu, E., *Principles of Laser Materials Processing*. Wiley: 2009.
46. Günther, H., *NMR Spectroscopy: Basic Principles, Concepts and Applications in Chemistry*. Wiley: Hoboken, 2013.
47. Balci, M., 1 - Introduction. In *Basic 1H- and 13C-NMR Spectroscopy*, Balci, M., Ed. Elsevier Science: Amsterdam, 2005; pp 3-8.
48. Conte, P.; Spaccini, R.; Piccolo, A., State of the art of CPMAS 13C-NMR spectroscopy applied to natural organic matter. *Progress in Nuclear Magnetic Resonance Spectroscopy* **2004,** *44* (3), 215-223.
49. Cao, X.; Pignatello, J. J.; Li, Y.; Lattao, C.; Chappell, M. A.; Chen, N.; Miller, L. F.; Mao, J., Characterization of Wood Chars Produced at Different Temperatures Using Advanced Solid-State 13C NMR Spectroscopic Techniques. *Energy & Fuels* **2012,** *26* (9), 5983-5991.
50. Maunu, S. L., NMR studies of wood and wood products. *Progress in Nuclear Magnetic Resonance Spectroscopy* **2002,** *40* (2), 151-174.
51. Mandal, P. K.; Majumdar, A., A comprehensive discussion of HSQC and HMQC pulse sequences. *Concepts in Magnetic Resonance Part A* **2004,** *20A* (1), 1-23.
52. Yelle, D. J.; Ralph, J.; Frihart, C. R., Characterization of nonderivatized plant cell walls using high-resolution solution-state NMR spectroscopy. *Magnetic resonance in chemistry : MRC* **2008,** *46* (6), 508-517.
53. Heikkinen, S.; Toikka, M. M.; Karhunen, P. T.; Kilpeläinen, I. A., Quantitative 2D HSQC (Q-HSQC) via Suppression of J-Dependence of Polarization Transfer in NMR Spectroscopy: Application to Wood Lignin. *Journal of the American Chemical Society* **2003,** *125* (14), 4362-4367.
54. Conley, R. T., *Infrared spectroscopy*. Allyn and Bacon: Boston U6 - ctx_ver=Z39.88-2004&ctx_enc=info%3Aofi%2Fenc%3AUTF-8&rfr_id=info:sid/summon.serialssolutions.com&rft_val_fmt=info:ofi/fmt:kev:mtx:book&rft.genre=book&rft.title=Infrared+spectroscopy&rft.au=Conley%2C+Robert+T&rft.series=The+Allyn+and+Bacon+chemistry+series&rft.date=1972-01-01&rft.pub=Allyn+and+Bacon&rft.externalDocID=b11100710&paramdict=en-US U7 - Book U8 - FETCH-vt_catalog_b111007101, 1972.
55. Berthomieu, C.; Hienerwadel, R. *Fourier transform infrared (FTIR) spectroscopy*; Springer Science & Business Media: Dordrecht, Sep 2009, 2009; pp 157-70.
56. Faix, O., Practical uses of FTIR spectroscopy in wood science and technology. *Mikrochim Acta* **1988,** *94* (1-6), 21-25.
57. Pandey, K. K., A study of chemical structure of soft and hardwood and wood polymers by FTIR spectroscopy. *Journal of Applied Polymer Science* **1999,** *71* (12), 1969-1975.
58. Emandi, A.; Vasiliu, C. I.; Budrugeac, P.; Stamatin, I., QUANTITATIVE INVESTIGATION OF WOOD COMPOSITION BY INTEGRATED FT-IR AND THERMOGRAVIMETRIC METHODS. *CELLULOSE CHEMISTRY AND TECHNOLOGY* **2011,** *45* (9-10), 579-584.
59. Pleul, D.; Simon, F., X-Ray Photoelectron Spectroscopy. Springer Berlin Heidelberg: Berlin, Heidelberg, 2008; pp 71-89.
60. Lee, H.-L.; Flynn, N. T., X-RAY PHOTOELECTRON SPECTROSCOPY. Springer US: Boston, MA, 2006; pp 485-507.
61. Popescu, C.-M.; Tibirna, C.-M.; Vasile, C., XPS characterization of naturally aged wood. *Applied Surface Science* **2009,** *256* (5), 1355-1360.

62. Inari, G. N.; Petrissans, M.; Lambert, J.; Ehrhardt, J. J.; Gérardin, P., XPS characterization of wood chemical composition after heat-treatment. *Surface and Interface Analysis* **2006,** *38* (10), 1336-1342.
63. Delange, P. J.; Dekreek, A. K.; Vanlinden, A.; Coenjaarts, N. J., WEATHERING OF WOOD MEASURED BY XPS AND IMAGING XMA. *INSTITUTE OF PHYSICS CONFERENCE SERIES* **1993,** (130), 439-442.
64. Shen, Q.; Mikkola, P.; Rosenholm, J. B., Quantitative characterization of the subsurface acid–base properties of wood by XPS and Fowkes theory. *Colloids and Surfaces A: Physicochemical and Engineering Aspects* **1998,** *145* (1–3), 235-241.
65. D'Ascenzo, G.; Nicolini, N., Evolution of paper chromatography: from Runge's perceptions to Tswett's adsorption. *Fresenius J Anal Chem* **1990,** *337* (2), 232-234.
66. Farradane, J., History of chromatography. *Nature* **1951,** *167* (4238), 120-120.
67. Lee, T. D., Introduction to Modern Liquid Chromatography, Third Edition: Lloyd R. Snyder, Joseph J. Kirkland, John W. Dolan, Authors John Wiley & Sons, Inc. Hoboken, NJ, USA ISBN 978-0-470-16754-0 2010, Hardcover, $125.00 US, 912 pp. *Journal of The American Society for Mass Spectrometry* **2011,** *22* (1), 196-196.
68. Sluiter, A.; National Renewable Energy, L., *Determination of structural carbohydrates and lignin in biomass: laboratory analytical procedure (LAP) : issue date, 4/25/2008*. National Renewable Energy Laboratory: Golden, Colo U6 - ctx_ver=Z39.88-2004&ctx_enc=info%3Aofi%2Fenc%3AUTF-8&rfr_id=info:sid/summon.serialssolutions.com&rft_val_fmt=info:ofi/fmt:kev:mtx:book&rft.genre=book&rft.title=Determination+of+structural+carbohydrates+and+lignin+in+biomass&rft.au=Sluiter%2C+A&rft.series=Technical+report&rft.date=2008-01-01&rft.pub=National+Renewable+Energy+Laboratory&rft.volume=NREL%2FTP-510-42618&rft.externalDocID=b25726547 U7 - eBook U8 - FETCH-vt_catalog_b257265471, 2008; Vol. NREL/TP-510-42618.
69. (a) Kim, H.; Ralph, J., Solution-state 2D NMR of ball-milled plant cell wall gels in DMSO-d6/pyridine-d5. *Org. Biomol. Chem.* **2010,** *8* (3), 576-591; (b) Mansfield, S. D.; Kim, H.; Lu, F.; Ralph, J., Whole plant cell wall characterization using solution-state 2D NMR. *Nat. Protoc.* **2012,** *7* (9), 1579-1589.
70. Heikkinen, S.; Toikka, M. M.; Karhunen, P. T.; Kilpeläinen, I. A., Quantitative 2D HSQC (Q-HSQC) via suppression of J-dependence of polarization transfer in NMR spectroscopy: application to wood lignin. *Journal of the American Chemical Society* **2003,** *125* (14), 4362-4367.
71. Yelle, D. J.; Ralph, J.; Frihart, C. R., Characterization of nonderivatized plant cell walls using high-resolution solution-state NMR spectroscopy. *Magn. Reson. Chem.* **2008,** *46* (6), 508-517.
72. Sette, M.; Wechselberger, R.; Crestini, C., Elucidation of lignin structure by quantitative 2D NMR. *Chem. Eur. J.* **2011,** *17* (34), 9529-9535.
73. Del Río, J. C.; Rencoret, J.; Prinsen, P.; Martínez, A. T.; Ralph, J.; Gutiérrez, A., Structural characterization of wheat straw lignin as revealed by analytical pyrolysis, 2D-NMR, and reductive cleavage methods. *J. Agric. Food. Chem.* **2012,** *60* (23), 5922-5935.
74. Serrano, E., A numerical study of the shear-strength-predicting capabilities of test specimens for wood–adhesive bonds. *International Journal of Adhesion and Adhesives* **2004,** *24* (1), 23-35.
75. Laboratory, F. P.; Agriculture, U. S. D. o., *The Encyclopedia of Wood*. Skyhorse Pub.: 2007.
76. Yasuda, S.; Fukushima, K.; Kakehi, A., Formation and chemical structures of acid-soluble lignin I: sulfuric acid treatment time and acid-soluble lignin content of hardwood. *J Wood Sci* **2001,** *47* (1), 69-72.
77. Rowell, R. M.; LeVan-Green, S. L., Wood Chemistry and Wood Composites USDA, Ed. CRC Press: 2005; pp 121-137.
78. Hequet, E. F.; Henneberry, T. J.; Nichols, R. L.; United States. Agricultural Research, S., *Sticky cotton: causes, effects, and prevention*. US. Dept. of Agriculture, Agricultural Research Service: Washington, D.C. U6 - ctx_ver=Z39.88-2004&ctx_enc=info%3Aofi%2Fenc%3AUTF-8&rfr_id=info:sid/summon.serialssolutions.com&rft_val_fmt=info:ofi/fmt:kev:mtx:book&rft.genre=book

&rft.title=Sticky+cotton&rft.au=Hequet%2C+Eric+F&rft.au=Henneberry%2C+T.+J&rft.au=Nichols%2C+R.+L&rft.series=Technical+bulletin&rft.date=2007-01-01&rft.pub=US.+Dept.+of+Agriculture%2C+Agricultural+Research+Service&rft.volume=no.+1915&rft.externalDocID=b29625634&paramdict=en-US U7 - eBook U8 - FETCH-vt_catalog_b296256341, 2007; Vol. no. 1915.

79. Brebu, M.; Vasile, C., THERMAL DEGRADATION OF LIGNIN - A REVIEW. *CELLULOSE CHEMISTRY AND TECHNOLOGY* **2010,** *44* (9), 353-363.

80. Melkior, T.; Jacob, S.; Gerbaud, G.; Hediger, S.; Le Pape, L.; Bonnefois, L.; Bardet, M., NMR analysis of the transformation of wood constituents by torrefaction. *Fuel* **2012,** *92* (1), 271-280.

81. Kamide, K., *Cellulose and Cellulose Derivatives*. Elsevier Science: 2005.

82. Terinte, N.; Ibbett, R.; Schuster, K. C., Overview on Native Cellulose and Microcrystalline cellulose I structure studied by X-ray Diffraction (WAXD): Comparison Between Measurement Techniques. *Lenzinger Berichte* **2011,** (89), 118-131.

83. Borysiak, S.; Doczekalska, B., X-ray diffracfion study of pine wood treated with NaOH. *FIBRES & TEXTILES IN EASTERN EUROPE* **2005,** *13* (5), 87-89.

84. Kroon-Batenburg, L. M. J.; Kroon, J., The crystal and molecular structures of cellulose I and II. *Glycoconjugate Journal* **1997,** *14* (5), 677-690.

85. Hon, D. N.-S.; Shiraishi, N., *Wood and Cellulosic Chemistry*. 2 ed.; Marcel Dekker: 2001.

86. Houminer, Y.; Patai, S., Thermal polymerization of levoglucosan. *Journal of Polymer Science Part A-1: Polymer Chemistry* **1969,** *7* (10), 3005-3014.

87. Fowkes, F. M., ATTRACTIVE FORCES AT INTERFACES. *Industrial & Engineering Chemistry* **1964,** *56* (12), 40-52.

88. Fowkes, F. M.; Mostafa, M. A., Acid-Base Interactions in Polymer Adsorption. *Industrial & Engineering Chemistry Product Research and Development* **1978,** *17* (1), 3-7.

89. Van Oss, C. J.; Good, R. J.; Chaudhury, M. K., Additive and nonadditive surface tension components and the interpretation of contact angles. *Langmuir* **1988,** *4* (4), 884-891.

90. Wålinder, M. E. P., Study of Lewis Acid-Base Properties of Wood by Contact Angle Analysis. In *Holzforschung*, 2002; Vol. 56, p 363.

91. Colom, X.; Carrillo, F.; Nogués, F.; Garriga, P., Structural analysis of photodegraded wood by means of FTIR spectroscopy. *Polymer degradation and stability* **2003,** *80* (3), 543-549.

92. Papp, G.; Barta, E.; Preklet, E.; Tolvaj, L.; Berkesi, O.; Nagy, T.; Szatmári, S., Changes in DRIFT spectra of wood irradiated by UV laser as a function of energy. *Journal of Photochemistry and Photobiology A: Chemistry* **2005,** *173* (2), 137-142.

93. Oh, S. Y.; Yoo, D. I.; Shin, Y.; Kim, H. C.; Kim, H. Y.; Chung, Y. S.; Park, W. H.; Youk, J. H., Crystalline structure analysis of cellulose treated with sodium hydroxide and carbon dioxide by means of X-ray diffraction and FTIR spectroscopy. *Carbohydrate Research* **2005,** *340* (15), 2376-2391.

94. Kondo, T.; Sawatari, C., A Fourier transform infra-red spectroscopic analysis of the character of hydrogen bonds in amorphous cellulose. *Polymer* **1996,** *37* (3), 393-399.

95. Ciolacu, D.; Ciolacu, F.; Popa, V. I., AMORPHOUS CELLULOSE - STRUCTURE AND CHARACTERIZATION. *CELLULOSE CHEMISTRY AND TECHNOLOGY* **2011,** *45* (1-2), 13-21.

96. Zavarin, E., Activation of Wood Surface and Nonconventional Bonding. In *The Chemistry of Solid Wood*, American Chemical Society: 1984; Vol. 207, pp 349-400.

97. Fowkes, F. M., QUANTITATIVE CHARACTERIZATION OF THE ACID-BASE PROPERTIES OF SOLVENTS, POLYMERS, AND INORGANIC SURFACES. *JOURNAL OF ADHESION SCIENCE AND TECHNOLOGY* **1990,** *4* (8), 669-691.

98. Chen-Loung, C.; Hou-Min, C.; Cowling, E. B., Aporphine alkaloids and lignans in heartwood of Liriodendron tulipifera. *Phytochemistry* **1976,** *15* (4), 547-550.

99. (a) Hillis, W. E., Formation and properties of some wood extractives. *Phytochemistry* **1972,** *11* (4), 1207-1218; (b) Taylor, A. M.; Gartner, B. L.; Morrell, J. J., Heartwood formation and natural durability - A review. *Wood and Fiber Science* **2002,** *34* (4), 587-611.
100. Pizzi, A. M. K. L., *Handbook of adhesive technology*. M. Dekker: New York, 2003.
101. Tolvaj, L.; Persze, L.; Albert, L., Thermal degradation of wood during photodegradation. *Journal of Photochemistry and Photobiology B: Biology* **2011,** *105* (1), 90-93.
102. Cousins, W. J., Elastic modulus of lignin as related to moisture content. *Wood Sci.Technol.* **1976,** *10* (1), 9-17.
103. Cousins, W. J., Young's modulus of hemicellulose as related to moisture content. *Wood Sci.Technol.* **1978,** *12* (3), 161-167.
104. Eichhorn, S. J.; Young, R. J., The Young's modulus of a microcrystalline cellulose. *Cellulose* **2001,** *8* (3), 197-207.
105. Quéré, D., Rough ideas on wetting. *Physica A: Statistical Mechanics and its Applications* **2002,** *313* (1), 32-46.
106. Aydemir, D.; Gunduz, G.; Altuntas, E.; Ertas, M.; Sahin, H. T.; Alma, M. H., INVESTIGATING CHANGES IN THE CHEMICAL CONSTITUENTS AND DIMENSIONAL STABILITY OF HEAT-TREATED HORNBEAM AND ULUDAG FIR WOOD. *BioResources* **2011,** *6* (2), 1308-1321.
107. Beall, F. C.; Eickner, H. W.; Forest Products Lab Madison, W. I. S., THERMAL DEGRADATION OF WOOD COMPONENTS: A REVIEW OF THE LITERATURE. 1970.
108. Burhenne, L.; Messmer, J.; Aicher, T.; Laborie, M.-P., The effect of the biomass components lignin, cellulose and hemicellulose on TGA and fixed bed pyrolysis. *Journal of Analytical and Applied Pyrolysis* **2013,** *101* (0), 177-184.
109. Windeisen, E.; Bächle, H.; Zimmer, B.; Wegener, G., Relations between chemical changes and mechanical properties of thermally treated wood 10th EWLP, Stockholm, Sweden, August 25–28, 2008. *Holzforschung: International Journal of the Biology, Chemistry, Physics, & Technology of Wood* **2009,** *63* (6), 773-778.

Appendix A. Compression Shear Block Analysis Results and sample dimensions

	Lap specimens in compression shear (MPa)					
Treatment	1		2		3	
Sample	SYP	Yellow-poplar	SYP	Yellow-poplar	SYP	Yellow-poplar
1	8.4	5.8	4.1	3.7	5.9	6.3
2	6.4	3.4	3.2	3.9	5.7	9.9
3	6.0	7.1	3.2	3.8	3.7	6.8
4	6.5	3.8	6.0	3.4	8.5	4.1
5	0.2	3.2	1.3	3.3	6.6	8.3
6	2.3	6.3	6.2	2.9	5.5	6.0
7	7.3	6.5	1.6	0.0	7.2	6.8
8	6.3	3.9	2.6	0.0	6.9	6.7
9	5.2	3.8	4.0	0.0	8.9	5.8
10	2.3	2.7	0.7	0.0	4.7	6.5
11	7.2	5.9	3.7	0.0	5.5	4.8
12	6.8	3.0	1.9	0.0	9.2	7.4
13	6.6	2.7	3.9	0.0	6.5	8.4
14	6.2	5.4	3.5	0.0	6.6	5.2
15	3.3	5.5	2.8	0.0	7.4	5.0
16	5.2	4.7	1.3	0.0	8.6	7.5
17	6.3	4.5	2.8	0.0	7.6	6.7
18	5.3	3.5	0.0	0.0	3.5	8.1
19	5.0	5.0	0.0	0.0	5.6	4.4
20	6.7	3.6	0.0	0.0	7.6	5.3
21	7.0	5.7	0.0	0.0	9.3	6.1
22	6.2	4.3	0.0	0.0	5.6	7.5
23	5.0	6.3	0.0	0.0	6.9	6.4
24	6.4	4.4	0.0	0.0	7.6	7.5
Average	5.6	4.6	2.2	0.9	6.7	6.6
Standard Deviation	1.86	1.32	1.92	1.57	1.60	1.39

Sample Dimensions

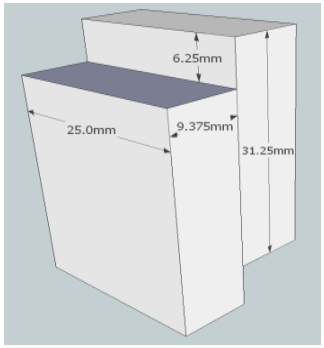

Appendix B. Scanning Electron Microscopy Ablated Channel Measurements

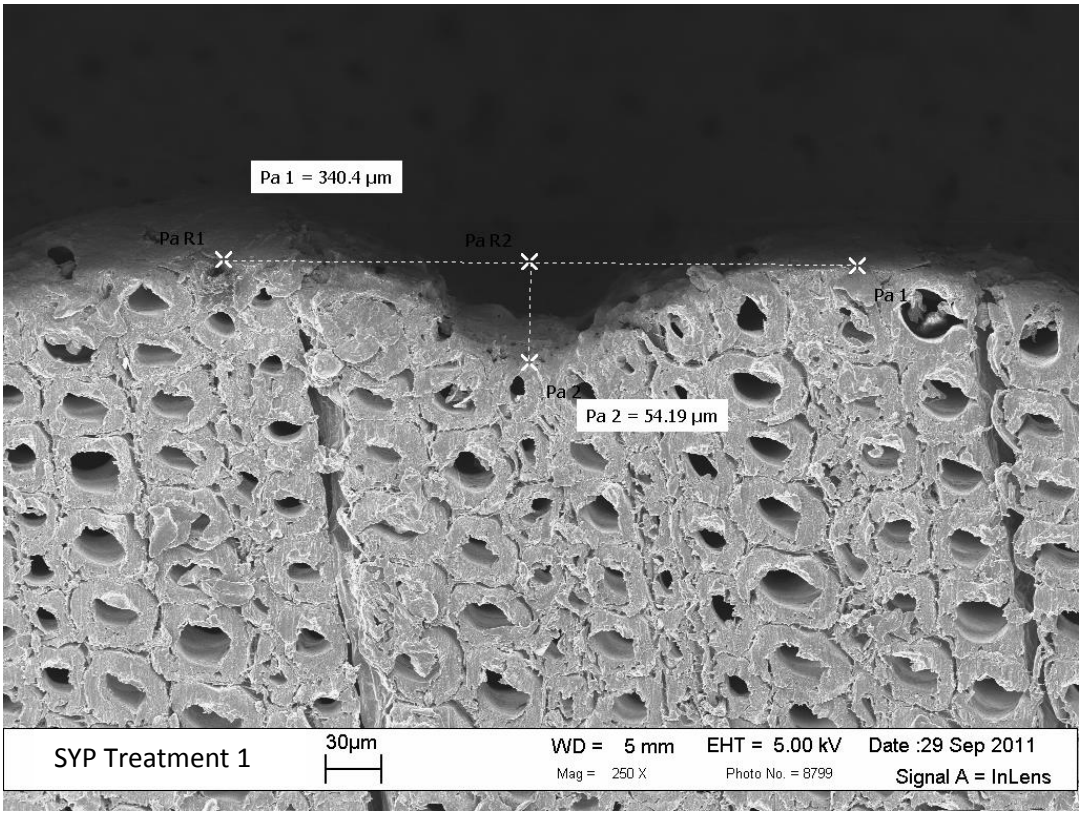

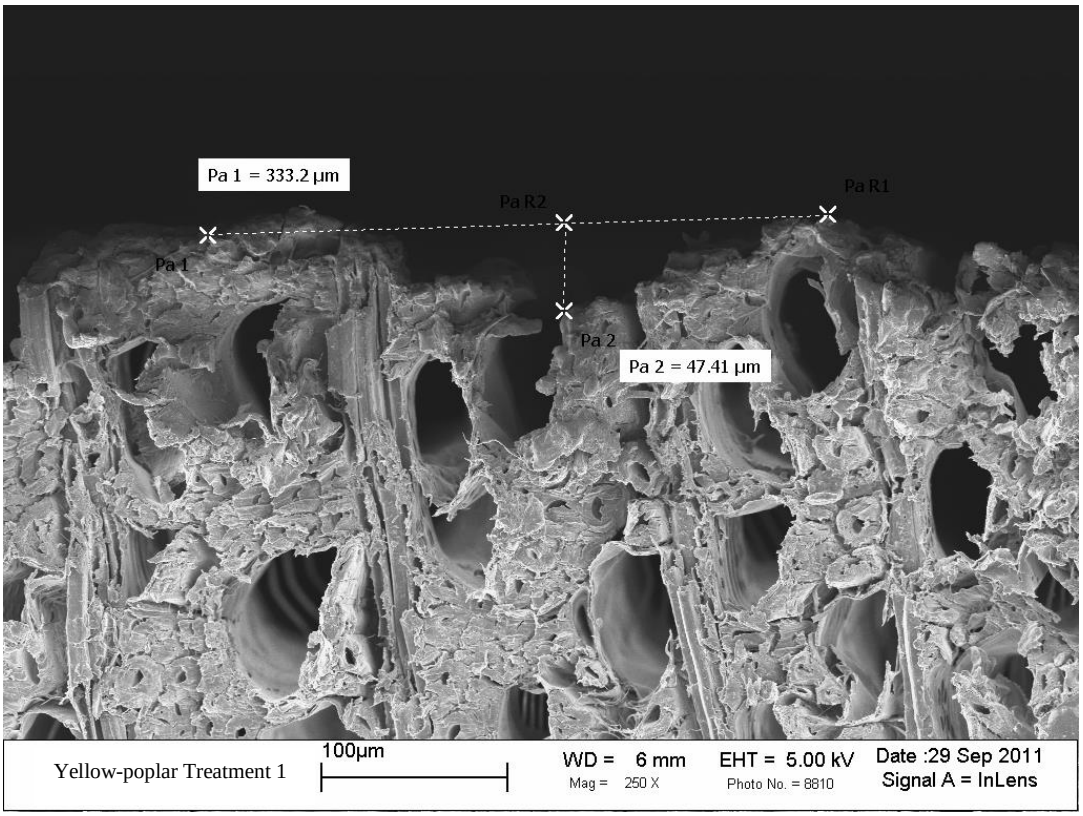

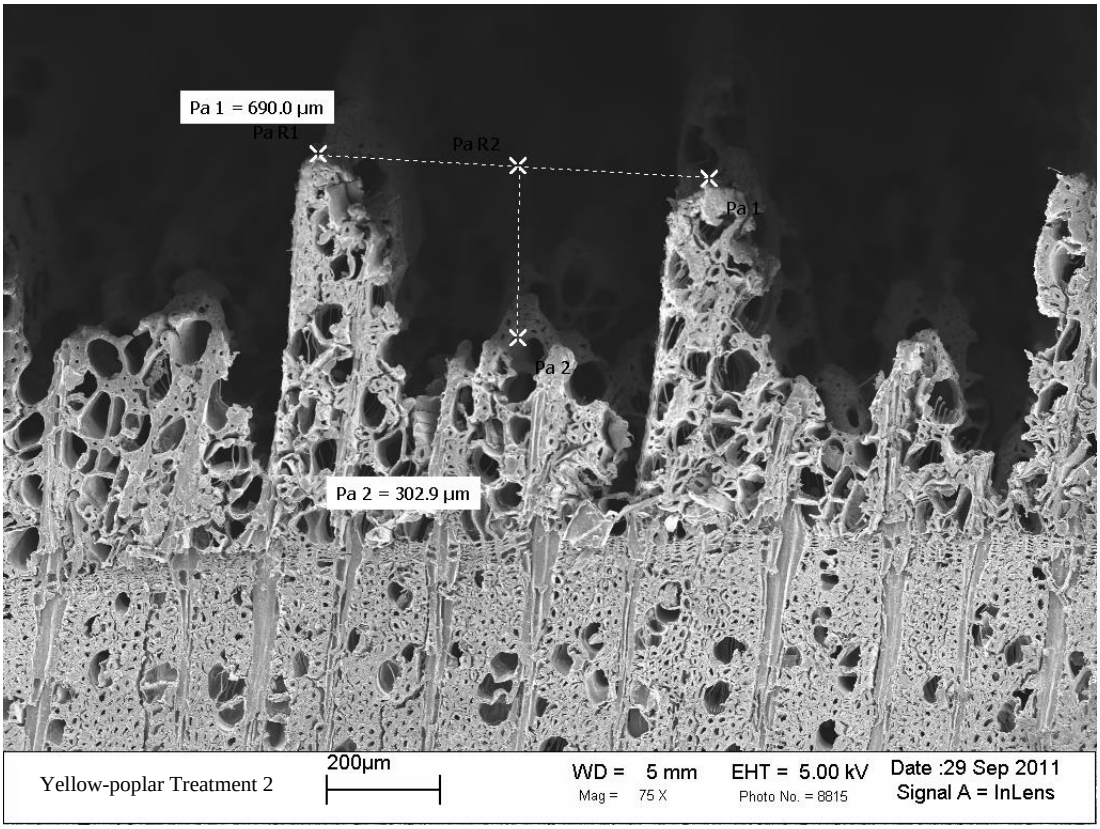
Pa 1 = 690.0 µm
Pa R1
Pa R2
Pa 1
Pa 2
Pa 2 = 302.9 µm
Yellow-poplar Treatment 2
200µm
WD = 5 mm
Mag = 75 X
EHT = 5.00 kV
Photo No. = 8815
Date :29 Sep 2011
Signal A = InLens

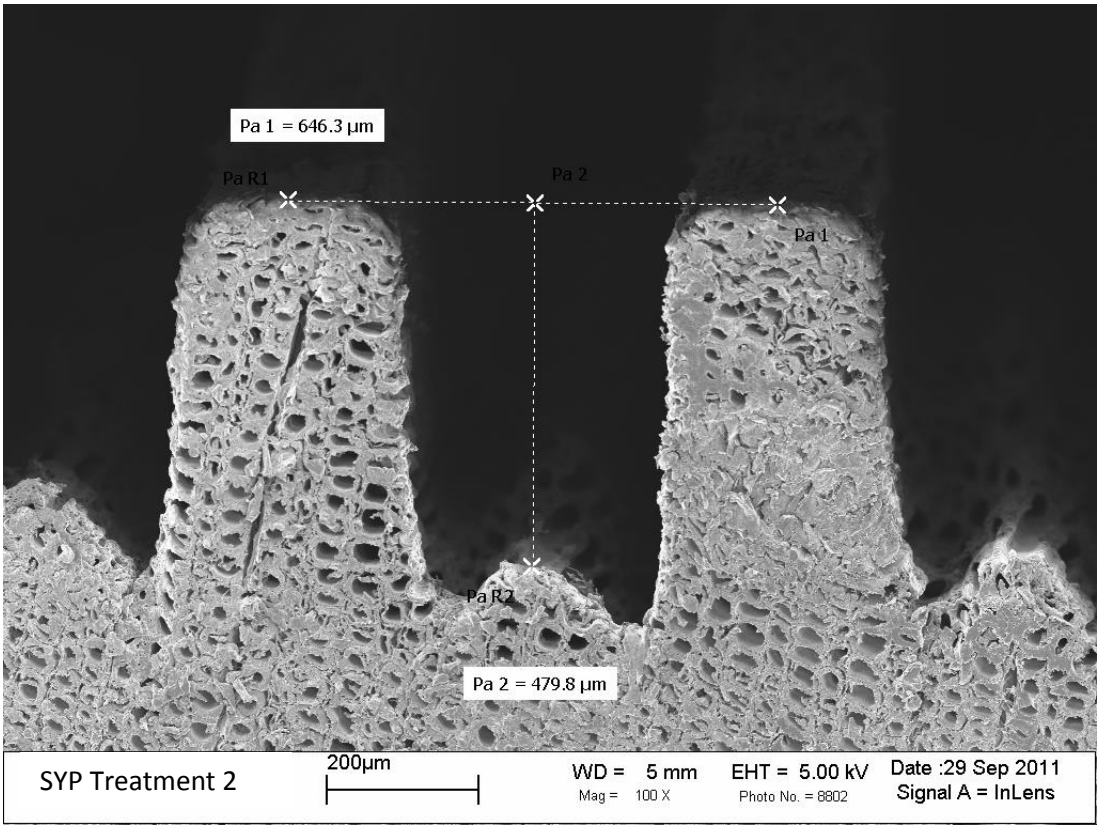
Pa 1 = 646.3 µm
Pa R1
Pa 2
Pa 1
Pa R2
Pa 2 = 479.8 µm
SYP Treatment 2
200µm
WD = 5 mm
Mag = 100 X
EHT = 5.00 kV
Photo No. = 8802
Date :29 Sep 2011
Signal A = InLens

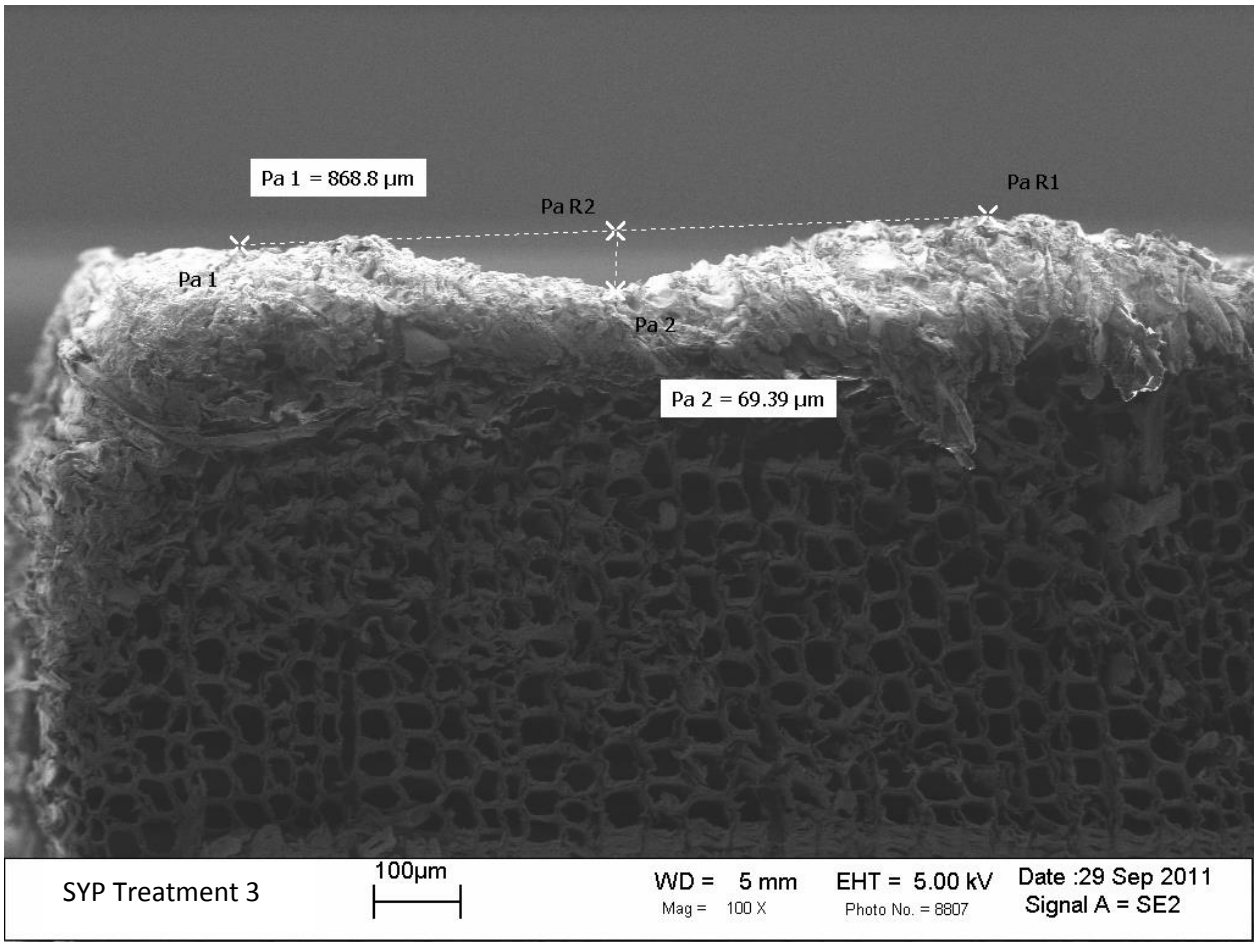
Pa 1 = 868.8 µm
Pa R2
Pa R1
Pa 1
Pa 2
Pa 2 = 69.39 µm
SYP Treatment 3
100µm
WD = 5 mm
Mag = 100 X
EHT = 5.00 kV
Photo No. = 8807
Date :29 Sep 2011
Signal A = SE2

Appendix C. List of ^{13}C Solid State NMR Wood Spectra Assignments

Chemical Shift (ppm)	Assignment
172	Hemicelluloses: –<u>C</u>OO–R, CH_3–<u>C</u>OO–
152.6	Lignin: S-3(e), S-5(e)
148–147	Lignins: S-3(ne), S-5(ne), G-3(ne, e), G-4(ne, e)
138–138.5	Lignins: S-1(e), S-4(e), G-1(e)
134–133	Lignins: S-1(ne), S-4(ne), G-1(ne)
121	Lignin: G-6
114–106	Lignins: G-5, G-6, S-2, S-6
104.8	Cellulose: C-1
104–101	Hemicelluloses: C-1
88.7	Carbohydrates: C-4 cellulose (ordered)
83.8	Lignins: Cβ
	Carbohydrates: C-4 cellulose (disordered)
74.8	Lignins: Cα
	Carbohydrates: C-2,-3,-5
72.2	Carbohydrates: C-2,-3,-5
64.7	Carbohydrates: C-6 cellulose (ordered)
61.6	Lignins: Cγ
	Carbohydrates: C-6 cellulose (disordered)
55.7	Lignins: O<u>C</u>H_3
21	Hemicelluloses: <u>C</u>H_3–COO–
S= carbon in syringyl units, G=carbon in gauiacyl units, ne=in non-etherified arylglycerol β-aryl ethers, e= in etherified arylglycerol β-aryl ethers[80]	

Appendix D. 2D HSQC Peak Assignments and Spectra for untreated and laser modified Yellow-poplar

Assignments of carbohydrates/lignin ^{13}C-^{1}H correlation peaks in the 2D HSQC spectra of untreated and laser modified yellow-poplar

Region	Label	δ_C/δ_H (ppm)	Assignment
Aliphatic	A_α	71.8/4.83	C_α–H_α in β-O-4' substructures (**A**)
	$A_{\beta(G)}$	83.4/4.27	C_β–H_β in β-O-4' substructures (**A**) linked to a G unit
	$A_{\beta(S)}$	85.9/4.10	C_β–H_β in β-O-4' substructures linked (**A**) to a S unit
	B_α	86.8/5.43	C_α–H_α in β-5 phenylcoumaran substructures (**B**)
	C_α	84.8/4.65	C_α–H_α in β–β' resinol substructures (**C**)
	C_β	53.5/3.05	C_β–H_β in β–β' resinol substructures (**C**)
	C_γ	71.1/3.81 & 4.16	C_γ–H_γ in β–β' resinol substructures (**C**)
	E_γ	61.3/4.08	C_γ–H_γ in cinnamyl alcohol end-groups (**E**) overlaps with carbohydrate signals
	MeO (–OCH_3)	55.6/3.73	C–H in methoxyls
	X_2'	99.4/4.50	2-*O*-Ac-β-D-Xyl*p*(R)
	X_3'	101.5/4.39	3-*O*-Ac-β-D-Xyl*p*(R)
Aromatic	G_2	110.9/6.99	C_2–H_2 in guaiacyl units (**G**)
	G_5/G_6	114.9/6.72 and 6.94	C_5–H_5 and C_6–H_6 in guaiacyl units (**G**)
	G_5	118.7/6.77	C_5–H_5 in guaiacyl units (**G**)
	$S_{2,6}$	103.8/6.69	C_2–H_2 and C_6–H_6 in etherified syringyl units (**S**)
Anomeric	(1-4)-β-D-Glc*p*		Cellulose
	D-α-Glc*p*(R)		C_α–H_α reducing end of glucose
	D-β-Glc*p*(R)		C_β–H_β reducing end of glucose
	(1-4)-β-D-Xyl*p*		Xylan
	D-α-Xyl*p*(R)		C_α–H_α reducing end of xylose
	D-β-Xyl*p*(R)		C_β–H_β reducing end of xylose
	2-*O*-Ac-β-D-Man*p*		O-2 acetylated mannan
	3-*O*-Ac-β-D-Man*p*		O-3 acetylated mannan

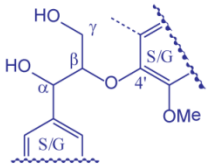

A
β-aryl ether (β-O-4)

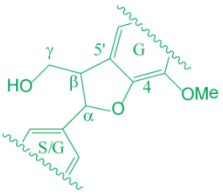

B
Phenylcoumaran (β-5)

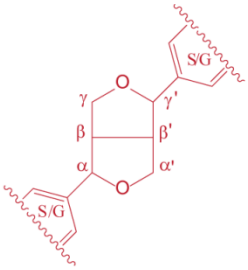

C
Resinol (β-β)

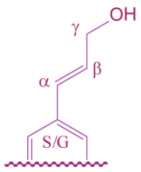

E
Cinnamyl alcohol end-groups

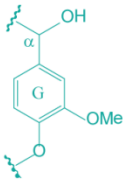

G
Guaiacyl

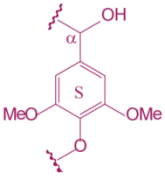

S
Syringyl

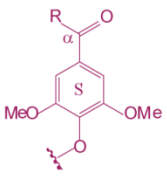

S'
Oxidized syringyl

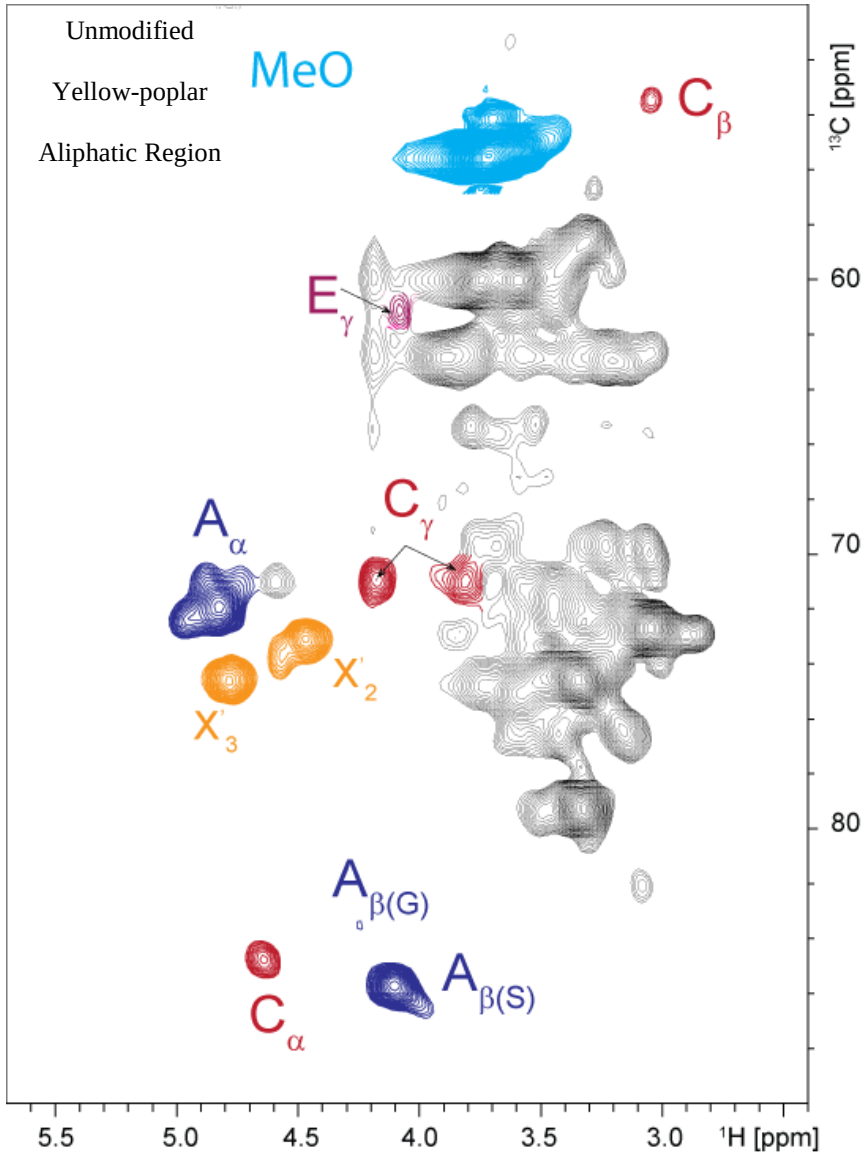
Unmodified
Yellow-poplar
Aliphatic Region
MeO
C β
E γ
C γ
A α
X' 2
X' 3
A β(G)
A β(S)
C α
60
70
80
13C [ppm]
5.5
5.0
4.5
4.0
3.5
3.0
1H [ppm]

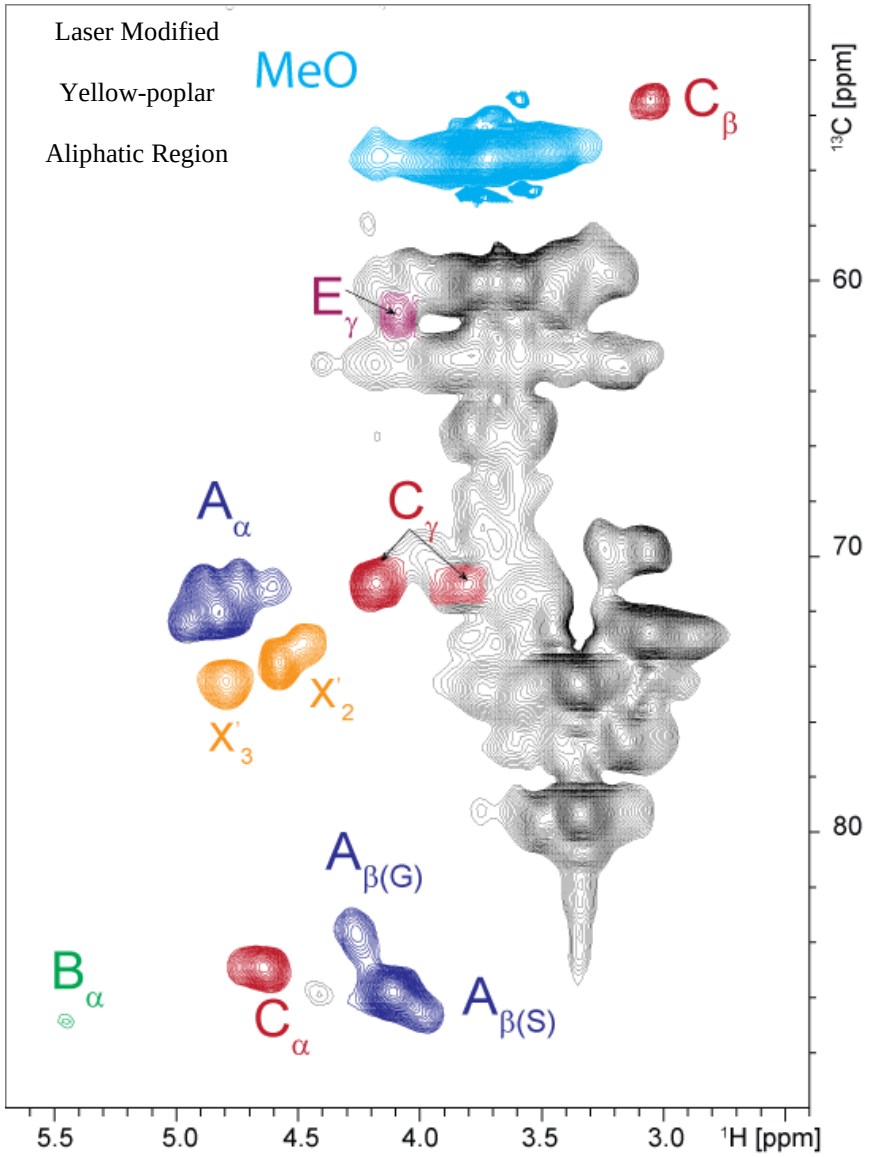
Laser Modified
Yellow-poplar
Aliphatic Region
MeO
C β
E γ
C γ
A α
X' 2
X' 3
A β(G)
B α
C α
A β(S)
60
70
80
13C [ppm]
5.5
5.0
4.5
4.0
3.5
3.0
1H [ppm]

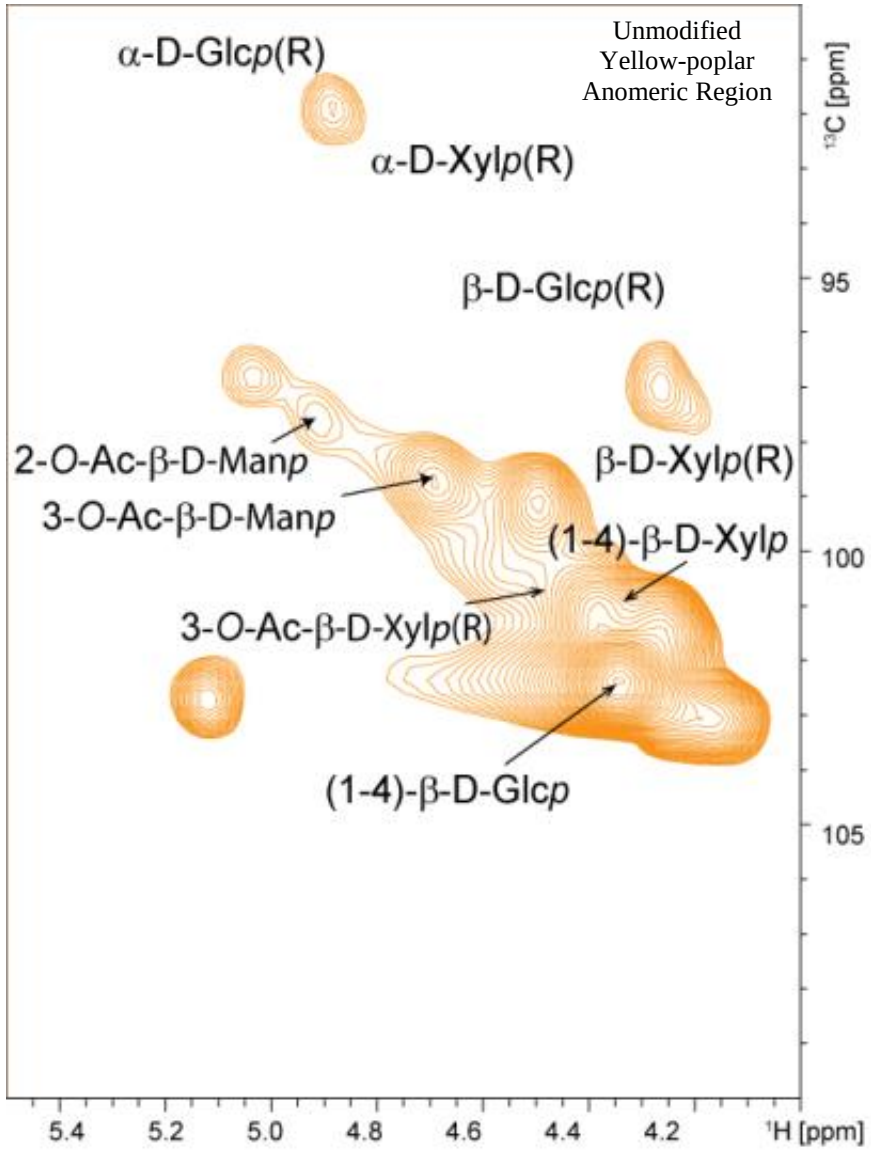
Unmodified
Yellow-poplar
Anomeric Region
α-D-Glcp(R)
α-D-Xylp(R)
β-D-Glcp(R)
β-D-Xylp(R)
2-O-Ac-β-D-Manp
3-O-Ac-β-D-Manp
(1-4)-β-D-Xylp
3-O-Ac-β-D-Xylp(R)
(1-4)-β-D-Glcp
95
100
105
13C [ppm]
5.4
5.2
5.0
4.8
4.6
4.4
4.2
1H [ppm]

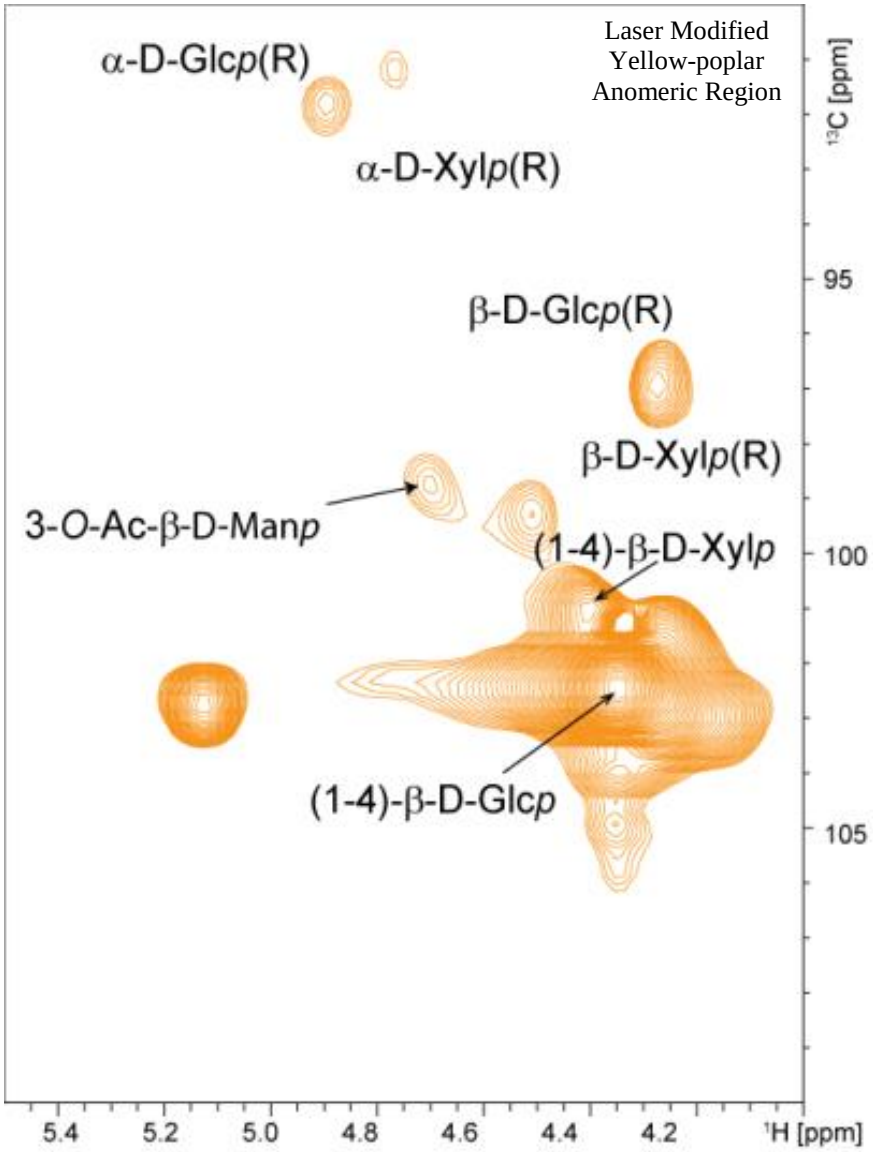
Laser Modified
Yellow-poplar
Anomeric Region
α-D-Glcp(R)
α-D-Xylp(R)
β-D-Glcp(R)
β-D-Xylp(R)
3-O-Ac-β-D-Manp
(1-4)-β-D-Xylp
(1-4)-β-D-Glcp
95
100
105
13C [ppm]
5.4
5.2
5.0
4.8
4.6
4.4
4.2
1H [ppm]

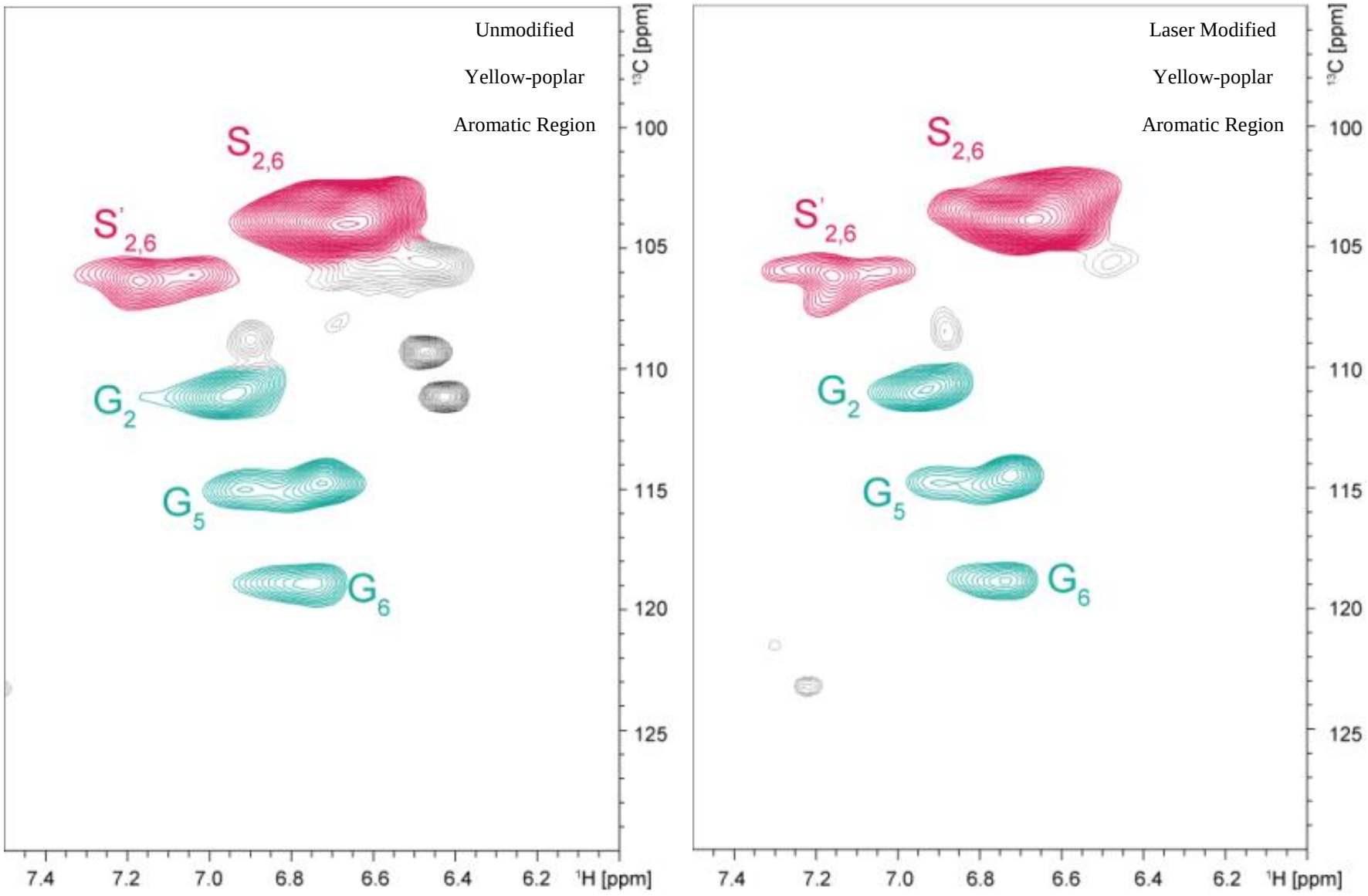
Unmodified
Yellow-poplar
Aromatic Region
S2,6
S'2,6
G2
G5
G6
13C [ppm]
100
105
110
115
120
125
7.4
7.2
7.0
6.8
6.6
6.4
6.2
1H [ppm]
Laser Modified
Yellow-poplar
Aromatic Region
S2,6
S'2,6
G2
G5
G6
13C [ppm]
100
105
110
115
120
125
7.4
7.2
7.0
6.8
6.6
6.4
6.2
1H [ppm]

Appendix E. X-Ray Photoelectron High Resolution Peak fit data and Wide Scan compositional summary

Peak Fit Data Carbons

Heartwood Yellow-poplar

r^2 Coef Det 0.999

Peak	Type	Amplitude	Center	% Area
1	Gauss	5090	284.8	51.7
2	Gauss	2877	286.2	39.0
3	Gauss	709	287.9	6.2
4	Gauss	308	289.1	3.1

Sapwood Yellow-poplar

r^2 Coef Det 0.999

Peak	Type	Amplitude	Center	% Area
1	Gauss	5988	284.7	50.4
2	Gauss	4380	286.2	36.9
3	Gauss	1233	287.8	10.4
4	Gauss	277	289.0	2.3

Laser Modified Sapwood

r^2 Coef Det 0.9995

Peak	Type	Amplitude	Center	% Area
1	Gauss	5943	284.8	59.6
2	Gauss	2564	285.9	35.0
3	Gauss	353	287.6	4.6
4	Gauss	97	289.2	0.8

Laser Modified Heartwood

r^2 Coef Det 0.9995

Peak	Type	Amplitude	Center	% Area
1	Gauss	5825	284.7	58.2
2	Gauss	2597	286.0	31.4
3	Gauss	682	287.2	7.8
4	Gauss	267	289.0	2.6

200C Heated Heartwood

r^2 Coef Det 0.999

Peak	Type	Amplitude	Center	% Area
1	Gauss	5349	284.8	57.5
2	Gauss	2610	286.3	33.0
3	Gauss	650	287.9	6.2
4	Gauss	322	289.0	3.3

200C Heated Laser Modified Heartwood

r^2 Coef Det 0.999

Peak	Type	Amplitude	Center	% Area
1	Gauss	5092	284.8	58.7
2	Gauss	2772.55	286.3	30.9
3	Gauss	498.283	287.4	7.7
4	Gauss	289.37	289.2	2.7

Wide Scan Atomic Concentration Table (%)

Sample ID	C1s	N1s	O1s	P2p	Ca2p
Heartwood	78.4	2.04	19.08	0.2	0.27
Heated Heartwood	74.89	2.88	21.78	0.14	0.32
Laser Modified Heartwood	83.25	0.31	16.4	0	0.04
Heat treated Laser Modified Heartwood	78.57	0.22	21.2	0.01	0
Sapwood	76.48	1.82	21.67	0	0.04
Laser Modified Sapwood	86.87	0.4	12.69	0.04	0